Casey, J.F., and Miller, D.J. (Eds.)
Proceedings of the Ocean Drilling Program, Scientific Results Volume 179

2. Igneous Petrology of Gabbros from Hole 1105A: Oceanic Magma Chamber Processes[1]

P. Thy[2]

ABSTRACT

Hole 1105A penetrated 158 m of gabbros at a site offset 1.3 km east-northeast from Hole 735B on the Atlantis Bank near the Atlantis II Fracture Zone. A total of 118 m of dominantly medium- to coarse-grained intercalated Fe-Ti oxide gabbro and olivine gabbro was recovered from Hole 1105A that shows many petrographic features similar to those recovered from the upper part of Hole 735B. The main rock types are distinguished based on the constituent cumulus phases, with the most primitive gabbros consisting of olivine, plagioclase, and clinopyroxene. The inferred crystallization order is subsequently Fe-Ti oxides (ilmenite and titanomagnetite), followed by orthopyroxene, then apatite, and finally biotite. Orthopyroxene appears to replace olivine in a narrow middle interval. The magmatic evolution is likewise reflected in the mineral compositions. Plagioclase varies from An_{66} to An_{28}. Olivine varies from Fo_{78} to Fo_{35}. The gap in olivine crystallization occurs between Fo_{46} and Fo_{40} and coincides approximately with the appearance of orthopyroxene (~En_{50}). The clinopyroxenes show large compositional variation in $Mg/(Mg+Fe^{total})$ from 0.84 to 0.51. The nonquadrilateral cations of clinopyroxene similarly show large variations with Ti increasing for the olivine gabbros and decreasing for the Fe-Ti oxide gabbros with the decrease in $Mg/(Mg+Fe^{total})$. The apatites are mainly flourapatites. The compositional variation in the gabbros is interpreted as a comagmatic suite resulting from fractional crystallization. Pyroxene geothermometry suggests equilibration temperatures from 1100°C and below. The coexisting Fe-Ti oxide minerals indicate subsolidus equilibration temperatures from 900°C for olivine gabbros to 700°C for the

[1]Thy, P., 2003. Igneous petrology of gabbros from Hole 1105A: oceanic magma chamber processes. *In* Casey, J.F., and Miller, D.J. (Eds.), *Proc. ODP, Sci. Results,* 179, 1–76 [Online]. Available from World Wide Web: <http://www-odp.tamu.edu/publications/179_SR/VOLUME/CHAPTERS/SR179_02.PDF>. [Cited YYYY-MM-DD]
[2]Department of Geology, University of California, One Shields Avenue, Davis CA 95616, USA.
thy@geology.ucdavis.edu

Initial receipt: 10 November 2000
Acceptance: 11 March 2003
Web publication: 23 June 2003
Ms 179SR-017

most evolved apatite-bearing gabbros. The cryptic variation in the olivine gabbros defines two or three lenses, 40 to 60 m thick, each characterized by a distinct convex zoning with a lower segment indicating upward reverse fractionation, a central maximum, and an upper segment showing normal fractionation. The Fe-Ti oxide gabbros show cryptic variations independent of the host olivine gabbros and reveal a systematic upward normal fractionation trend transgressing host olivine gabbro boundaries. Forward fractional crystallization modeling, using a likely parental magma composition from the Atlantis II Fracture Zone (MgO = 7.2 wt%; $Mg/[Mg+Fe^{2+}] = 0.62$), closely matches the compositions of coexisting olivine, plagioclase, and clinopyroxene. This modeling suggests cosaturation of olivine, plagioclase, and clinopyroxene from 1155°C and the addition of Fe-Ti oxides from 1100°C. The liquid line of descent initially shows increasing FeO with moderately increasing SiO_2. After saturation of Fe-Ti oxides, the liquid strongly decreases in FeO and TiO_2 and increases in SiO_2, reaching dacitic compositions at ~10% liquid remaining. The calculations indicate that formation of olivine gabbros can be accounted for by <65% fractionation and that only the residual 35% liquid was saturated in Fe-Ti oxides. The modeling of the solid fractionation products shows that both the olivine gabbro and the Fe-Ti oxide gabbros contain very small amounts of trapped liquid (<5%). The implications are that the gabbros represent crystal mush that originated in a recharging and tapping subaxial chamber. Compaction and upward melt migration in the crystal mush appear to have been terminated with relatively large amounts of interstitial liquid remaining in the upper parts of the cumulate mush. This termination may have been caused by tectonic disturbances, uplift, and associated withdrawal of magma into the subaxial dike and sill system. Prolonged compaction and cooling of the trapped melt in the mush formed small differentiated bodies and lenses by pressure release migration and crystallization along syntectonic channels. This resulted in differentiation products along lateral and vertical channelways in the host gabbro that vary from olivine gabbro, to Fe-Ti oxide gabbro, gabbronorite, and apatite gabbros and show large compositional variations independent of the host olivine gabbros.

INTRODUCTION

Crustal accretion at slow-spreading ridges is controlled by relatively low magma supply rates. This results in periods of amagmatic spreading and pronounced lateral and vertical variations in crustal architecture and thickness. Magma migration in slow-spreading crust will consequently be influenced by tectonic processes that will lead to the emplacement of dikes and sills and small ephemeral chambers at all crustal levels. Despite this, the internal evolution of such magma reservoirs will fundamentally be controlled by the same processes that control magma evolution at fast-spreading centers. Cooling and crystallization will proceed by the formation of crystal mush zones along chamber margins and floors. Slow spreading and low magma supply will result in less frequent chamber tapping and replenishment and restrict magma mixing compared to chambers at fast-spreading centers. The restricted flux of magma at the same time will provide conditions for efficient fractionation processes. Crystal mush in slow-spreading chambers will solidify by compaction and vertical and horizontal melt migration partially in response to deformation processes affecting the mush zone.

Compaction and plastic flow in the crystal mush will result in or intensify preexisting modal layering and lamination. The differentiation of magma at slow-spreading ridges may further be affected by tectonic uplift and withdrawal of magma from the melt lens and cessation or reduction in compaction. Trapped interstitial liquid of crystal mushes may crystallize in the host rock to form intercalated, small differentiated bodies and lenses as a result of predominantly lateral migration and syn- and post-tectonic melt-channeled movement into uplift- and deformation-induced pressure release zones.

The gabbro and ferrogabbro complex recovered from Hole 1105A near the Atlantis II Fracture Zone, Southwest Indian Ridge, records fractionation and melt migration processes in chambers at a slow-spreading regime (Shipboard Scientific Party, 1999). In this contribution, the petrological results of a study of gabbroic cumulates from the 150-m, nearly continuous drill core that sampled parts of a small crustal magma chamber are presented. The results confirm the observations from Hole 735B and show that trapped interstitial melt migrates and differentiates largely without reequilibrating with the primitive olivine gabbro host.

HOLE 1105A

Tectonic Setting

Hole 1105A was drilled during Leg 179 in a water depth of 703 m on the block-faulted and wave-cut platform of the Atlantis Bank at approximately longitude 57°E (Fig. **F1A**), only 18–20 kilometers from the eastern rim of the Atlantis II Fracture Zone, Southwest Indian Ridge (Fig. **F1B**) (Pettigrew, Casey, Miller, et al., 1999). The position of Site 1105 is offset 1.3 km toward the east-northeast from Hole 735B, drilled during Legs 118 and 176 (Robinson, Von Herzen, et al., 1989; Dick, Natland, Miller, et al., 1999). Both sites are located east of the north-south–trending Atlantis II Transform that left-lateral offsets the Southwest Indian Ridge (Fig. **F1C**) (Dick et al., 1991b). The age offset is ~20 m.y., and the Atlantis II Fracture Zone grew at an average of 0.4 cm/yr (Dick et al., 1991b). Both ridge-transform intersections display asymmetric rift valleys with inside corner highs, outer corner lows, and nodal basins. The relief of the northern inner rift valley wall is nearly double that of the outer valley wall as a result of low-angle detachment faulting and unroofing of the plutonic footwall block (Fig. **F1D**).

Both Holes 735B and 1105A sampled gabbroic massifs formed at the inner corner of the northern median rift valley. The crustal section penetrated by Hole 735B represents thin crust relatively unaffected by the adjacent transform and formed beneath the median valley ~15–19 km away from the transform-ridge intersection ~11 m.y. ago (Dick et al., 1991a, 1991b; Muller et al., 1997). The massif was subsequently uplifted 5–6 km as a transverse ridge to above sea level, eroded, and later subsided to its present water depth. Thus, the Atlantis Bank may represent the remains of a fossil magma chamber formed near the midpoint of a volcanic ridge segment and unroofed by transform tectonics (Dick et al., 1991b, p. 396). Site 1105 is located in crust of approximately similar age and origin as that at Site 735 and represents crust formed farther distal from the transform-ridge intersection. Hole 1105A probably penetrated crust that originated from the same volcanic ridge segment as Hole 735B, only slightly farther away from the transform-ridge intersec-

F1. Main tectonic features and location of site, p. 25.

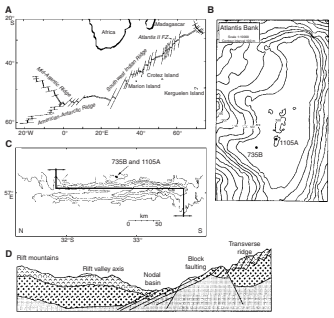

tion. The results from Hole 1105A, therefore, can elucidate the lateral variation in magma supply and magma processes along active slow-spreading centers.

Principal Lithostratigraphy

Hole 1105A penetrated to a depth of 158 m and recovered a total of 118 m of dominantly medium- to coarse-grained gabbro intervals (Fig. F2). The grain size ranges from coarse to pegmatitic in extreme cases. The lithologic intervals were divided into three major units by the Shipboard Scientific Party (1999). Gabbroic rocks constitute by far the majority of the recovered igneous lithologies with only a very minor component of felsic veins (<0.1%). The gabbros are composed of olivine gabbro (52%), gabbro (16%), Fe-Ti oxide olivine gabbro (14%), Fe-Ti oxide gabbro (16%), and minor amounts of Fe-Ti oxide gabbronorite (2%). The main components can largely be grouped into Fe-Ti oxide–free (78%) and Fe-Ti oxide–bearing gabbros (22%) that are intercalated throughout the recovered gabbro interval on a scale from a few millimeters to meters. Apatite is a characteristic index mineral in some relatively evolved Fe-Ti oxide gabbros and gabbronorites. A minor component of granular textured microgabbros is also occasionally present.

Igneous layering is seen mainly as irregularly developed modal, textural, and grain size variations in all gabbro components. Mostly this layering is defined by grain size variation from medium to coarse grained (Fig. F3A). The gabbros are texturally granular, often with large poikilitic clinopyroxenes, particularly in the pegmatitic components (<60 mm). Rhythmic modal layering and laminations (Fig. F3B) are only occasionally identified. Many of the gabbros show a distinctive penetrative foliation (Fig. F3C) that may have overprinted a primary igneous fabric. The Fe-Ti oxides and sulfides are irregularly distributed as granular to interstitial and disseminated grains that are often highly concentrated in patches and bands. There is a strong tendency for ductile deformation to be channeled along Fe-Ti oxide–rich bands and to be accompanied by grain fining and neoblast and porphyroblast formation (Fig. F3D) and sometimes the development of mylonitic bands (Fig. F3E). In the relatively undeformed gabbros and olivine gabbros, the effects of deformation are seen as kinking of albite twins and the development of tapering twins (Fig. F3F), irregular zoning, and incipient neoblast formation along grain boundaries. The pyroxenes similarly show kinking of exsolution lamellae and twin planes. Most preserved olivine grains show signs of kink banding and recrystallization. The Shipboard Scientific Party (1999) estimated that gabbroic rocks with deformation and recrystallization textures represent >40% of the rock intervals present in Hole 1105A.

The principal divisional units were defined by the Shipboard Scientific Party (1999) by the relative proportion of Fe-Ti oxide gabbro layers and lenses in dominantly massive Fe-Ti oxide–free gabbro and olivine gabbro. The assigned unit divisions are illustrated in Figure F2, together with a schematic breakdown in the two principal gabbroic components.

Lithologic Unit I (15–48.14 meters below seafloor [mbsf]) is composed of medium- to coarse-grained, alternating gabbro, olivine gabbro, and Fe-Ti oxide gabbro. Fe-Ti oxide gabbro (8%) is confined to the lower part of the unit (Fig. F2), whereas the rest of the unit is medium- to coarse-grained massive gabbro and olivine gabbro (92%). The Fe-Ti ox-

F2. Lithologic summary, p. 26.

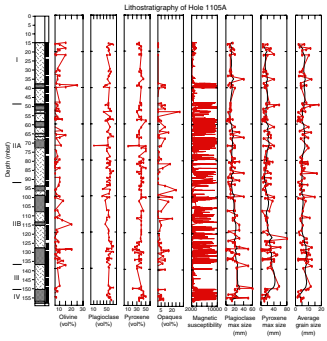

F3. Gabbro structures, p. 27.

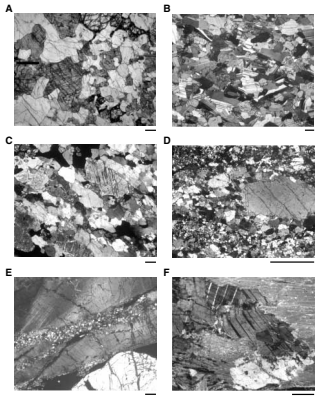

ide gabbro is characterized by irregularly distributed, interstitial, and disseminated Fe-Ti oxides and sulfides that may be highly concentrated in localized patches and bands.

Lithologic Unit II (48.14–136.38 mbsf) is composed of alternating gabbro, Fe-Ti oxide gabbro, and olivine gabbro. The upper boundary is defined by the appearance of a higher proportion of Fe-Ti oxide gabbro and is also clearly reflected in the magnetic susceptibility (Fig. F2). Unit II is composed of medium- to coarse-grained Fe-Ti oxide gabbro (29%), gabbro (55%), and olivine gabbro (16%), without systematic distribution of the three main gabbro types. Fe-Ti oxide minerals are a minor component in all gabbros and olivine gabbros. The gabbro and olivine gabbro vary modally widely and are composed of olivine (2%–20%), plagioclase (55%–70%), and clinopyroxene (20%–35%) with anhedral to subhedral granular textures and larger poikilitic clinopyroxene grains. The Fe-Ti oxide gabbros are typically composed of olivine (0%–15%), plagioclase (50%–60%), clinopyroxene (25%–40%), Fe-Ti oxide minerals (5%–15%), minor amounts of sulfides, and, occasionally, orthopyroxene and apatite. The Shipboard Scientific Party (1999) observed that the average grain size in the lower part of the unit appeared to be larger than that in the upper part of the unit (Fig. F2). This allows Unit II to be divided into two subunits. Subunit IIA is defined between 48.14 and 92.79 mbsf and Subunit IIB between 92.79 and 136.38 mbsf. This subdivision corresponds to the magnetic susceptibility measurements, which show a significant drop in average values at this boundary (Shipboard Scientific Party, 1999).

Lithologic Unit III (136.38–150.60 mbsf) is composed of gabbro (9%), olivine gabbro (88%), and minor amounts of Fe-Ti oxide gabbro (3%). The lower boundary is defined by an increase in the modal abundance of Fe-Ti oxide minerals and in the intensity of the magnetic susceptibility (Fig. F2). Unit III is a sequence of dominantly olivine gabbro that is separated from the units above and below, both of which are characterized by the ubiquitous presence of Fe-Ti oxide–rich gabbros.

Lithologic Unit IV (150.60 mbsf to the bottom of the hole at 157.44 mbsf) is composed of Fe-Ti oxide gabbro (37%) and gabbro (63%) in alternating intervals. The contact with Unit III is marked by an abrupt increase in the modal abundance of Fe-Ti oxide and in the intensity of the magnetic susceptibility (Fig. F2). The Fe-Ti oxide content in the Fe-Ti oxide gabbros ranges from 5% to 10%, and the remainder is mainly composed of plagioclase and clinopyroxene, the former volumetrically generally exceeding the latter.

The gabbro units drilled from Hole 1105A are principally defined by the relative proportions of Fe-Ti oxide–bearing and Fe-Ti oxide–free gabbros. Except for a coarsening downward in the average grain size in the core (Fig. F2), there is no additional systematic petrographic and textural variation that can be related to stratigraphic position (Shipboard Scientific Party, 1999).

Sampling and Analytical Techniques

A total of 99 samples (Table T1) were selected from Hole 1105A to represent the main gabbroic rock types. This number includes 67 shipboard-prepared thin sections for which extensive petrographic and modal data exist (Shipboard Scientific Party, 1999). Primary igneous minerals were analyzed for each thin section with an CAMECA SX-50 electron microprobe operated at accelerating voltage = 15 kV, beam current = 10 nA, and count time = 10 s. Because of extensive exsolution

T1. Silicate mineral compositions, p. 53

lamellae in pyroxenes and Fe-Ti oxides, these minerals were analyzed with a broad beam (~10 µm). Further, the possibility for loss of sodium from albitic plagioclase also necessitated that this mineral be analyzed with the broad beam. Olivine and apatite were analyzed with a narrow beam (~1–2 µm), the latter because of its relatively small size. Multiple analyses of primary igneous phases were compiled for each individual petrographically distinct part of the thin sections. The analytical results are summarized in Table T1 for plagioclase, clinopyroxene, olivine, and orthopyroxene as averages and standard deviations of characteristic cation ratios. Plagioclase is described by the An content (Ca/[Ca+Na+K]). Olivine is described by the Fo content (Mg/[Mg+Fe]). Clinopyroxene and orthopyroxene are described by either their $Mg/(Mg+Fe^{total})$ or $Mg/(Mg+Fe^{2+})$ ratios, with Fe^{2+} and Fe^{3+} estimated based on charge balancing cations (Papike et al., 1974). Fe-Ti oxide minerals (ilmenite and titanomagnetite) are described by the ilmenite-hematite and ulvöspinel-magnetite fractions, respectively, with Fe^{2+} and Fe^{3+} estimated by assuming perfect stoichiometries (Andersen and Lindsley, 1988).

IGNEOUS PETROGRAPHY

Classification

The main rock types are principally distinguished by the presence or absence of the main minerals plagioclase, clinopyroxene, orthopyroxene, olivine, Fe-Ti oxides, and apatite. Sulfide minerals, brown hornblende, and biotite are additionally present in many of the examined samples in total proportions <1%–2%. The classification used in this study contrasts to the usage adopted during Leg 179 (Shipboard Scientific Party, 1999), as well as to IUGS classification (Le Maitre, 1989). The justification is that the relatively coarse grained nature of the gabbros makes it difficult to obtain representative estimates of rock modes. An additional consideration is the need to use a nomenclature that facilitates the petrogenetic discussion.

The relatively coarse grained nature of many of the gabbros and their low modal olivine content question the significance of distinguishing between gabbro and olivine gabbro based on sampling a volume represented by a thin section. Therefore, gabbro and olivine gabbro are grouped together in this work and are described in general terms as olivine gabbro. This contrasts with the nomenclature adopted during Legs 118, 176, and 179.

The Shipboard Scientific Party (1999) defined Fe-Ti oxide gabbros drilled during Leg 179 as containing at least 5% modal Fe-Ti oxide minerals. This definition contrasts with the usage adopted by the Shipboard Scientific Parties of both Legs 118 and 176 (Robinson, Von Herzen, et al., 1989; Dick, Natland, Miller, et al., 1999), which defined petrographic and modal varieties of Fe-Ti oxide gabbros as containing at least 1% Fe-Ti oxide minerals. The present work follows Legs 118 and 176 in the modal definition of Fe-Ti oxide gabbros.

Gabbronorite and apatite gabbro are defined by the presence of orthopyroxene and apatite, respectively, as primary igneous phases irrespective of their absolute modes. The mode of orthopyroxene in many of the rocks, here referred to as gabbronorites, is often too low to classify these as gabbronorites stricto sensu (Le Maitre, 1989). The presence of orthopyroxene is a diagnostic feature for monitoring the petrogenesis of the gabbros, and its inclusion in the nomenclature is thus justi-

fied. Similarly, the presence of apatite is used to classify the gabbro (or gabbronorite) as apatite gabbro. Pigeonite, or its low-temperature inversion products, was not detected as a primary igneous phase in this study, despite being described from Hole 735B (Robinson, Von Herzen, et al., 1989; Dick, Natland, Miller, et al., 1999).

The Hole 1105A gabbros are modified to variable degrees by hydrothermal alteration, ductile to brittle deformation, extensive development of secondary and metamorphic minerals, and dynamic recrystallization of primary mineral assemblages. The secondary neocrystallized minerals include talc, serpentine, smectite, magnetite, calcite, epidote, chlorite, green hornblende, and actinolite. Recrystallization of primary igneous minerals (olivine, pyroxene, and plagioclase) is likewise extensive in many gabbros. The secondary and metamorphic mineral assemblages suggest that overall the dominant alteration and metamorphism took place under greenschist facies conditions (Stakes et al., 1991). These modifications of primary igneous textures and mineralogies are not dealt with in this contribution to any significant extent.

Olivine Gabbro

Olivine gabbro is the most abundant rock type in all lithologic units (Fig. F2) (Scientific Shipboard Party, 1999). The average modal composition of olivine gabbros is olivine = 9 vol%, plagioclase = 60 vol%, and clinopyroxene = 31 vol%. All major mineral phases show wide modal variations (Fig. F4), mainly due to variations in amounts of plagioclase and pyroxene, with occasional troctolitic and anorthositic variants. Additional trace amounts of brown hornblende and opaque minerals (Fe-Ti oxide and sulfide minerals) are present in many gabbros in amounts <0.4%. The grain sizes of the olivine gabbros are dominantly medium to mostly coarse grained (~75 vol%). The textures are granular with interlocking plagioclase and clinopyroxene grains (Fig. F5A). Most of the coarse-grained and pegmatitic olivine gabbros, however, have poikilitic or subophitic textures in which large subhedral poikilitic clinopyroxene (Fig. F5B) encloses or partly encloses small euhedral to subhedral plagioclase and, sometimes, olivine. Plagioclase grains are commonly homogeneous and in undeformed gabbros rarely show signs of compositional zoning (Fig. F5C). Because of incipient deformation, plagioclase often contains tapering twin lamellae and has undulatory extinction. Plagioclase of the olivine gabbros shows very wide compositional ranges from An_{66} to An_{40} (Fig. F6; Tables T1, T2). Olivine is present as rounded to anhedral homogeneous grains that vary in composition from Fo_{78} to Fo_{50} (Fig. F7; Table T1). Olivine is often recrystallized and forms clusters of grains with fine-grained polygonal, mosaic textures (Fig. F5D). Deformation bands and undulatory extinction occur in most olivine grains (Fig. F5E). Clinopyroxene is present as homogeneous grains without obvious compositional zoning. Fine exsolution lamellae of low-Ca pyroxene are ubiquitously present in most clinopyroxene grains. The clinopyroxene is augitic with $Mg/(Mg+Fe^{total})$ ratios from 0.84 to nearly 0.60 (Fig. F8; Tables T1, T3). Often, clinopyroxene shows consertal intergrowth and replacement textures with adjacent clinopyroxene (Fig. F5F). Clinopyroxene is commonly clouded by acicular opaque minerals that are aligned and regularly spaced. Brown hornblende is an accessory mineral that is present in most gabbros as rims to clinopyroxene grains as well as patchy blebs in clinopyroxene and as coronas around Fe-Ti oxide and olivine. Biotitic mica is also occasionally present as a late-

F4. Modal variation in gabbros, p. 28.

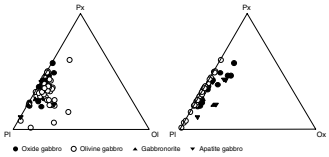

F5. Petrography, mineralogy, and textures of olivine gabbros, p. 29.

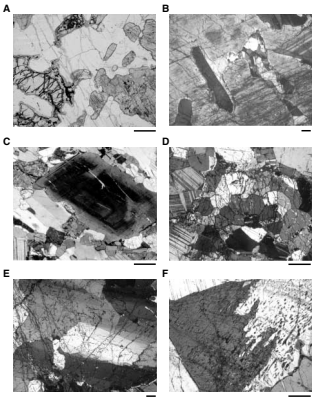

F6. An content of plagioclase for main lithologic components, p. 30.

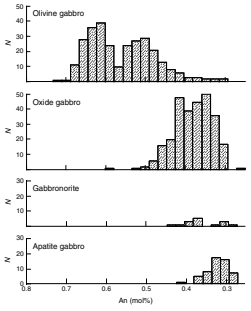

T2. Compositions of cumulus plagioclase, p. 56.

F7. Fo content of olivine for main lithologic components, p. 31.

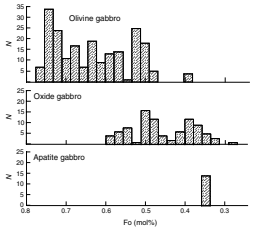

crystallizing phase. Apatite is characteristically absent from the olivine gabbros.

Fe-Ti Oxide Gabbro

The modal composition of Fe-Ti oxide gabbro averages olivine = 3 vol%, plagioclase = 58 vol%, clinopyroxene = 35 vol%, and Fe-Ti oxides and sulfides = 5 vol%. Additional trace amounts of brown hornblende and biotite are often present. As for the olivine gabbros, the modal variation of the Fe-Ti oxide gabbros varies considerably but is mainly restricted to variations in plagioclase and pyroxene contents (Fig. F4). Olivine appears to be present in the Fe-Ti oxide gabbros in lower modal amounts than in the olivine gabbros. However, the presence or absence and absolute amounts of olivine may have little petrogenetic significance because of the relatively coarse grained nature of the gabbros. The Fe-Ti oxide minerals are mostly ilmenite and are present in amounts that do not exceed a total of 12% (Fig. F4) (Shipboard Scientific Party, 1999).

The undeformed Fe-Ti oxide gabbros are in many respects similar to the olivine gabbros, especially in terms of rock textures, mineral morphologies, and mineral intergrowth. The difference is the presence of Fe-Ti oxide minerals that are generally <0.5 mm in grain size in the olivine gabbro and are present as late interstitial patches often intergrown with brown hornblende and metamorphic amphiboles and other secondary phases. In contrast, the Fe-Ti oxide minerals in the Fe-Ti oxide gabbros may reach grain sizes generally up to 10 mm in an interstitial fabric to silicate minerals and as elongated aggregates forming irregular seams and bands.

The composition of olivine in the Fe-Ti oxide gabbros, when present, is between Fo_{51} and Fo_{36} and is significantly more iron rich than that for the olivine gabbros (Fig. F7; Tables T1, T4). Similarly, the coexisting plagioclase (An_{49}–An_{29}) and clinopyroxene ($Mg/[Mg+Fe^{total}]$ = 0.66–0.58) reveals more evolved compositions compared to the olivine gabbros (Figs. F6, F8; Tables T1, T2, T3).

Gabbronorite

Orthopyroxene, along with plagioclase and clinopyroxene, is present as a primary igneous phase in a few gabbros without any apparent stratigraphic relations. These gabbronorites contain up to 8% modal orthopyroxene and appear not to contain olivine. Only two gabbronorites were examined in this study; both contain a few percent Fe-Ti oxide minerals. It thus appears that orthopyroxene–bearing gabbros are also Fe-Ti oxide bearing and, further, lack olivine. Orthopyroxene is often slightly prismatic elongated and is present in granular intergrowths with plagioclase and clinopyroxene. Orthopyroxene contains abundant, thin exsolution lamellae and blebs of clinopyroxene (Fig. F9C). Some samples reveal replacement textures of orthopyroxene by secondary clinopyroxenes.

The composition of the primary igneous orthopyroxenes is relatively Fe rich, with Mg/(Mg+Fe) ratios of 0.48–0.52 (Fig. F8; Tables T1, T3) without detectable differences between the apatite-bearing and apatite-free gabbros. The orthopyroxene compositions correspond to the generally more sodium- and iron-rich compositions of coexisting plagioclase (An_{37}–An_{33}) and clinopyroxene ($Mg/[Mg+Fe^{total}]$ = 0.63–0.51) (Figs. F6,

F8. Mg/(Mg+Fe^{2+}) of pyroxenes for main lithologic components, p. 32.

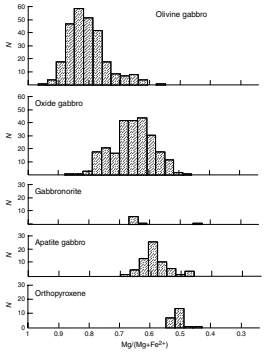

T3. Compositions of cumulus pyroxene, p. 61.

T4. Compositions of cumulus olivine, p. 66.

F9. Petrography, mineralogy, and textures of Fe-Ti oxide–bearing gabbros, p. 33.

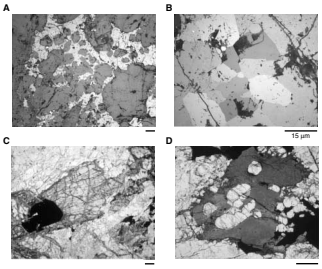

F8; Tables T1, T2, T3). Thus, the gabbronorites appear to be relatively more evolved than the most primitive of the Fe-Ti oxide gabbros.

Low-Ca pyroxenes also appear as secondary minerals in minor amounts in many Fe-Ti oxide gabbros and are relatively more Mg rich than the primary igneous orthopyroxenes. These secondary pyroxenes are not dealt with in this study.

Apatite Gabbro

Apatite was found and analyzed in 11 samples and is present in close association with Fe-Ti oxide seams (Fig. F9D). Three of these samples also contain orthopyroxene. Apatite generally ranges up to 5 vol% and contains saline fluid inclusions. The presence of considerable amounts of apatite is one of the significant features that characterize some of the Fe-Ti oxide gabbros from Hole 1105A. Apatite was not fully recognized in the gabbros of Hole 735B (Robinson, Von Herzen, et al., 1989). Biotitic mica is only found in one sample as prismatic grains enclosed by Fe-Ti oxide minerals that texturally signify a primary igneous origin (Sample 179-1105A-27R-1, 71–75 cm). The apatite gabbros are, in most respects, similar to the Fe-Ti oxide gabbros and the gabbronorites. They are typically medium to coarse grained and have granular textures. The apatite is present as <0.1-mm, large euhedral grains, most often in interstitial Fe-Ti oxide seams and patches, but may also be found included in other primary or secondary minerals.

The compositions of the silicate minerals in apatite gabbro show that these are among the most evolved gabbros. The olivine compositions are relatively restricted around Fo_{35} (Fig. F7; Tables T1, T4). Similarly, plagioclase compositions are below An_{31} and clinopyroxene Mg/(Mg+Fe^{total}) ratios are <0.68 (Figs. F6, F8; Tables T1, T2, T3).

Microgabbro

Fine-grained gabbros are occasionally present and are of considerable interest, as they may represent quenched liquid. Three samples were included in this study (Samples 179-1105A-8R-1, 68–70 cm; 13R-1, 24–25 cm; and 15R-2, 71–74 cm). Microgabbros appear to be generally confined to bands or lenses (Fig. F10), but no clear discordant relationships and chill effects were observed against the coarser-grained gabbros (Fig. F10). The microgabbros are mineralogically highly variable but share common fine-grained homogeneous, equigranular textures with polyhedral mutual grain boundaries and are void of phenocrysts (or porphyroblasts) (Fig. F10). The latter distinguish them from mylonitic gabbros. The mineralogies of the microgabbros vary from gabbronorite, gabbro, and olivine gabbro and they appear to represent a range of relatively evolved compositions with olivine compositions of Fo_{40} (Sample 179-1105A-15R-2, 71–74 cm), plagioclase of An_{46} to An_{31}, and clinopyroxene of Mg/(Mg+Fe^{total}) between 73 and 62 (Table T1). The orthopyroxene present in one of the microgabbros has a Mg/(Mg+Fe^{total}) ratio of 51 (Sample 179-1105A-8R-1, 68–70 cm). The petrographic, textural, and compositional similarities between the microgabbros and the gabbros are striking and suggest that the microgabbros may be recrystallized gabbros and not quenched melts.

F10. Microgabbro banding, p. 34.

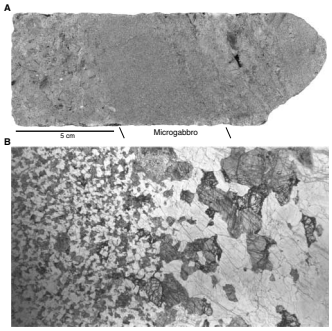

IGNEOUS MINERAL CHEMISTRY

The analyzed samples and the resultant average mineral analyses are summarized in Table T1. More compositional details are given in Table T2 (plagioclase), Table T3 (clinopyroxene and orthopyroxene), Table T4 (olivine), Table T5 (titanomagnetite and ilmenite), Table T6 (apatite), and Table T7 (biotite).

Plagioclase

Plagioclase shows extensive solid solutions from $An_{70}Ab_{30}$ to $An_{30}Ab_{69}$ concurrently with a systematic increase in potassium from $Or_{0.4}$ to $Or_{1.0}$ (Fig. F11). The iron content of plagioclase is relatively low (FeO = 0.21 wt%) and only weakly increases with Ab content. The systematic variations in Ab and Or point toward a cogenetic suite from olivine gabbros to Fe-Ti oxide gabbros, gabbronorites, and apatite gabbros.

Olivine

Despite the limited preservation and restricted appearance of olivine, its composition parallels the evolution of plagioclase. Olivine shows strong iron enrichment and varies in composition from Fo_{88} to Fo_{35} in the general sequence from olivine gabbros to Fe-Ti oxide gabbros and apatite gabbros (Fig. F12). There are two intervals of olivine crystallization with a gap between approximately Fo_{46} and Fo_{40}. This interval without olivine crystallization appears to correspond to the appearance of orthopyroxene. The most fayalitic olivine is found in the apatite gabbros (Fo_{36}–Fo_{35}). Manganese shows a systematic increase with increasing fayalite content of the olivine (Fig. F12), but other analyzed minor elements (Ni and Cr) show no systematic variation.

Clinopyroxene

Extensive variation is revealed by the clinopyroxene compositions in both minor and major elements. The quadrilateral components (94%–91%) (Fig. F13) define the clinopyroxenes as dominantly augitic to slightly ferroaugitic (Poldervaart and Hess, 1951). Pyroxene quadrilateral geothermometry suggests equilibration temperatures from 1100°C and down to 700°C (Fig. F13) (Lindsley, 1983).

The nonquadrilateral cations include Na, Al, Mn, Ti, and Cr (Fig. F14). Chromium shows a strong decrease for the olivine gabbros with decreasing $Mg/(Mg+Fe^{2+})$ ratio but remains low in the Fe-Ti oxide–bearing gabbros. Manganese shows systematic increases and Al shows a systematic decrease with decreasing $Mg/(Mg+Fe^{2+})$ ratios throughout the gabbro suite. Despite large variation, Ti shows an increase in the olivine gabbros but indicates a moderate decrease in the Fe-Ti oxide–bearing gabbros. This break in the Ti variation is also revealed by the Ti/Al ratios, for which the olivine gabbros suggest an increase and the Fe-Ti oxide gabbros suggest relatively constant ratios (Fig. F15).

The major elements show a strong negative correlation between Mg and Fe^{2+} and only a small decrease in Ca with increasing Fe^{2+} (Fig. F16). The Mg and Fe^{2+} variation deviates from the trend expected from a dominating $Fe^{2+} \leftrightarrow Mg$ cation exchange. The deviation increases with increasing Fe^{2+}, in part due to $(Mg,Fe^{2+}) \leftrightarrow Ca$ exchange as well as cou-

T5. Compositions of coexisting ilmenite and titanomagnetite, p. 69.

T6. Compositions of cumulus apatite, p. 74.

T7. Composition of cumulus biotite, p. 75.

F11. Orthoclase vs. An content of plagioclase, p. 35.

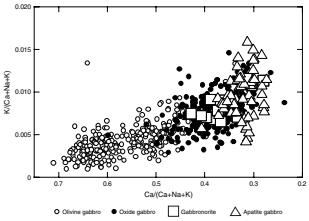

F12. Mn vs. Fo content of olivine, p. 36.

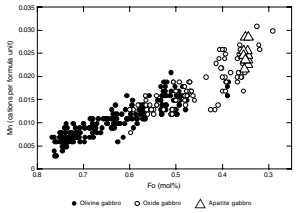

F13. Quadrilateral components of pyroxenes, p. 37.

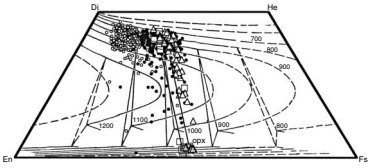

pled exchange mechanisms such as $TiAl_2 \leftrightarrow (Mg,Fe^{2+})Si_2$. The exchange mechanisms can be further evaluated by assigning cations to likely site positions in the pyroxene structure. The pyroxene compositions have been recalculated with all Si assigned to tetrahedral position and Fe^{3+}, Ti, and Cr to the M1 position in the structure. The Al is distributed between tetrahedral and M1 positions, assuming that the total amounts of tetrahedral cations is 2. Ca and Na occur only in M2 positions, and Fe^{2+}, Mn, and Mg may occur in either M1 or M2 octahedral positions (Lindsley and Andersen, 1983). The distribution of iron between Fe^{2+} and Fe^{3+} has been estimated based on charge balancing the cations (Papike et al., 1974). The results suggest Fe^{3+}/Fe^{2+} ratios of 0.4–0.1, with a systematic fall in the average values for each group of gabbros from olivine gabbro to Fe-Ti oxide gabbro and apatite gabbro. Both tetrahedral Al^{IV} and octahedral Al^{VI} slightly decrease in the same sequence. The Ti vs. Al^{IV} variation suggests wide variations in the Ti/Al ratios from between 1:2 and 1:8 (Fig. **F15**). The Na content is relatively constant without any systematic dependence on Fe or Mg contents. Based on simplified partitionings, the nonquadrilateral cations can be broken down as aegerine (2.6%–2.9%; $NaFe^{3+}Si_2O_6$), jadeite (0.5%–0.7%; $NaAlSi_2O_6$), fassaite (1.3%–1.7%; $CaFe^{3+}AlSiO_6$), Ti-tschermakite (1.3%–1.9%; $CaTiAl_2O_6$), and Ca-tschermakite (0.8%–2.8%, $CaAlAlSiO_6$) (Lindsley, 1983). These components show little systematic variation with the quadrilateral components, with the exception of Ti-tschermakite, which shows a maximum for an intermediate ferrosilite composition.

Orthopyroxene

The low-Ca pyroxene is an orthopyroxene with generally <4% wollastonite and $Mg/(Mg+Fe^{total})$ ratios narrowly between 0.49 and 0.51 (Fig. **F13**). The apparent closure of the gap between Ca-rich and Ca-poor pyroxenes, seen on Figure **F13** and also reflected on Figure **F16** for analyses with high Mg and low Ca, in part reflects the inability of the broad analytical microbeam technique always to consistently average unexsolved pyroxene composition.

There is no detectable difference in the compositions of the orthopyroxenes in the apatite-bearing and the apatite-free gabbros. The nonquadrilateral elements are mostly Ti and Al (Fig. **F14**) and amount to <2% of the total. The exchange coefficient for Mg and Fe between the two pyroxenes $([Mg/Fe]^{cpx}/[Mg/Fe]^{opx})$ range between 0.500 and 0.763 (N = 5), mainly due to variation in the coexisting augites. As a result, the slope of the tie-lines between coexisting orthopyroxene and augite (Fig. **F13**) appears to correspond better to experimentally determined augite-pigeonite than to augite-orthopyroxene pairs (Lindsley, 1983). Therefore, it is possible that the orthopyroxenes reflect subsolidus inversion or granule exsolution from high-temperature pigeonite.

Fe-Ti Oxide Minerals

The Fe-Ti oxide minerals of the oxide gabbros are present as granular intergrowth between ilmenite and titanomagnetite. The ilmenite is generally free of hematite lamellae, whereas titanomagnetite often contains lamellar to granule exsolution of titanomagnetite. The analytical technique attempted to incorporate the exsolved component by using a broad beam and by analyzing the relatively unexolved parts of the grains. Figure **F17** illustrates the extent of solid solution in the two Fe-Ti

F14. Ti, Al, Mn, Na, and Cr in clinopyroxenes vs. $Mg/(Mg+Fe^{2+})$, p. 38.

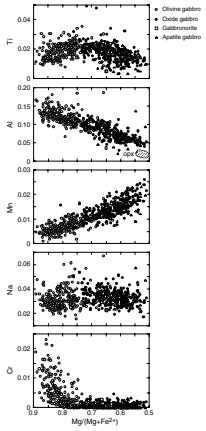

F15. Ti and Al in clinopyroxenes, p. 39.

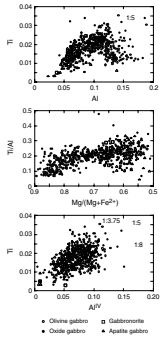

F16. Mg and Ca in clinopyroxenes vs. Fe^{2+}, p. 40.

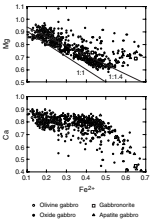

F17. Fe^{2+}-Ti-Fe^{3+} variation of coexisting ilmenite and titanomagnetite, p. 41.

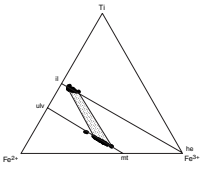

oxide minerals as well as the range of tie-lines between coexisting titanomagnetite and ilmenite. The minor elements in the two Fe-Ti oxide series show little correlation with rock types (Fe-Ti oxide or apatite gabbros). The only exception is Mn, which is negatively correlated with Mg content of ilmenite (Fig. F18). The ilmenite in the apatite gabbros has the highest Mn content. This is consistent with the increase of Mn seen in olivine and augite with increasing Fe^{2+} or decreasing $Mg/(Mg+Fe^{2+})$ ratio.

The compositions of the coexisting ilmenite and titanomagnetite can be used to calculate the equilibration temperature and oxygen fugacity (f_{O2}) (Buddington and Lindsley, 1964; Andersen and Lindsley, 1988). The result of these calculations for average compositions of individual samples is shown in Figure F19. The equilibration temperatures range from 850° to 675°C, and the apatite gabbros have the lowest equilibrium temperatures. These results generally correspond to the equilibrium temperatures determined for augite (1100°–700°C) and suggest that the Fe-Ti oxide pairs continued to reequilibrate past closure of the silicate assemblage. The calculated oxygen fugacity clusters around the fayalite-magnetite-quartz (FMQ) oxygen buffer at relatively high temperatures, but deviates for lower temperatures vary by up to 0.5 log units below the FMQ.

Apatite

Apatite contains various amounts of anionic fluorine, chlorine, and hydroxyl. The fluorine content is >2.6 wt%, and the chlorine content is <0.40 wt%. The OH content can be estimated from the deficiency in the total cations (F+Cl+OH = 2) and is <30% of the total anions. Cations in minor concentrations (Fe, Mn, Mg, and Na) are generally well below 0.2 wt%. The solid solutions of the apatites are illustrated in Figure F20 in terms of the F+Cl+OH component as dominantly flourapatites to hydroxyapatites with minor amounts of chlorapatite.

Biotite

Mica was detected in one of the most evolved apatite gabbros (Fo_{32}) as a few grains of likely primary igneous origin. The average composition is illustrated in Table T7 and defines the mica as a typical biotite with a Mg/Fe ratio of 1:2.

CRYPTIC VARIATION

Gabbro Compositions

The compositional variation of the gabbros from Hole 1105A can be evaluated by the shipboard X-ray fluorescence (XRF) analyses (Shipboard Scientific Party, 1999). Selected elements as a function of depth in the hole (Fig. F21) confirm the petrographic observations of two distinct compositional groups. The volumetrically dominant and relatively primitive olivine gabbros have low TiO_2 and Fe_2O_3 (total iron) contents, high Mg/(Mg+Fe) ratios, and anorthitic normative plagioclase compositions (weight percent CIPW norm). The Fe-Ti oxide–bearing gabbros have high TiO_2 and Fe_2O_3 contents, low Mg/(Mg+Fe) ratios,

F18. Mn vs. Mg in ilmenite, p. 42.

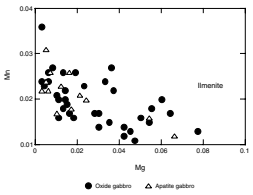

F19. Oxygen fugacity vs. temperature for coexisting ilmenite and titanomagnetite, p. 43.

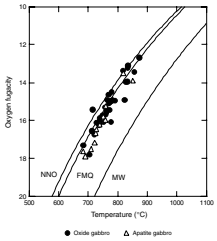

F20. Anionic F, Cl, and OH components of apatite, p. 44.

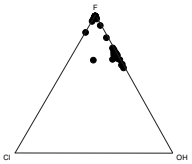

F21. Compositional variation in Fe-Ti oxide- and Fe-Ti oxide–free bulk rocks, p. 45.

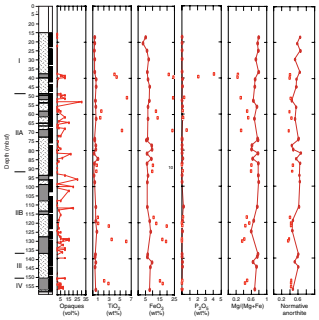

and albitic normative plagioclase compositions. The apatite gabbros, in addition, have high P_2O_5 content (<4 wt%), reflecting modal apatite.

The interpretation of the compositional variation is complicated because the gabbros represent mixtures of the constituent primocryst minerals as well as interstitial crystallization and overgrowth. The problem of sampling the two closely intermixed gabbro components also attributes to the complications. The relative proportions and compositions of minerals control the bulk rock compositions. This means that volumetric combinations determined by the accumulative or segregative processes of up to eight minerals (olivine, plagioclase, augite, orthopyroxene, ilmenite, magnetite, apatite, and biotite) control the gabbro compositions. Thus, it cannot a priori be assumed that the two predominant gabbro groups identified by differences in the major oxide compositions also represent distinct liquid compositions. It is plausible, for example, that the compositional variation in TiO_2 and Fe_2O_3 reflects variations in crystallization and accumulation processes and not the existence of two distinct liquid compositions. This is illustrated in Figure **F22,** which shows the Mg/(Mg+Fe^{total}) ratio as a function of the normative plagioclase composition (anorthite). The olivine gabbros show distinct positive correlation that may reflect the constituent minerals and, thus, the hidden cryptic variation in the dominant minerals. In contrast, the Fe-Ti oxide–bearing gabbros show limited variation in anorthite but large variation in Mg/(Mg+Fe^{total}) ratios. This latter likely reflects variable modal content of Fe-Ti oxide minerals and not necessarily the Mg/(Mg+Fe^{total}) ratio of the constituent minerals.

F22. Bulk rock Mg/(Mg+Fe^{total}) vs. CIPW normative composition of plagioclase, p. 46.

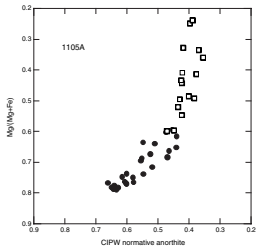

Mineral Compositions

The compositions of the three main constituent minerals (olivine, plagioclase, and clinopyroxene) are illustrated as a function of depth in Figure **F23,** showing all analyses, and in Figure **F24** as the averaged mineral compositions. The results confirm that the two main groups of gabbros observed from the bulk rock compositions are retained when mineral compositions are considered. At any depth interval in the core where both groups are represented, the gabbros show variation between primitive and evolved mineral compositions, often with an indication for a bimodal distribution. Only at some intervals can a near-complete compositional continuum be seen between the two groups. As already demonstrated, the olivine gabbros are relatively primitive, with Mg-rich mafic minerals and anorthitic plagioclases, and the Fe-Ti oxide gabbros are evolved, with Fe-rich mafic minerals and albitic plagioclases. The average compositions for each sample (Fig. **F24**) reveal the same compositional variation shown by the complete analytical data set but tend to enhance the compositional bimodality of the gabbros. The mineral compositions at any specific interval vary considerably between the two end-members because of crystallization and reequilibration. It is also apparent that some samples contain mixed populations of minerals grains (e.g., ~80 mbsf), probably resulting from mechanical redistribution during shear deformation. These latter are not further considered. It is the consistent variations in the most primitive and most evolved gabbro compositions that provides important first-order petrogenetic information and that is the principal object of the present discussion.

The olivine gabbros show large compositional variations, only tentatively defined based on the available sampling. If the most primitive

F23. Cryptic mineral variation revealed by cumulus olivine, plagioclase, augite, and orthopyroxene (all data), p. 47.

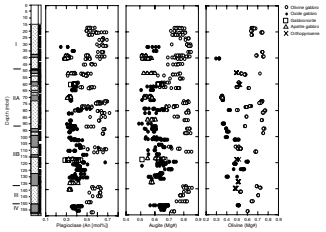

F24. Cryptic mineral variation revealed by cumulus olivine, plagioclase, augite, and orthopyroxene (averages), p. 48.

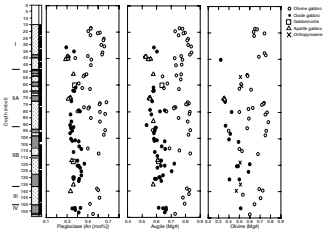

compositions are considered, the observed variation appears to define two and possibly three large-scale, convexly zoned gabbro lenses. These lenses vary in thickness from 40 to 60 m, despite uncertainties such as limited sampling at certain intervals and lack of base and top of the core. There is a surprising lack of olivine gabbros between ~115 and 137 mbsf (Fig. F23); despite this, olivine gabbros were identified by Scientific Shipboard Party (1999) to dominate this interval. It is possible that the host gabbros of this interval were relatively evolved and saturated or near saturated in Fe-Ti oxides and, therefore, cannot petrographically easily be distinguished from the oxide gabbros. It is equally possible that this interval completely lacks olivine gabbros despite shipboard observations.

Each convexly zoned lens includes a lower segment that shows upward reversed zoning, a central maximum, and an upper segment that shows normal zoning upward, all for $Mg/(Mg+Fe^{total})$ ratios of augite and olivine and An mole percent content of plagioclase. There is a tendency for a symmetric zoning pattern in the olivine gabbro lenses. If this interpretation is correct, we can distinguish lens I from the bottom of the hole to 115 mbsf (42 m), lens II between 115 and 55 mbsf (60 m), and lens III from 55 mbsf to the top of the hole (39 m) (Fig. F24). Despite the large uncertainty in this interpretation (Figs. F23, F24), it is nevertheless clear that the cryptic variation preserved by the olivine gabbros is distinctly different from that preserved by the Fe-Ti oxide gabbros.

The Fe-Ti oxide gabbros show systematic upward normal variation toward decreasing $Mg/(Mg+Fe^{total})$ ratios of the mafic minerals and An mole percent of plagioclase irrespective of the variation in the host olivine gabbros. The upward variation in the most evolved plagioclase compositions amounts to ~10 mol% from An_{40} to An_{30}. This is a normal differentiation trend typically observed from many layered intrusions and ophiolitic complexes.

QUANTITATIVE CRYSTALLIZATION MODEL

Provided that parental melts for the gabbros are known or can be reasonably predicted, fractional crystallization models can be formulated that allow the compositions of liquids, minerals, and bulk solids to be calculated as a function of temperature or liquid fraction remaining. The fractional crystallization models presented here are based on existing experimental results on mostly ferrobasaltic lavas (e.g., Thy and Lofgren, 1992, 1994; Toplis and Carroll, 1995). The models employ mass balance calculations for each oxide as a function of the solid fraction incrementally going from 0 to 1 in small and constant steps of the remaining liquid (<0.01). The compositions of the stable phase assemblage in equilibrium with the coexisting liquid are determined from simple and complex experimentally determined exchange coefficients, either as constants or as linear functions of temperature. In addition, stoichiometric constraints have been imposed on all silicate minerals. The temperature for each increment is estimated from a linear relationship with liquid MgO content. The redox conditions are constrained by the FMQ oxygen buffer using the equations formulated by Kilinc et al. (1983). The FMQ buffer is suggested by the coexisting Fe-Ti oxide minerals (Fig. F19). The instantaneous solid modes along the cotectics are modeled as constants based on the results of Thy and Lofgren (1994) and Toplis and Carroll (1995). The plagioclase-olivine cotectic is ap-

proximated by 0.264 olivine and 0.736 plagioclase (as total solids in weight fractions). The olivine-plagioclase-augite cotectic is constrained by 0.092 olivine, 0.463 plagioclase, and 0.446 augite. The Fe-Ti oxide minerals are modeled by 0.13 ilmenite and 0.07 magnetite, based on Thy and Lofgren (1994). Because of insufficient experimental constraints, the model calculations exclude low-Ca pyroxene and apatite and have been terminated at temperatures of 1000°C. Because the petrographic observations suggest that low-Ca pyroxene replaces olivine as a fractionating phase, this exclusion will have little effect on the liquid line of descent. The saturation of augite is based on Sugawara (2000), whereas the saturation of Fe-Ti oxides is based on Thy and Lofgren (1994) and Toplis and Carroll (1995). Details of the calculation method can be obtained from the author.

The parental magmas for the gabbros are not preserved in the recovered core, and no example of chilled margins has been identified from Hole 1105A (Shipboard Scientific Party, 1999) or from the nearby Hole 735B (Robinson, Von Herzen, et al., 1989; Dick, Natland, Miller, et al., 1999). However, possible parental basalts have been dredged from the Atlantis II Fracture Zone at several locations (Dick et al., 1991b; Natland et al., 1991; Johnson and Dick, 1992). Two glass analyses from pillow lavas have been tested as parental magma in the calculations. The first is from the rim of a pillow dredged from the northeastern side of the transform (Natland et al., 1991, table 1, anal. 5-3; Johnson and Dick, 1992, table 5). The other and more primitive glass analysis is from a sample dredged from the triple junction (Mahoney et al., 1989; Natland et al., 1991, table 1, anal. AII93-5, 6-1).

The results of modeling perfect fractional crystallization based on these possible parental magmas are illustrated in Figures **F25** and **F26.** The modeling for sample 5-3 assumes coprecipitation of olivine (Fo_{84}) and plagioclase (An_{69}) from 1184°C, augite ($Mg/[Mg+Fe^{total}] = 0.82$) in addition from 1155°C, and magnetite and ilmenite from 1100°C. The calculations are terminated at a liquid fraction of 0.13 (equal to 1000°C). The modeling result for sample 5-3 is summarized in Table **T8** with the first entry (zero solid fraction) being the starting composition normalized to 100%. The modeling for sample AII93-5 (only shown in Fig. **F25**) assumes coprecipitation of olivine (Fo_{88}) and plagioclase (An_{69}) from 1221°C, augite ($Mg/[Mg+Fe^{total}] = 0.80$) in addition from 1139°C, and magnetite and ilmenite from 1100°C. The calculations are terminated at liquid fractions of 0.14. The compositions of the mafic silicates when Fe-Ti oxides appear on the liquidus are very similar for the two models, whereas plagioclase compositions reflect differences in sodium content of the two compositions. The calculations show that olivine gabbro differentiation can be accounted for by up to 65% fractionation and that only the residual 35% will be saturated in Fe-Ti oxide minerals.

The resultant liquid lines of descent initially show increasing FeO with moderate increases in SiO_2. After Fe-Ti oxides appear, FeO and TiO_2 decrease while SiO_2 increases markedly to dacitic compositions at temperatures of ~1000°C and liquid fractions remaining of 0.15–0.10 (Fig. **F26A;** Table **T8**). The actual liquid iron enrichment path will be strongly dependent on the composition of the assumed starting composition. This is illustrated in Figure **F26A,** where the two liquid curves represent the two slightly different compositions for the same sample 5-3 given by Natland et al. (1991) and Johnson and Dick (1992), respectively (the highest iron enrichment in Fig. **F26A** results from the analysis of Johnson and Dick, 1992). The calculated liquid line of de-

F25. Fo of olivine vs. An of plagioclase and Mg# of augite vs. An of plagioclase, p. 49.

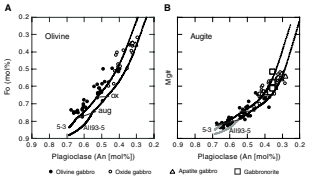

F26. Compositions of bulk gabbros compared to modeled liquid line of descent and solid fractionates, p. 50.

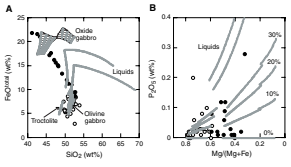

T8. Modeling of fractional crystallization, p. 76.

scent is typically tholeiitic and not very different than that suggested by Toplis and Carroll (1996) for the Skaergaard intrusion.

The average mode of the Hole 1105A olivine gabbros suggests a solid fractionate with higher plagioclase content (olivine = 11 wt%, plagioclase = 54 wt%, and augite = 35 wt%) than used in the modeling. Using such high plagioclase modes result in unrealistic fractionation paths, with Al_2O_3 being depleted from the liquid at fairly high temperatures (~1020°–1030°C) and thus the inability of plagioclase to be in equilibrium with the late-stage melts. Also the Fe-Ti oxide modes actually observed in the Hole 1105A gabbros suggest much lower contents of 0.12 ilmenite and 0.02 magnetite (maximum values). Despite this, the adopted model calculation for sample 5-3 duplicates reasonably well the observed cryptic variation (Fig. **F25**). The early income of augite suggests that few, if any, of the gabbros are troctolitic. However, it should be taken into account that the actual temperature of appearance of augite is a best estimate and need not be accurate for the particular starting composition. The actual income of Fe-Ti oxides is poorly predicted by the modeling, which suggests a later appearance of Fe-Ti oxides relative to the model assumption. Delays in Fe-Ti oxide crystallization may principally be caused by departures from the FMQ oxygen buffer toward reduced conditions (e.g., closed-system crystallization with respect to oxygen).

The crystallization modeling additionally allows the bulk solid fractionate and liquid compositions to be calculated for the chosen parental melt composition. Models for a range of trapped liquids contents (0%, 10%, 20%, and 30%) are shown in Figure **F26.** Several features can be observed:

1. Consistent with the petrographic observations, there are no troctolites among the analyzed gabbros (Fig. **F26A**).
2. There is an exceptionally good correspondence between the modeled and the observed olivine gabbro compositions.
3. The Fe-Ti oxide gabbros define a near-linear trend between evolved olivine gabbros and a group of high–Fe-Ti oxide gabbros. The latter Fe-Ti oxide gabbros are relatively similar to the modeled Fe-Ti oxide gabbros (Fig. **F26A**).
4. Both groups of gabbros contain very low amounts of trapped liquid (<5%) as inferred from the concentrations of incompatible elements like P_2O_5 (Fig. **F26B**). The exception is some Fe-Ti oxide gabbros with high P_2O_5 (<4 wt%) that indicate cumulus apatite.

Most of these observations were expected and support the fractional crystallization modeling. The strong linear variation in the Fe-Ti oxide gabbros between the two apparent end-members is not consistent with perfect fractional crystallization, which predicts trends perpendicular to the observed variation (Fig. **F26A**). It is possible, although not experimentally predicted, that the instantaneous mode of Fe-Ti oxides initially shows exponential increase. This would amount to a delay in the effects of Fe-Ti oxide fractionation on the liquid line of descent. It is perhaps equally or more likely that the strong linear trend is caused by failure to sample the pure end-member gabbros (olivine and Fe-Ti oxide gabbros) (Fig. **F26A**).

DISCUSSION

The gabbroic rocks recovered from Hole 1105A are cumulates composed of a framework of touching minerals concentrated through fractional crystallization (Irvine, 1982). The relatively unzoned nature of the cumulus phases (±5% An) (Fig. F27) and their granular interlocking textures suggest that the amount of postcumulus material is small and most of the gabbroic rocks are classified as mesocumulates, adcumulates, and poikilitic adcumulates (or heteradcumulates) (Wager et al., 1960; Irvine, 1982). The large interstitial but homogeneous clinopyroxene grains found in many of the gabbros appear to have grown in equilibrium with the coexisting, largely unzoned plagioclase and pyroxene and do not represent intercumulus crystallization. Further evidence for intercumulus crystallization, such as the appearance of low-temperature mineral phases, is also commonly lacking in the gabbros.

F27. An histograms, p. 51.

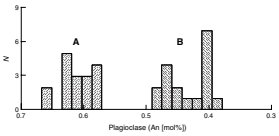

Additional support for the cumulate nature of the gabbros is provided by the modal layering (including nearly monomineralic anorthositic layers) (Fig. F4) and the occasional preferred mineral orientations or lamination defined by plagioclase laths (Fig. F3A). Layering is an integral part of most gabbroic intrusions, mainly in the form of modally graded and rhythmically repeated layers (Irvine, 1982, 1987). Rhythmic layering is synonymous with crystal fractionation and is thought to reflect mechanical and density sorting, compaction and flow, fluctuations in nucleation and growth rates, or multiple injection of melt batches (Wager and Brown, 1967; Boudreau and McBirney, 1997; McBirney and Nicolas, 1997; Irvine et al., 1998). The layering observed in the Hole 1105A gabbros, in general, is caused by size variations and to a lesser extent by modal variations. As such, this layering differs from the typical modally graded rhythmic layering in the layered series of the Skaergaard intrusion and in many other intrusions. The grain-size layering in the Hole 1105A gabbros can be attributed to fluctuations in nucleation and growth rates in a boundary layer along the margins of the chamber (cf. Bloomer et al., 1991). In many respects, the Hole 1105A style of layering may be more akin to the layering observed in the marginal border groups of the Skaergaard intrusion (Naslund, 1984; Hoover, 1989; Irvine et al., 1998). The near-cotectic mineral proportions of the shipboard-analyzed olivine gabbros indicate that these are average gabbros without little redistribution into layers (Fig. F26A). The modes of Fe-Ti oxide minerals in the Fe-Ti oxide gabbros vary from a few percent to near the inferred cotectic proportions (Fig. F26A). The reasons for this apparent variation in the proportions of the Fe-Ti oxide minerals appear most likely to record mixed sampling of the intermixed olivine and Fe Ti oxide gabbros.

The strongest support for the cumulate nature of the gabbros is provided by the whole-rock concentrations of major oxides and excluded trace elements. The high $Mg/(Mg+Fe^{total})$ ratios and low incompatible element abundances (e.g., TiO_2 and P_2O_5) in the olivine gabbros (Fig. F26B) clearly identified these as cumulates when compared to typical Atlantis II Fracture Zone basalts (Natland et al., 1991; Johnson and Dick, 1992). The low incompatible element content indicates low amounts of intercumulus material. This was also concluded by Natland et al. (1991) from a study of Hole 735B gabbros. The Fe-Ti oxide gabbros are compositionally highly variable in Fe_2O_3 and TiO_2 and have low concentrations of excluded trace elements similar to the olivine gab-

bros. The relatively high P_2O_5 in some of the analyzed Fe-Ti oxide gabbros suggests that these contain apatite cumulus minerals.

The planar fabric and deformation textures, seen in most of the Site 1105 gabbros, point toward compaction as a factor in the development of the cumulate textures (Hunter, 1996). The effects of load on a crystal mush zone is to compact, reorganize, deform, and recrystallize the solid framework and to move the interstitial liquid upward toward lower pressure regimes (Irvine, 1980; Hunter, 1996). The amount of liquid in a crystal mush depends on many factors, including accumulation, solidification processes, and cooling rates (Sparks et al., 1985). The residual porosity of the cumulates may be estimated to be >20% from the porosity of the olivine gabbros (<5%) and the average amount of Fe-Ti oxide gabbros (~22%) in the core, assuming that the Fe-Ti oxide gabbro component represents redistributed and segregated residual liquid. The results from the lower part of Hole 735B (Dick et al., 2000) show that the amount of Fe-Ti oxides decreases significantly in the lower parts of the cores to a few percent. More than 20% trapped liquid near the top of a compacting crystal mush appears reasonable and is certainly much less than a plausible maximum attainable initial porosity (Wager and Brown, 1967; Irvine, 1980; Shirley, 1986).

It is significant that the olivine gabbros at Site 1105 suggest an extent of solidification approximately similar to the middle part of the lower zone (LZb) of the Skaergaard intrusion (35%–50%, depending on the trapped liquid). Despite this, the LZb of the Skaergaard reflects a much higher extent of compaction (5%–10% trapped liquid), although both cumulate packages predict the presence of comparable thick masses of cumulates and a magma reservoir amounting to a total of at least 50% by volume. The reasons for the preservation of a zone with high porosity and high trapped liquid in the upper parts of Sites 1105 and 735 gabbros may be a sudden uplift and removal of the residual liquid from the chamber, thus effectively terminating melt migration and trapping the residual liquid in the crystal mush (Thy and Dilek, 2000). Such removal may be caused by tectonic uplift and melt extraction, possibly by injection into a subaxial dike and sill system. It is possible that the trapped liquid distribution in the Site 1105 gabbros represents a "fossil" compaction profile in an interrupted or decapitated magma chamber.

Cooling and crystallization of the cumulate pile during liquid migration and final compaction will change the stable assemblage and eventually saturate the migrating liquid first in Fe-Ti oxide minerals (~1100°C) and subsequently in apatite (~1030°C). Continued flux through the same vertical or lateral channels may result in Fe-Ti oxide and silicate proportions that greatly differ from the cotectic proportions, leaving behind a trail of "second" cumulus zones either intermingled with the host or as narrow bands and networks. Although the gabbros from Hole 1105A do not allow cumulus zone divisions to be defined, crystallization orders of the mineral phases and the petrogenesis of the rocks can still be inferred from careful petrographic observations. Troctolitic gabbros were recovered from Hole 735B as bands in the most primitive gabbros (Dick et al., 1991a, 1992, 2000; Bloomer et al., 1991). This is an indication that the primitive liquids for Hole 735B were saturated, or nearly saturated, with respect to olivine and plagioclase. The dominant lithology of Hole 1105A indicates mutual equilibrium of olivine, plagioclase, and augite cumulus phases. Fe-Ti oxide minerals are present additionally in many gabbros and show that these minerals appear next in the crystallization order. Orthopyroxene (or perhaps inverted pigeonite) cumulus grains occur additionally in a few examined

gabbros together with Fe-Ti oxides and suggest that this mineral appears after the Fe-Ti oxides in the crystallization order. The Fe-Ti oxide minerals are dominantly ilmenite, but magnetite also appears in significant amounts in textures, suggesting that both of these phases are primary in origin. Apatite is present in considerable amounts in some Fe-Ti oxide- and orthopyroxene-bearing gabbros. Finally, biotite is present in the most evolved gabbros together with apatite and Fe-Ti oxides. Thus, the petrographic information suggests the following crystallization order: olivine, plagioclase, clinopyroxene; ilmenite, magnetite; orthopyroxene; apatite; biotite. The results from the deepening of Hole 735B to ~1500 mbsf (Dick et al., 2000) do not suggest the presence of more primitive plutonic rocks below the deepest level of penetration of Hole 1105A (troctolites, dunites, and anorthosites). The petrographic observations further suggest that a gap may exist in olivine crystallization with the appearance of orthopyroxene as indicated by a decrease in abundance or the lack of olivine in gabbros that contain orthopyroxene. Regardless, this inferred crystallization order, in general, is similar to the crystallization order (or zone divisions) seen in the Skaergaard intrusion, as well as that predicted from low-pressure anhydrous experimental work on tholeiitic basalts. This was also pointed out by Meyer et al. (1989) in a study of dredge samples from the Southwest Indian Ridge (54°S–7°16′E). The complication, however, is that the rocks did not accumulate or accrete to the walls of the chamber in a systematic fashion that allows easy identification of cumulus zones, the volume relations, and the extent of fractionation. Therefore, we are unable to relate the magmatic evolution to any simple stratigraphic and volumetric scale as can be done to a certain extent for the Skaergaard intrusion (Wager, 1960).

The compositional variation in coexisting plagioclase, olivine, and augite can be relatively well duplicated by the modeling of perfect fractional crystallization (Figs. **F26, F28**). The small compositional differences between the gabbros from Holes 735B and 1105A can easily be accounted for by small differences in the parental melt compositions, such as $Fe/(Mg+Fe^{total})$ ratios and Na_2O contents. The strong effect of the parental melt is particularly well illustrated by differences in cumulus plagioclase compositions seen between the Atlantis II gabbros (Holes 735B and 1105A) and the Skaergaard intrusion (Fig. **F28**). Despite the success in modeling the composition of the coexisting minerals, the actual income or zone boundaries for cumulus augite and Fe-Ti oxides are less perfectly predicted by the modeling (Fig. **F26**). This is probably understandable, considering the uncertainty in predicting the parental melt, as well as the actual crystallization temperatures, for major cumulus phases without direct experimental confirmation.

The cryptic variation in the Hole 1105A gabbros shows as a function of depth several features at odds with observations from Hole 735B (Ozawa et al., 1991; Bloomer et al., 1991; Natland et al., 1991; Hébert et al., 1991; Thy and Dilek, 2000). The olivine gabbros from Hole 735B record several small reversals to relatively more primitive compositions that may reflect relatively abrupt replenishment and mixing of the residual magma with more primitive magma similar in appearance to many layered continental and ophiolitic complexes (Jackson, 1961; Irvine, 1980; Wilson and Larsen, 1985; Thy et al., 1989). The present results from Hole 1105A suggest a somehow different pattern in the cryptic variation (Figs. **F23, F24**) and at a much smaller scale than that for Hole 735B. The olivine gabbros appear to define several symmetric and convexly zoned gabbro lenses in thicknesses from 40 to 60 m that

F28. Compositional variation of coexisting plagioclase, olivine, and augite, p. 52.

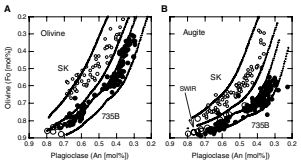

may signify much slower chamber filling than for the Hole 735B gabbros. The pattern in the cryptic variation for Hole 1105A is relatively similar to that seen for the upper gabbros of the Troodos ophiolite (Thy et al., 1989). Such large-scale repeated variations in cumulus compositions can be used to impose limitations on chamber height (Browning, 1984). Indications from the Semail ophiolite suggest maximum chamber height of a few hundred meters (Browning, 1984; MacLeod and Yaouancq, 2000). Similar estimates for the Hole 1105A gabbros suggest chamber heights in the same range as those inferred for the Semail ophiolite (100–150 m). This is in contrast to estimates for the Hole 735B gabbros, which predict chamber heights easily approaching 1000 m or more. The cryptic variation in the Hole 1105A gabbros returns to approximately similar compositions after each cycle, showing little depth dependence. This may be seen as an indication that the gabbro cumulate sections were emplaced through a same size-limited magma lens at an active spreading center (Quick and Denlinger, 1993; Phipps Morgan et al., 1994). These observations are interesting because they imply that the gabbros associated with the ultraslow-spreading Southwest Indian Ridge show many features in common with gabbros from the fast-spreading Semail ophiolite.

The Fe-Ti oxide gabbros of Hole 1105A show cryptic variations as a function of depth that are independent of the host olivine gabbros (Figs. **F23, F24**). All silicate cumulus phases show systematic upward variations toward more evolved compositions and follow normal fractionation trends that lack the characteristic convex cryptic variation seen for the olivine gabbros. The cryptic variation in the Hole 735B Fe-Ti oxide gabbros shows irregular downward repeated trends toward evolved compositions (Ozawa et al., 1991; Thy and Dilek, 2000). These individual trends are the reverse of the normal fractionation trend seen in the host olivine gabbro cumulates. Ozawa et al. (1991) identified three cycles in the Fe-Ti oxide gabbros, each showing downward increasing fractionation. The Hole 1105A Fe-Ti gabbros are dominated by normal fractionation trends, whereas the Hole 735B Fe-Ti oxide gabbros are dominated by punctuated and repeated reversed fractionation trends. The results show that the cryptic variation in Hole 1105A systematically differs from that seen in Hole 735B. Thus, perhaps contrary to expectations, lithostratigraphic correlation between the two closely located holes is not possible based on the present information.

Despite the differences, the observations from Hole 1105A reinforce the conclusions from Hole 735B (Dick et al., 1991a) that the interstitial liquid, now represented by the Fe-Ti oxide gabbros, evolved independently of the host partially molten olivine gabbros. Flow distance and efficiency of fractionation of the interstitial trapped melt controlled differentiation of the migrating liquid, as measured in the mineralogy and compositions of the constituent minerals. Dick et al. (1991a, 1992), based on observations from the Hole 735B, suggested that partially molten gabbro bodies were affected by syntectonic compaction and ductile deformation during cooling, causing interstitial melt to migrate toward areas of pressure release. The irregular and punctuated pattern seen for the Hole 735B Fe-Ti oxide gabbros supports the suggestion of Dick et al. (1991a) that syntectonic processes in part controlled solidification. The interaction of ductile deformation bands with the partially consolidated crystal mush may be responsible for the localized reversed fractionation trends repeatedly seen in Hole 735B (Ozawa et al., 1991). The implications from Hole 1105A are that the trapped melt in the crystal mush experienced a significant component of upward migration,

transgressing compositional boundaries in host olivine gabbro cells, and is reminiscent of compaction and upward migration prior to final solidification of the interstitial melt. There is no strong indication for ductile deformation and melt migration into deformation zones for the Hole 1105A gabbros.

CONCLUSIONS

The principal conclusions based on a petrographic investigation of the Hole 1105A gabbros largely confirm the conclusions from Hole 735B (Dick et al., 1991a; Natland et al., 1991). The suggestion is that the gabbros represent crystal mush originated in a subaxial chamber. Compaction and upward melt migration in the crystal mush was terminated with relatively large amounts of interstitial liquid remaining. Cooling of the trapped melt in the mush formed differentiated bodies and lenses by migration and crystallization along syntectonic channels induced by unroofing and pressure release deformation. This resulted in differentiation products along lateral and vertical channelways in the host gabbro that vary from olivine gabbro, to Fe-Ti oxide gabbro, gabbronorite, and apatite gabbros and show large compositional variations independent of the host olivine gabbros. Although the results from Hole 1105A imply strong similarities with the gabbros from Hole 735B, any direct correlation between the two nearby holes utilizing petrographic criteria is not possible.

ACKNOWLEDGMENTS

This work was supported by grants from the JOI/US Science Advisory Committee for participation in ODP Legs 179 (Hammer Drilling and NERO). The manuscript benefited from helpful reviews by Y. Niu and an anonymous reviewer. The Scientific Shipboard Party petrologists J.F. Casey, D.J. Miller, Z.P. Guo, D.G. Rao, and T. Shibata to a large extent collected the basic data on which this paper is based and provided much stimulating shipboard discussions.

This research used samples and data provided by the Ocean Drilling Program (ODP). The ODP is sponsored by the U.S. National Science Foundation (NSF) and participating countries under management of Joint Oceanographic Institutions (JOI), Inc.

REFERENCES

Andersen, D.J., and Lindsley, D.H., 1988. Internally consistent solution models for Fe-Mg-Mn-Ti oxides: Fe-Ti oxides. *Am. Mineral.,* 73:714–726.

Bloomer, S.H., Meyer, P.S., Dick, H.J.B., Ozawa, K., and Natland, J.H., 1991. Textural and mineralogic variations in gabbroic rocks from Hole 735B. *In* Von Herzen, R.P., Robinson, P.T., et al., *Proc. ODP, Sci. Results,* 118: College Station, TX (Ocean Drilling Program), 21–39.

Bloomer, S.H., Natland, J.H., and Fisher, R.L., 1989. Mineral relationships in gabbroic rocks from fracture zones of Indian Ocean ridges: evidence for extensive fractionation, parental diversity, and boundary-layer recrystallization. *In* Saunders, A.D., and Norry, M.J. (Eds.), *Magmatism in the Oceanic Basins.* Spec. Publ.—Geol. Soc. London, 42:107–124.

Boudreau, A.E., and McBirney, A.R., 1997. The Skaergaard layered series, Part III. Nondynamic layering. *J. Petrol.,* 38:1003–1020.

Brooks, C.K., and Nielsen, T.F.D., 1990. A discussion of Hunter and Sparks (Contrib Mineral Petrol 95:451–461). *Contrib. Mineral. Petrol.,* 104:235–247.

Browning, P., 1984. Cryptic variation within the cumulate sequence of the Oman ophiolite: magma chamber depth and petrological implications. *In* Gass, I.G., Lippard, S.J., and Shelton, A.W. (Eds.), *Ophiolites and Oceanic Lithosphere.* Spec. Publ.—Geol. Soc. London, 13:71–82.

Buddington, A.F., and Lindsley, D.H., 1964. Iron-titanium oxide minerals and synthetic equivalents. *J. Petrol.,* 5:310–357.

Dick, H.J.B., Meyer, P.S., Bloomer, S., Kirby, S., Stakes, D., and Mawer, C., 1991a. Lithostratigraphic evolution of an in-situ section of oceanic Layer 3. *In* Von Herzen, R.P., Robinson, P.T., et al., *Proc. ODP, Sci. Results,* 118: College Station, TX (Ocean Drilling Program), 439–538.

Dick, H.J.B., Natland, J.H., Alt, J.C., Bach, W., Bideau, D., Gee, J.S., Haggas, S., Hertogen, J.G.H., Hirth, G., Holm, P.M., Ildefonse, B., Iturrino, G.J., John, B.E., Kelley, D.S., Kikawa, E., Kingdon, A., LeRoux, P.J., Maeda, J., Meyer, P.S., Miller, D.J., Naslund, H.R., Niu, Y., Robinson, P.T., Snow, J., Stephen, R.A., Trimby, P.W., Worm, H.-U., and Yoshinobu, A., 2000. A long in situ section of the lower ocean crust: results of ODP Leg 176 drilling at the Southwest Indian Ridge. *Earth Planet. Sci. Lett.,* 179:31–51.

Dick, H.J.B., Natland, J.H., Miller, D.J., et al., 1999. *Proc. ODP, Init. Repts.,*176 [CD-ROM]. Available from: Ocean Drilling Program, Texas A&M University, College Station, TX 77845-9547, U.S.A.

Dick, H.J.B., Robinson, P.T., and Meyer, P.S., 1992. The plutonic foundation of a slow-spreading ridge. *In* Duncan, R., Rea, D., Kidd, R., von Rad, U., and Weissel, J. (Eds.), *Synthesis of Results from Scientific Drilling in the Indian Ocean.* Geophys. Monogr., Am. Geophys. Union, 70:1–39.

Dick, H.J.B., Schouten, H., Meyer, P.S., Gallo, D.G., Bergh, H., Tyce, R., Patriat, P., Johnson, K.T.M., Snow, J., and Fisher, A., 1991b. Tectonic evolution of the Atlantis II Fracture Zone. *In* Von Herzen, R.P., Robinson, P.T., et al., *Proc. ODP, Sci. Results,* 118: College Station, TX (Ocean Drilling Program), 359–398.

Hébert, R., Constantin, M., and Robinson, P.T., 1991. Primary mineralogy of Leg 118 gabbroic rocks and their place in the spectrum of oceanic mafic igneous rocks. *In* Von Herzen, R.P., Robinson, P.T., et al., *Proc. ODP, Sci. Results,* 118: College Station, TX (Ocean Drilling Program), 3–20.

Hoover, J.D., 1989. Petrology of the marginal border series of the Skaergaard intrusion. *J. Petrol.,* 30:399–439.

Hunter, R.H., 1996. Texture development in cumulate rocks. *In* Cawthorn, R.G. (Ed.), *Layered Intrusions:* Amsterdam (Elsevier), 77–101.

Irvine, T.N., 1980. Magmatic infiltration metasomatism, double-diffusive fractional crystallization, and adcumulus growth in the Muskox intrusion and other layered

intrusions. *In* Hargraves, R.B. (Ed.), *Physics of Magmatic Processes:* Princeton, NJ (Princeton Univ. Press), 325–384.

————, 1982. Terminology for layered intrusions. *J. Petrol.,* 23:127–162.

————, 1987. Layering and related structures in the Duke Island and Skaergaard intrusions: similarities, differences, and origins. *In* Parsons, I. (Ed.), *Origins of Igneous Layering:* Dordrecht (Reidel), 185–245.

Irvine, T.N., Andersen, J.C.O., and Brooks, C.K., 1998. Included blocks (and blocks within blocks) in the Skaergaard intrusion: geological relations and the origins of rhythmic modally graded layers. *Geol. Soc. Am. Bull.,* 110:1398–1447.

Jackson, E.D., 1961. Primary textures and mineral associations in the ultramafic zone of the Stillwater complex, Montana. *Geol. Surv. Prof. Pap. U.S.,* 358.

Johnson, K.T.M., and Dick, H.J.B., 1992. Open system melting and temporal and spatial variation of peridotite and basalt at the Atlantis II Fracture Zone. *J. Geophys. Res.,* 97:9219–9241.

Kilinc, A., Carmichael, I.S.E., Rivers, M.L., and Sack, R.O., 1983. The ferric-ferrous ratio of natural silicate liquids equilibrated in air. *Contrib. Mineral. Petrol.,* 83:136–140.

Le Maitre, R.W., 1989. *A Classification of Igneous Rocks and Glossary of Terms:* Oxford (IUGS, Blackwell).

Lindsley, D.H., 1983. Pyroxene thermometry. *Am. Mineral.,* 68:477–493.

Lindsley, D.H., and Andersen, D.J., 1983. A two-pyroxene thermometer. *J. Geophys. Res.,* 88 (Suppl.): A887–A906.

Maaløe, S., 1976. The zoned plagioclase of the Skaergaard intrusion, East Greenland. *J. Petrol.,* 17:398–419.

MacLeod, C.J., and Yaouancq, G., 2000. A fossil melt lens in the Oman ophiolite: implications for magma chamber processes at fast spreading ridges. *Earth Planet. Sci. Lett.* 176:357–373.

Mahoney, J.J., Natland, J.H., White, W.M., Poreda, R., Bloomer, S.H., Fisher, R.L., and Baxter, A.N., 1989. Isotopic and geochemical provinces of the western Indian Ocean spreading centers. *J. Geophys. Res.,* 94:4033–4052.

McBirney, A.R., 1989. The Skaergaard layered series, I. Structure and average compositions. *J. Petrol.,* 30:363–397.

McBirney, A.R., and Nicolas, A., 1997. The Skaergaard layered series, Part II. Magmatic flow and dynamic layering. *J. Petrol.,* 38:569–580.

Meyer, P.S., Dick, H.J.B., and Thompson, G., 1989. Cumulate gabbros from the Southwest Indian Ridge, 54°S–7°16′E: implications for magmatic processes at a slow spreading ridge. *Contrib. Mineral. Petrol.,* 103:44–63.

Muller, M.R., Robinson, C.J., Minshull, T.A., White, R.S., and Bickle, M.J., 1997. Thin crust beneath Ocean Drilling Program borehole 735B at the Southwest Indian Ridge? *Earth Planet. Sci. Lett.,* 148:93–107.

Naslund, H.R., 1984. Petrology of the upper border series of the Skaergaard intrusion. *J. Petrol.,* 25:185–212.

Natland, J.H., Meyer, P.S., Dick, H.J.B., and Bloomer, S.H., 1991. Magmatic oxides and sulfides in gabbroic rocks from Hole 735B and the later development of the liquid line of descent. *In* Von Herzen, R.P., Robinson, P.T., et al., *Proc. ODP, Sci. Results,* 118: College Station, TX (Ocean Drilling Program), 75–111.

Nwe, Y.Y., 1976. Electron-probe studies of the earlier pyroxenes and olivines from the Skaergaard intrusion, East Greenland. *Contrib. Mineral. Petrol.,* 55:105–126.

Ozawa, K., Meyer, P.S., and Bloomer, S.H., 1991. Mineralogy and textures of iron-titanium oxide gabbros and associated olivine gabbros from Hole 735B. *In* Von Herzen, R.P., Robinson, P.T., et al., *Proc. ODP, Sci. Results,* 118: College Station, TX (Ocean Drilling Program), 41–73.

Papike, J.J., Cameron, K.L., and Baldwin, K., 1974. Amphiboles and pyroxenes: characterization of other than quadrilateral components and estimates of ferric iron from microprobe data. *Geol. Soc. Am. Abstr. Progr.,* 6:1053–1054. (Abstract)

Pettigrew, T.L., Casey, J.F., Miller, D.J., et al., 1999. *Proc. ODP, Init. Repts.,* 179 [CD-ROM]. Available from: Ocean Drilling Program, Texas A&M University, College Station, TX 77845-9547, U.S.A.

Phipps Morgan, J., Harding, A.J., Orcutt, J., Kent, G., and Chen, Y.J., 1994. An observational and theoretical synthesis of the magma chamber geometry and of crustal genesis along a mid-ocean ridge spreading center. *In* Ryan, M.P. (Ed.), *Magmatic Systems:* San Diego (Academic Press), 139–178.

Poldervaart, A., and Hess, H.H., 1951. Pyroxenes in the crystallization of basaltic magma. *J. Geol.,* 59:472–489.

Quick, J.E., and Denlinger, R.P., 1993. Ductile deformation and the origin of layered gabbro in ophiolites. *J. Geophys. Res.,* 98:14015–14027.

Robinson, P.T., Von Herzen, R., et al., 1989. *Proc. ODP, Init. Repts.,* 118: College Station, TX (Ocean Drilling Program).

Shipboard Scientific Party, 1999. Hammer Drill Site (1104 and 1106) and Site 1105. *In* Pettigrew, T.L., Casey, J.F., Miller, D.J., et al., *Proc. ODP, Init. Repts.,* 179, 1–183 [CD-ROM]. Available from: Ocean Drilling Program, Texas A&M University, College Station, TX 77845-9547, U.S.A.

Shirley, D.N., 1986. Compaction of igneous cumulates. *J. Geol.,* 94:795–809.

Sparks, R.S.J., Huppert, H.E., Kerr, R.C., McKenzie, D.P., and Tait, S.R., 1985. Postcumulus processes in layered intrusions. *Geol. Mag.,* 122:555–568.

Stakes, D., Mével, C., Cannat, M., and Chaput, T., 1991. Metamorphic stratigraphy of Hole 735B. *In* Von Herzen, R.P., Robinson, P.T., et al., *Proc. ODP, Sci. Results,* 118: College Station, TX (Ocean Drilling Program), 153–180.

Sugawara, T., 2000. Empirical relationships between temperature, pressure, and MgO content in olivine and pyroxene saturated liquid. *J. Geophys. Res.,* 105:8457–8472.

Thy, P., and Dilek, Y., 2000. Magmatic and tectonic controls on the evolution of oceanic magma chambers at slow-spreading ridges: perspectives from ophiolitic and continental layered intrusions. *Spec. Pap.— Geol. Assoc. Am.,* 349:87–104.

Thy, P., and Lofgren, G.E., 1992. Experimental constraints on the low-pressure evolution of transitional and mildly alkalic basalts: multisaturated liquids and coexisting augites. *Contrib. Mineral. Petrol.,* 112:196–202.

————, 1994. Experimental constraints on the low-pressure evolution of transitional and mildly alkalic basalts: the effect of Fe-Ti oxide minerals and the origin of basaltic andesites. *Contrib. Mineral. Petrol.,* 116:340–351.

Thy, P., Schiffman, P., and Moores, E.M., 1989. Igneous mineral stratigraphy and chemistry of the Cyprus Crustal Study Project drill core in the plutonic sequences of the Troodos ophiolite. *In* Gibson, I.L., Malpas, J., Robinson, P.T., and Xenophontos, C. (Eds.), *Cyprus Crustal Study Project: Initial Report, Hole CY-4.* Pap.—Geol. Surv. Can., 88-9:147–185.

Toplis, M.J., and Carroll, M.R., 1995. An experimental study of the influence of oxygen fugacity on Fe-Ti oxide stability, phase relations, and mineral-melt equilibria in ferro-basaltic systems. *J. Petrol.,* 36:1137–1170.

————, 1996. Differentiation of ferro-basaltic magmas under conditions open and closed to oxygen: implications for the Skaergaard Intrusion and other natural systems. *J. Petrol.,* 37:837–858.

Wager, L.R., 1960. The major element variation of the layered series of the Skaergaard intrusion and a re-estimation of the average composition of the hidden layered series and of the successive residual magmas. *J. Petrol.,* 1:364–398.

Wager, L.R., and Brown, G.M., 1967. *Layered Igneous Rocks:* San Francisco (W.H. Freeman).

Wager, L.R., Brown, G.M., and Wadsworth, W.J., 1960. Types of igneous cumulates. *J. Petrol.,* 1:73–85.

Wilson, J.R. and Larsen, S.B., 1985. Two-dimentional study of a layered intrusion—the Hyllingen series, Norway. *Geol. Mag.,* 122:97–124.

Figure F1. A. The main tectonic features of the Southwest Indian Ocean and location of the Atlantis Fracture Zone (FZ). **B.** Atlantis Bank with locations of Holes 735B and 1105A. The bathymetry is from Dick, Natland, Miller, et al. (1999). **C.** Atlantis Fracture Zone and location of Holes 735B and 1105A (based on Dick et al., 1991b). **D.** Schematic cross section of the rift valley of the Southwest Indian Ridge parallel to the spreading direction (north-south) drawn ~20 km west of the transform (north-south). The diagram illustrates that block uplift at the ridge-transform forms a transverse ridge (Dick et al., 1991b).

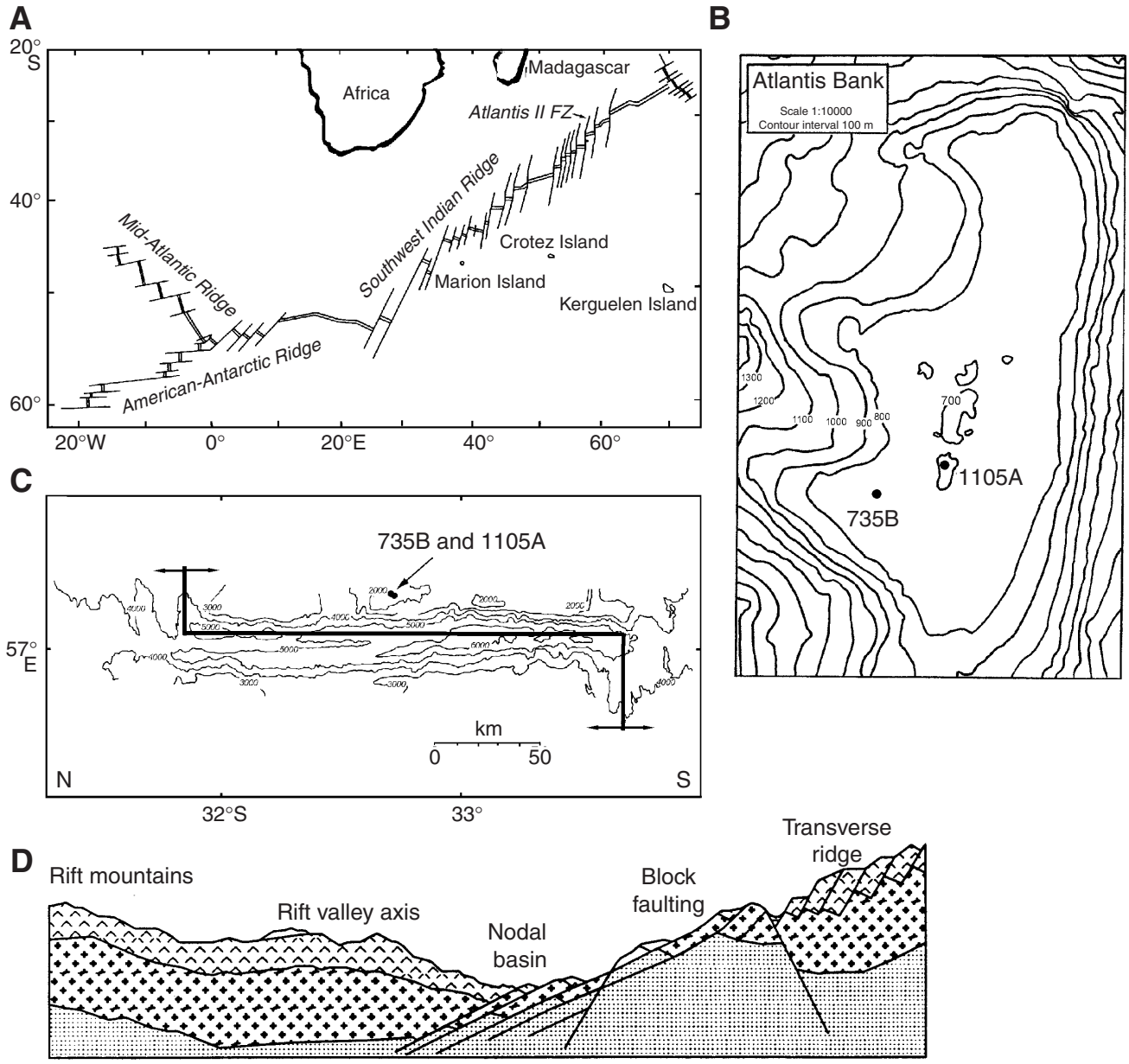

Figure F2. Summary of lithologic variation and units of Hole 1105A as defined by Shipboard Scientific Party (1999). Only the two main lithologic rock types are illustrated (cross-hatched = olivine gabbro; shaded = Fe-Ti oxide gabbro). Visual estimated downhole variation in modal mineralogy and shipboard measured magnetic susceptibility are shown. Opaques include Fe-Ti oxides and sulfides. Also shown are visual estimated downhole variation in maximum (plagioclase and pyroxene) and average gabbro grain size. The curves on the last three columns are running grain-size averages (in millimeters).

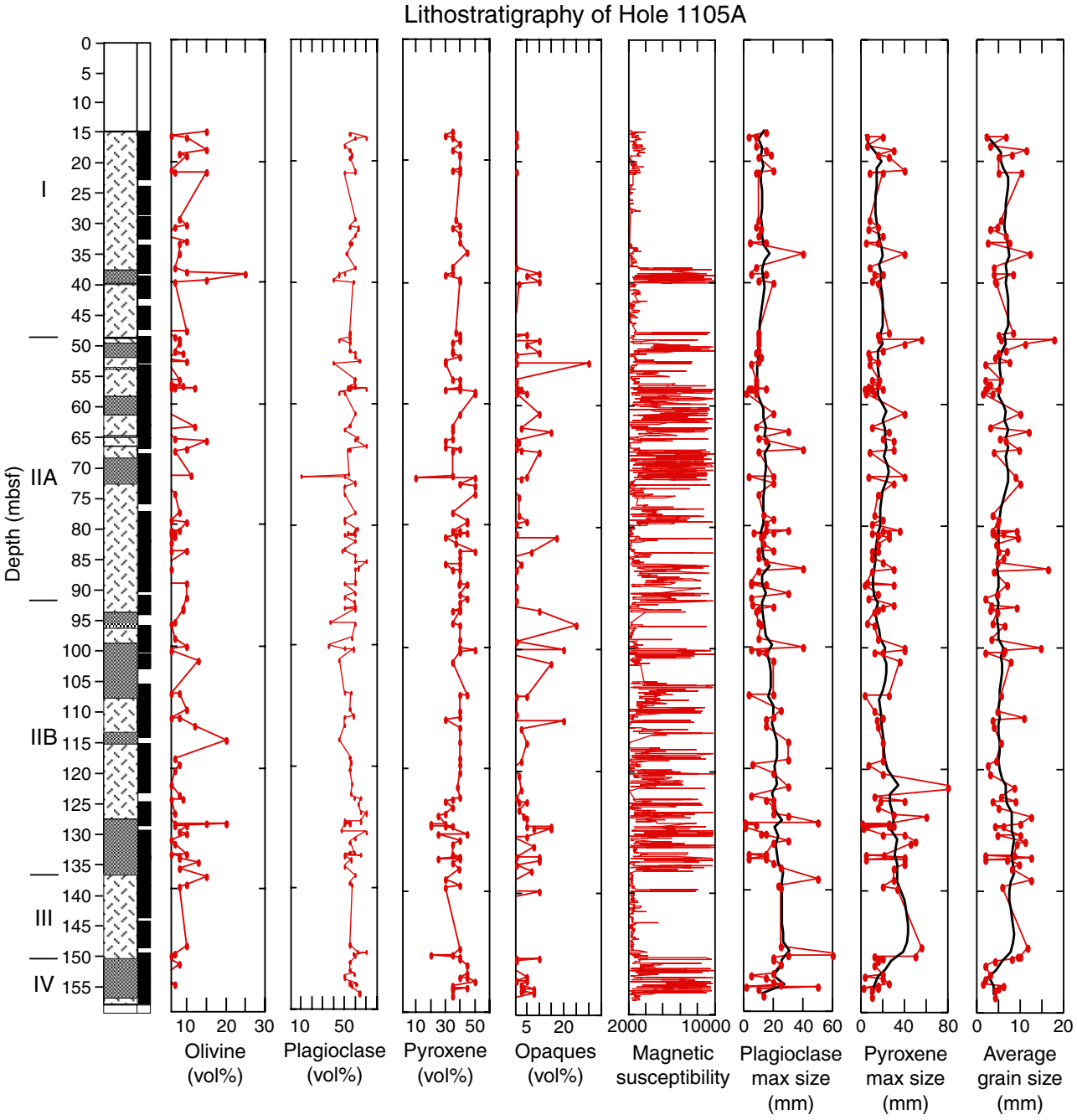

Figure F3. Photomicrographs illustrating structures of gabbros from Hole 1105A. Scale bar = 0.5 mm. **A.** Contact between fine-grained gabbro (right) and medium-grained gabbro (left) (Sample 179-1105A-13R-1, 24–26 cm). **B.** Laminated olivine gabbro (Sample 179-1105A-12R-2, 50–53 cm). **C.** Foliation in Fe-Ti oxide gabbro (Sample 179-1105A-30R-2, 109–113 cm). **D.** Plagioclase porphyroclast in a matrix of fine-grained neoblasts of mostly plagioclase in apatite Fe-Ti oxide olivine gabbro (Sample 179-1105A-5R-1, 144–147 cm). **E.** Deformation band of fine-grained neoblastic plagioclase through plagioclase grain in apatite Fe-Ti oxide olivine gabbro (Sample 179-1105A-5R-1, 115–118 cm). **F.** Kink deformation in plagioclase of relatively undeformed olivine gabbro (Sample 179-1105A-3R-1, 51–54 cm). Photomicrographs are by the Shipboard Scientific Party (1999).

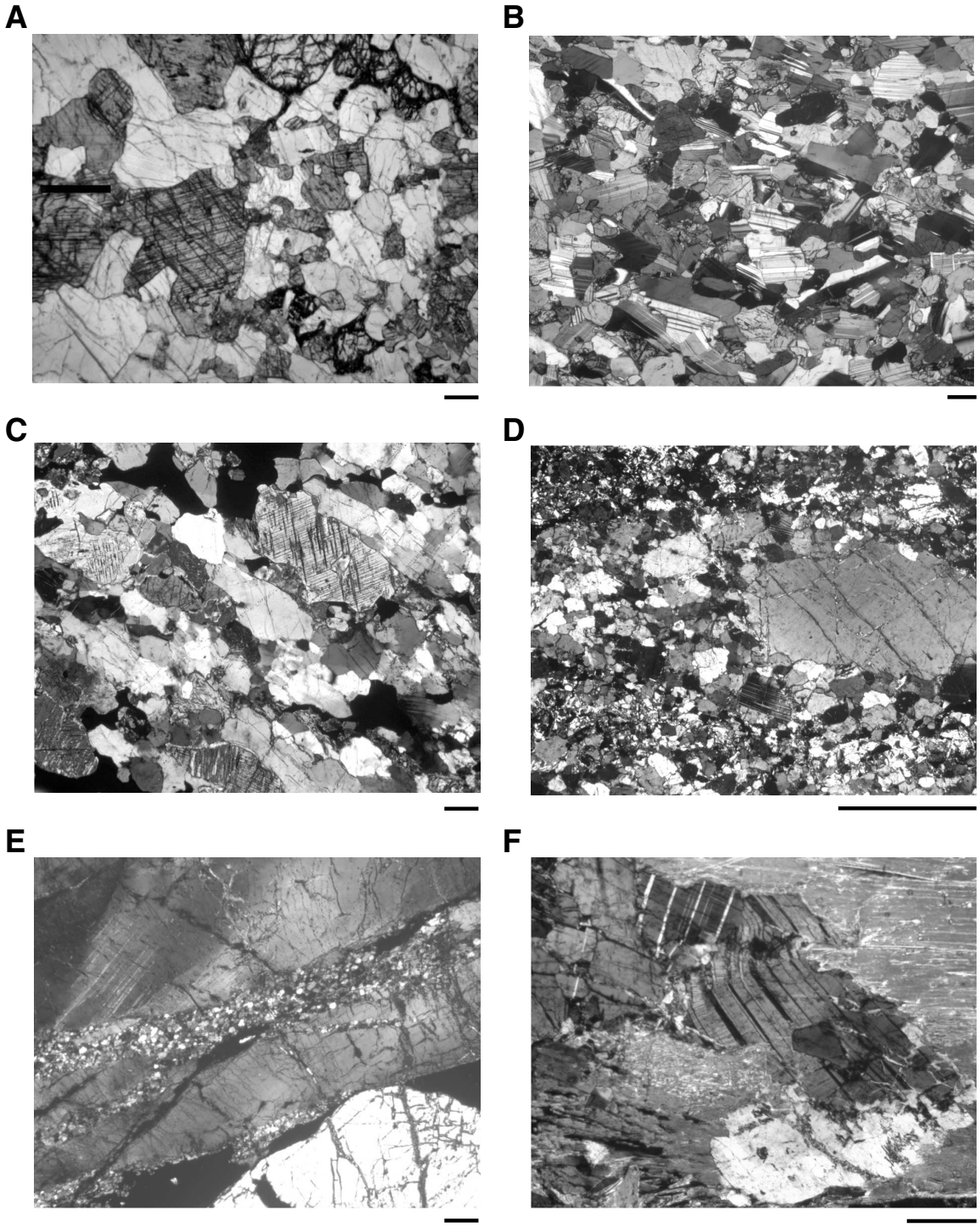

Figure F4. Modal variation in gabbros from Hole 1105A based on point counting of thin sections. **A.** Plagioclase-pyroxene-olivine (Pl-Px-Ol) relations. **B.** Plagioclase-pyroxene-Fe-Ti oxide mineral (Pl-Px-Ox) relations. Symbols are given for main petrographic groups of gabbros as discussed in text. Data are from Shipboard Scientific Party (1999).

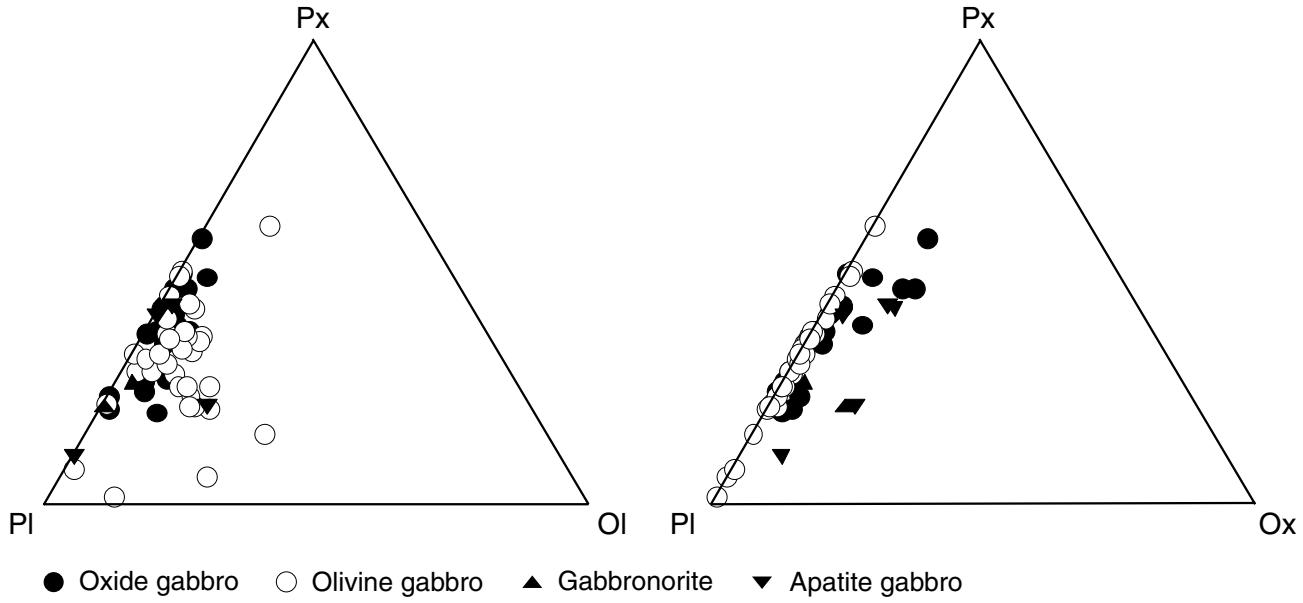

Figure F5. Photomicrographs illustrating the petrography, mineralogy, and textures of olivine gabbros from Hole 1105A. Scale bar = 0.5 mm. **A.** Typical olivine gabbro with cumulus olivine, augite, and plagioclase (Sample 179-1105A-1R-1, 88–91 cm). **B.** Large poikilitic augite with composite and resorbed plagioclase inclusions (Sample 179-1105A-21R-1, 49–52 cm). **C.** Complex zoning in plagioclase cumulus grain in laminated olivine gabbro (Sample 179-1105A-12R-2, 50–55 cm). **D.** Breakdown of primary olivine into a polyhedral aggregate of recrystallized olivine (Sample 179-1105A-10R-1, 38–42 cm). **E.** Deformation bands in olivine (Sample 179-1105A-1R-4, 137–141 cm). **F.** Replacement of primary augite by a secondary augite (Sample 179-1105A-3R-1, 51–54 cm). Photomicrographs are by the Shipboard Scientific Party (1999).

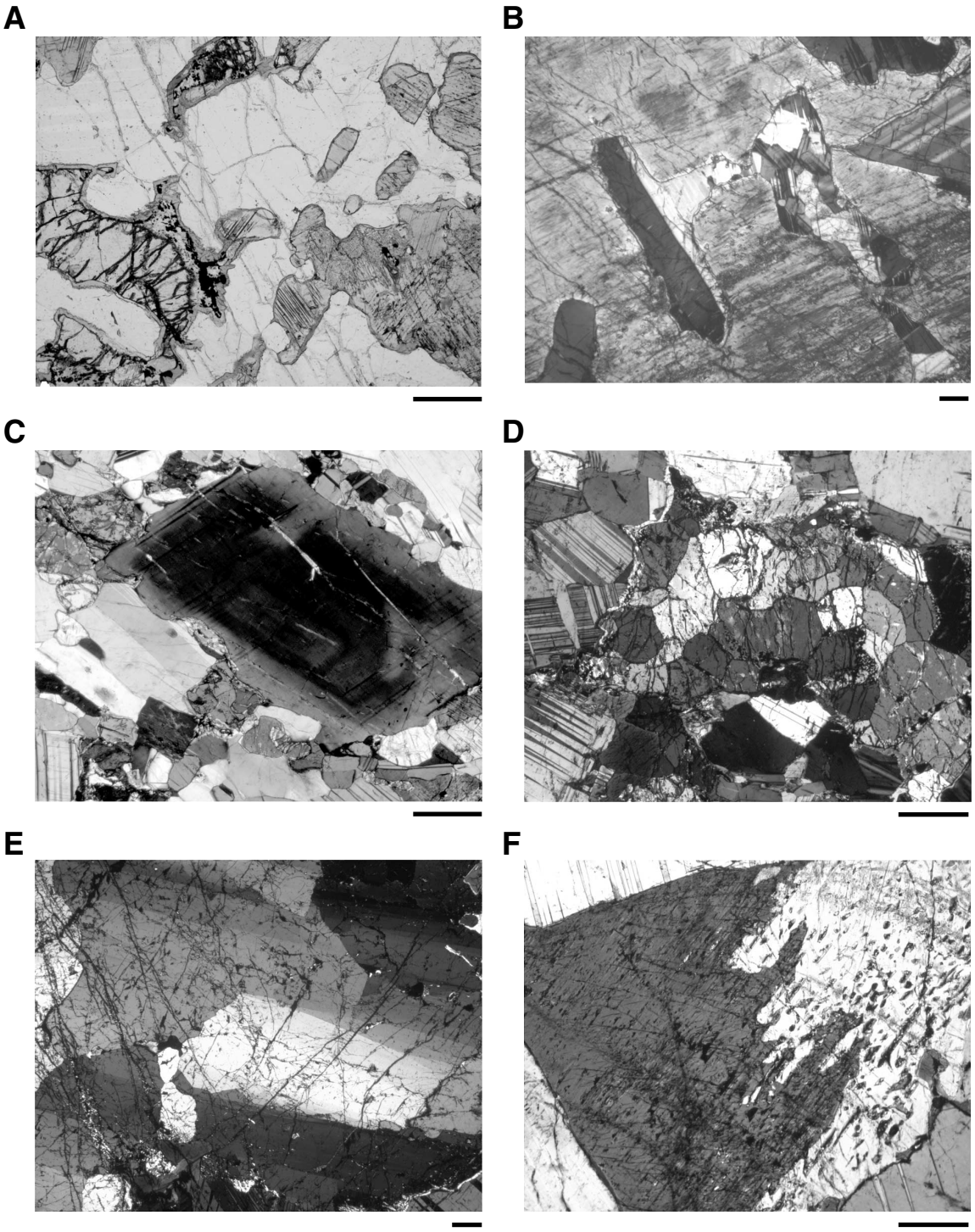

Figure F6. Anorthite mole percent content (Ca/[Ca+Na+K]) of plagioclase for the four main lithologic components. *N* = number of analyses.

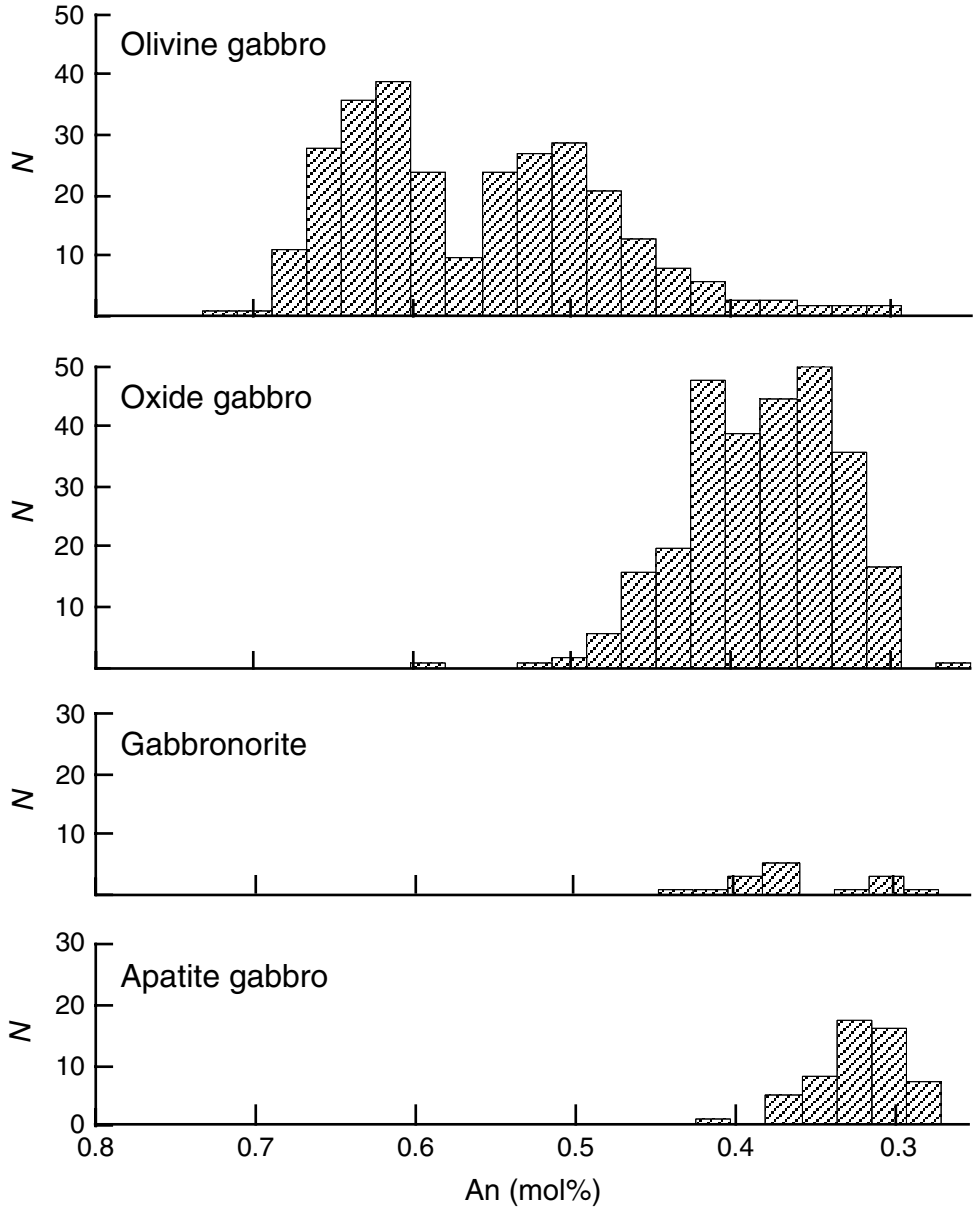

Figure F7. Forsterite mole percent content of olivine (Mg/[Mg+Fe]) for the three main lithologic components. Orthopyroxene bearing gabbros do not contain olivine. *N* = number of analyses.

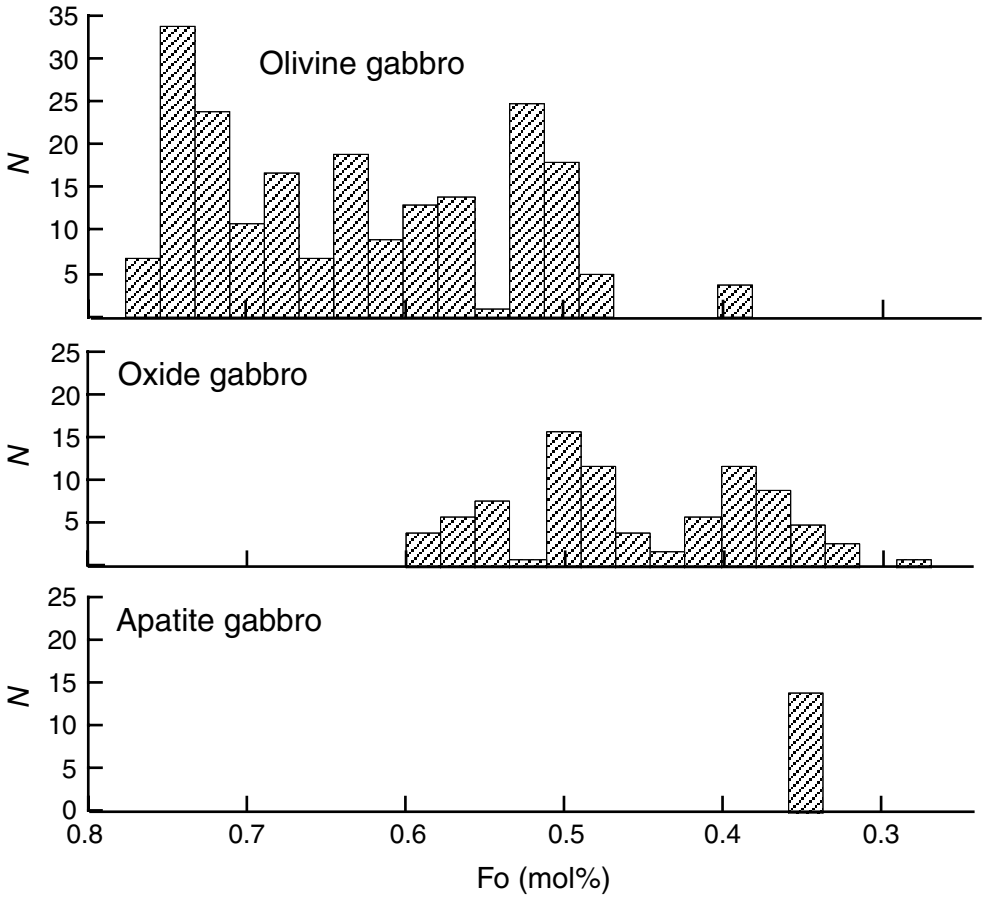

Figure F8. Mg/(Mg+Fe^{2+}) ratio of pyroxenes for the four main lithologic components. The lowermost histogram illustrates the composition of orthopyroxene in gabbronorites. Orthopyroxene is calculated with all iron as Fe^{2+}, whereas iron in augite has been redistributed between Fe^{3+} and Fe^{2+} by charge balancing the cations. *N* = number of analyses.

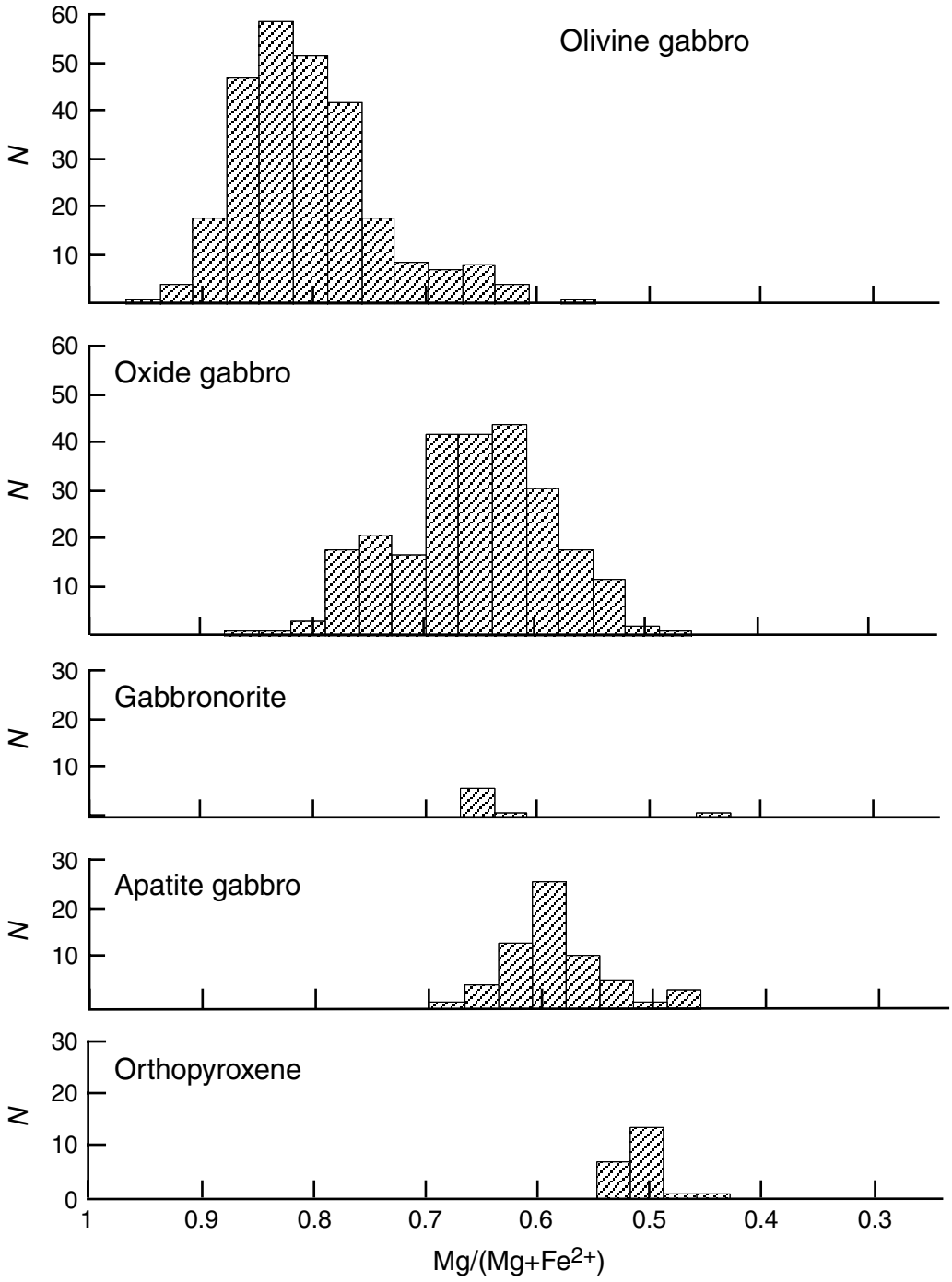

Figure F9. Photomicrographs illustrating the petrography, mineralogy, and textures of Fe-Ti oxide–bearing gabbros from Hole 1105A. Scale bar = 0.5 mm, except as noted. **A.** Interstitial ilmenite in orthopyroxene apatite Fe-Ti oxide gabbro (Sample 179-1105A-7R-3, 33–36 cm). **B.** Granular intergrowth of dominantly ilmenite and titanomagnetite (Sample 179-1105A-5R-1, 115–118 cm). Scale bar = 15 mm. **C.** Orthopyroxene intergrown with Fe-Ti oxide minerals in orthopyroxene Fe-Ti oxide gabbro (Sample 179-1105A-22R-2, 74–78 cm). **D.** Apatite in ilmenite and secondary amphibole in apatite Fe-Ti oxide gabbro (Sample 179-1105A-4R-4, 57–62 cm). Photomicrographs are by the Shipboard Scientific Party (1999).

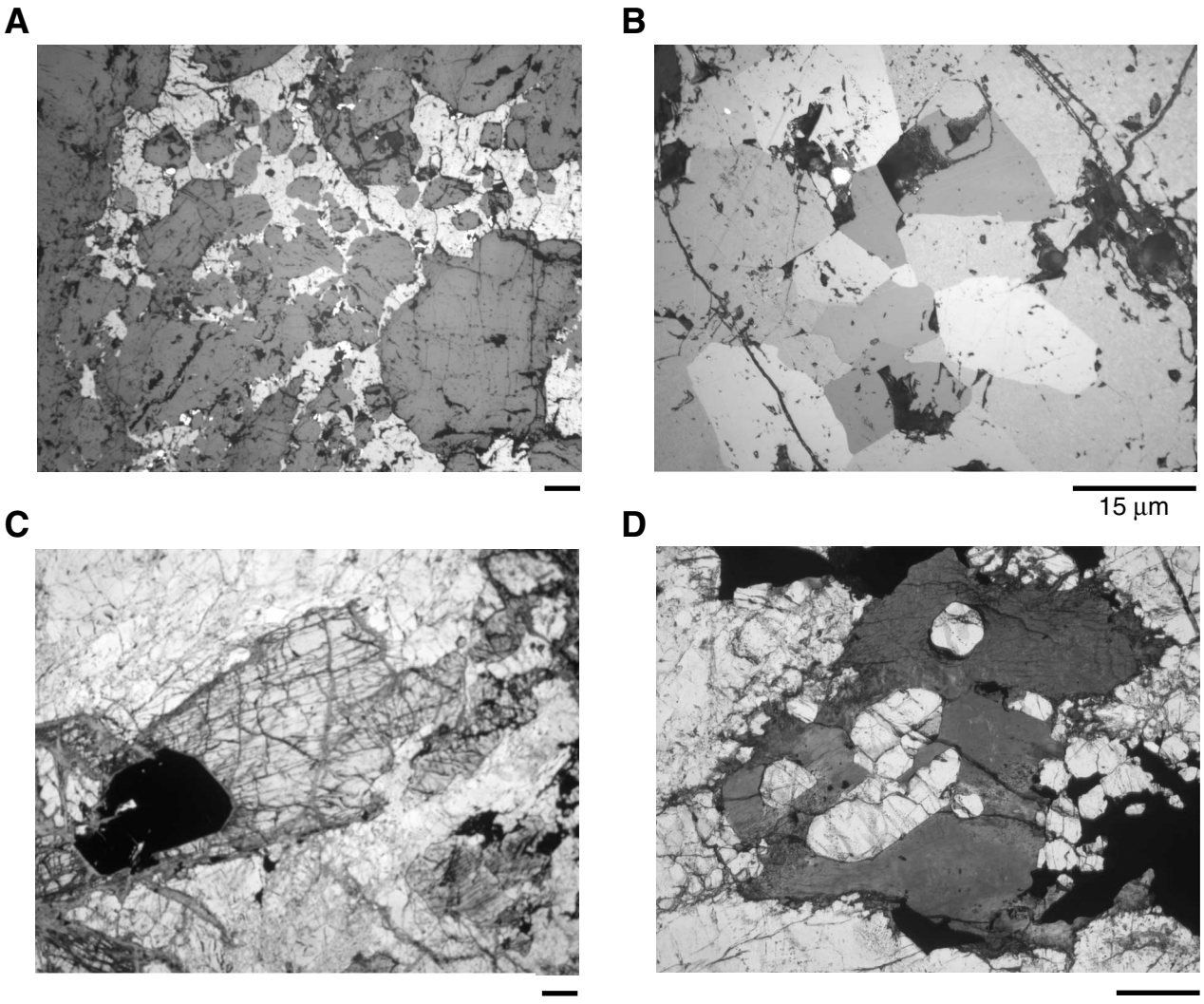

Figure F10. A. Close-up photograph of microgabbro band in medium-grained gabbro (Sample 179-1105A-16R-1, 116–132 cm). **B.** Microphotograph of the contact between medium-grained olivine gabbro and granular microgabbro (Sample 179-1105A-13R-1, 24–36 cm).

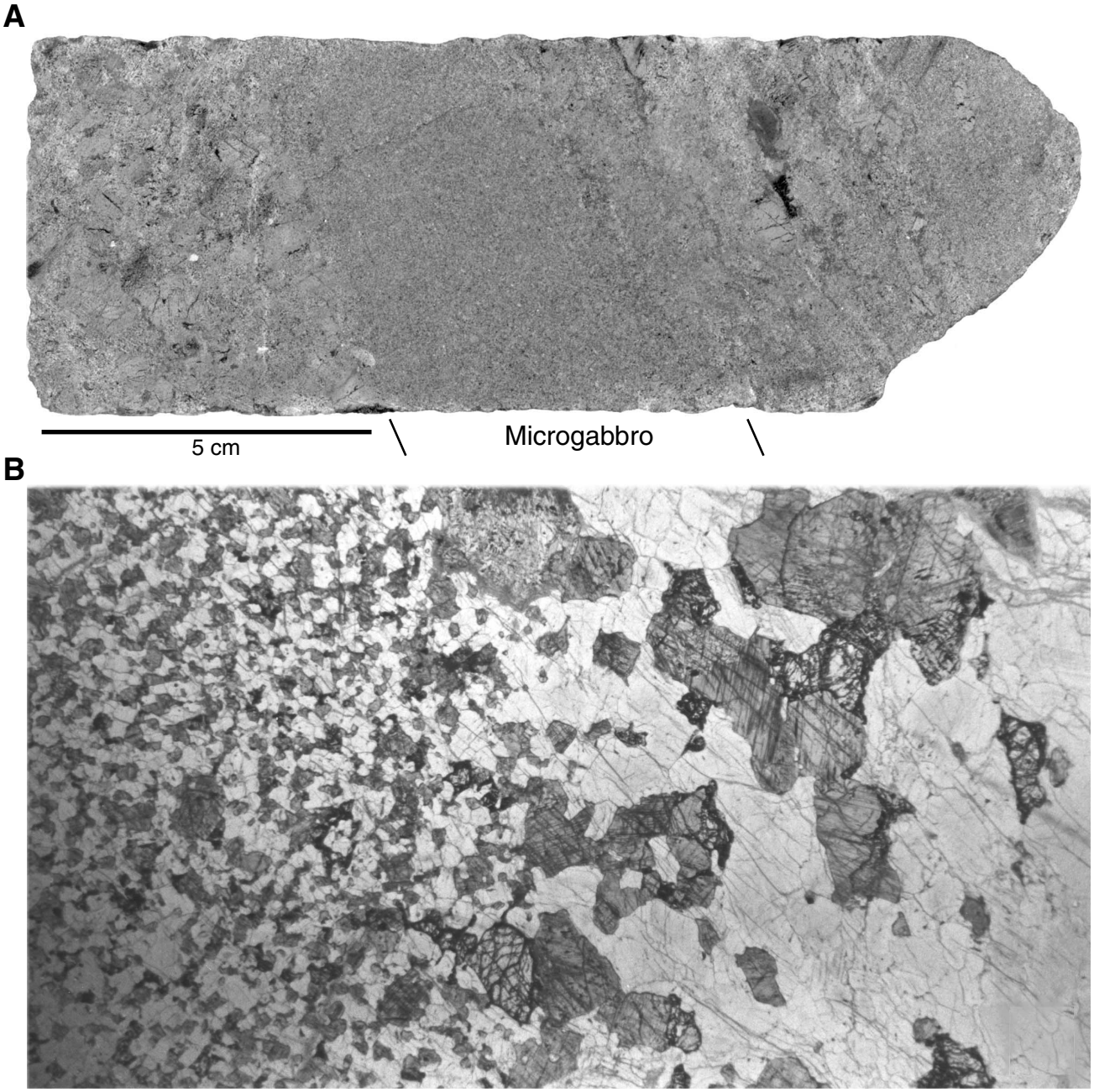

Figure F11. Orthoclase (K/[Ca+Na+K]) as a function of anorthite (Ca/[Ca+Na+K]) content of plagioclase (cation fractions). The lithologic grouping is the same as that in Figure F4, p. 28.

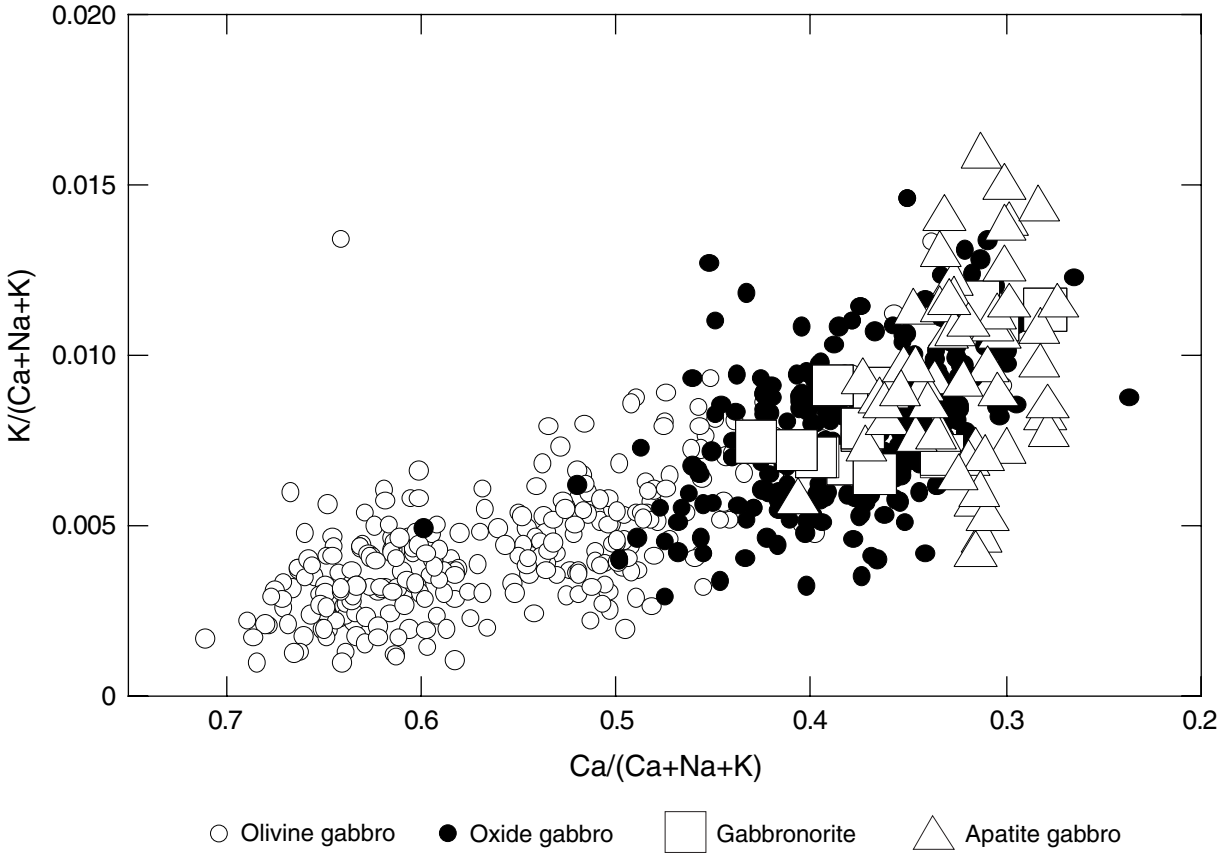

Figure F12. Manganese (cations to four oxygens) as a function of forsterite (Mg/[Mg+Fe]) content of olivine. The lithologic grouping is the same as that in Figure F4, p. 28, except that olivine is not present in gabbronorites.

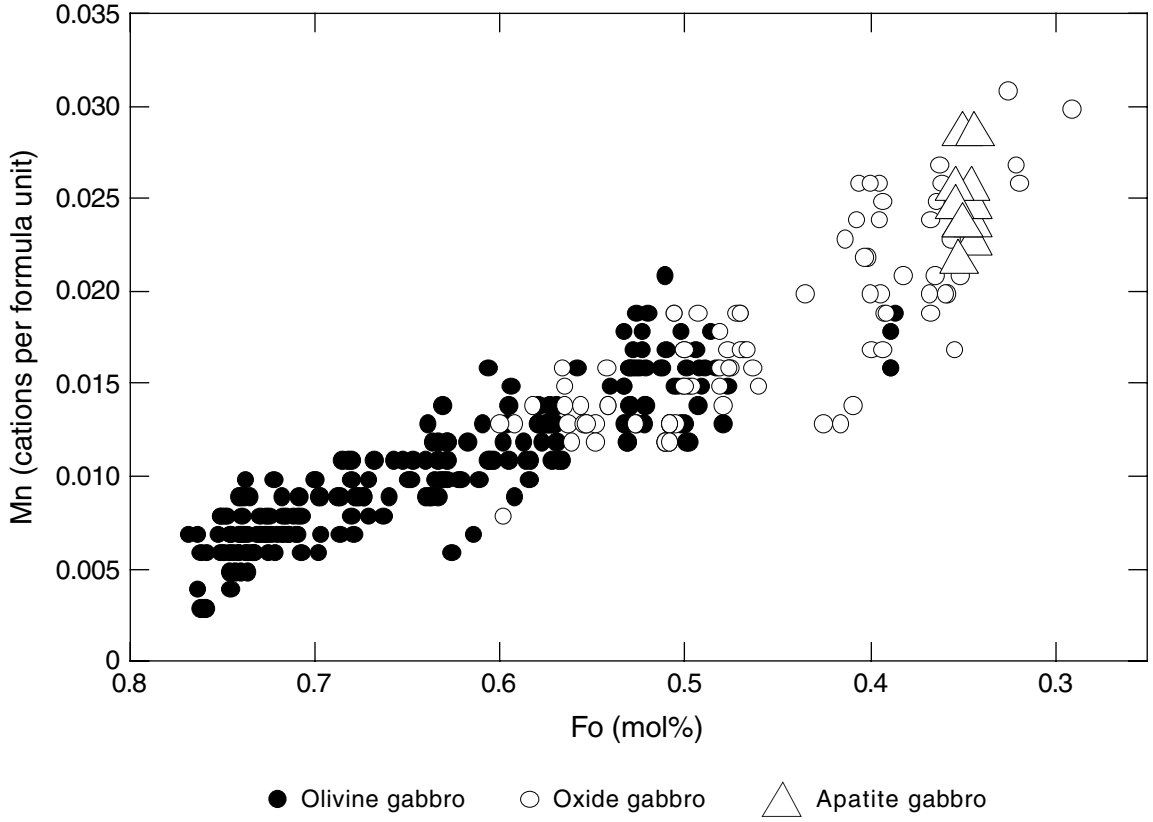

Figure F13. Quadrilateral components of pyroxenes. Fe^{2+} and Fe^{3+} are estimated from charge balancing the cations. All analyzed pyroxenes are shown. Tie-lines are shown between typical coexisting clinopyroxene and orthopyroxene (opx). Di = diopside, He = hedenbergite, En = enstatite, Fs = ferrosilite.Calculation of quadrilateral components is after Lindsley (1983). Experimental tie-lines between coexisting pyroxenes and isotherms are contoured at 100°C intervals between 700° and 1200°C after Lindsley (1983). The lithologic grouping is the same as those for previous figures.

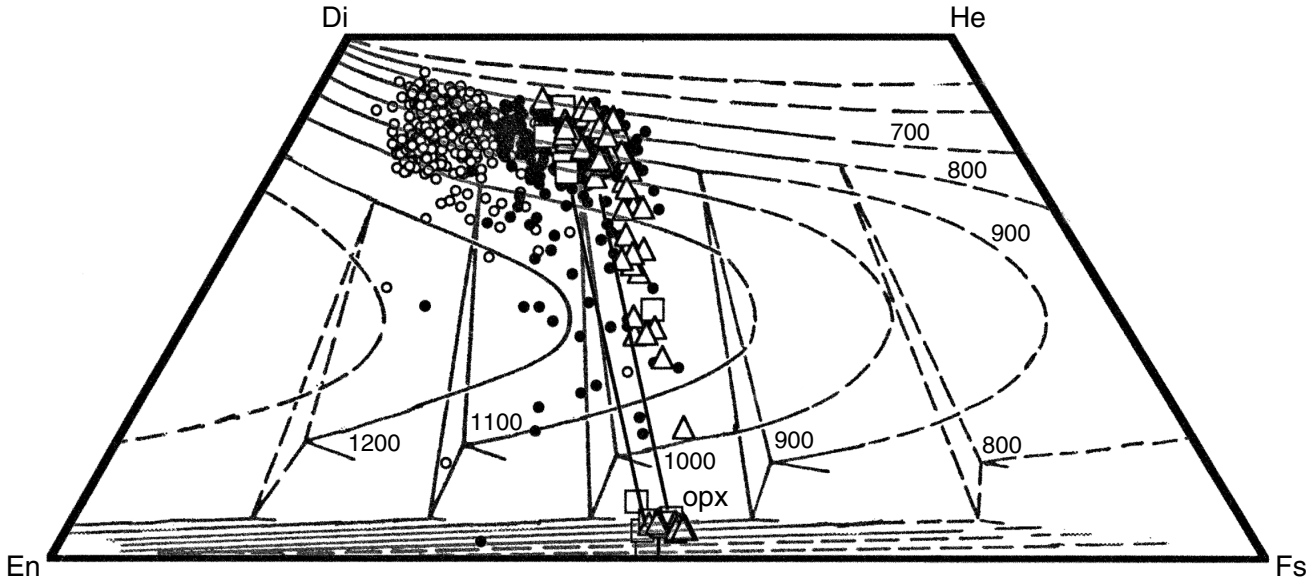

Figure F14. The minor elements Ti, Al, Mn, Na, and Cr (cations per formula unit) in clinopyroxenes as a function of $Mg/(Mg+Fe^{2+})$ with Fe^{2+} and Fe^{3+} estimated from charge balancing the cations. Pyroxenes with <10 wt% CaO are not included. opx = orthopyroxene. The lithologic grouping is the same as those for previous figures.

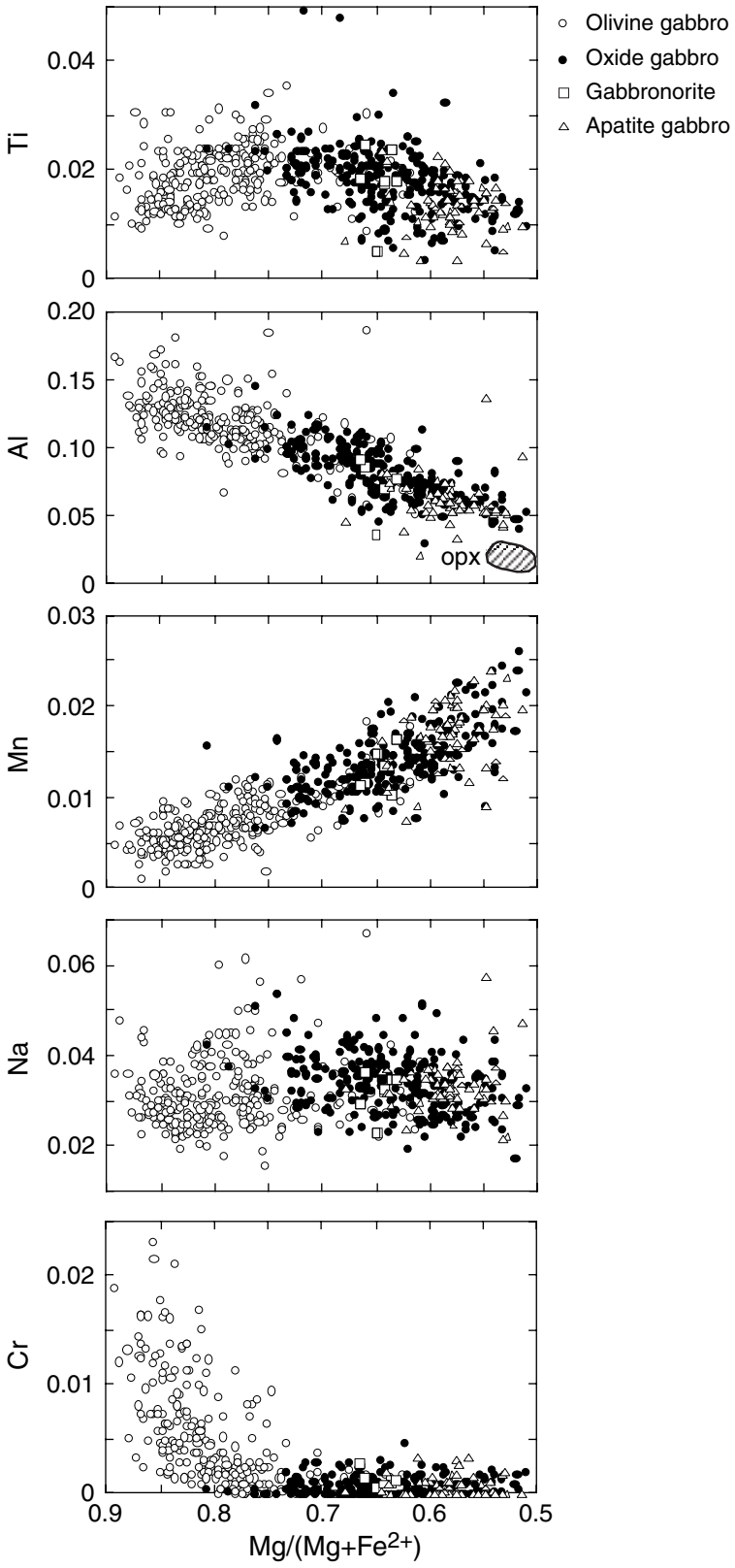

Figure F15. The Ti and Al relations (cations per formula unit) in clinopyroxenes. Ti vs. total Al contents; Ti/Al vs. Mg/(Mg+Fe^{2+}) ratios; Ti vs. Al^{IV} contents. Fe^{2+} was estimated from charge balancing the cations. The groups of gabbros are as for previous figures. Pyroxenes with <10 wt% CaO are not included.

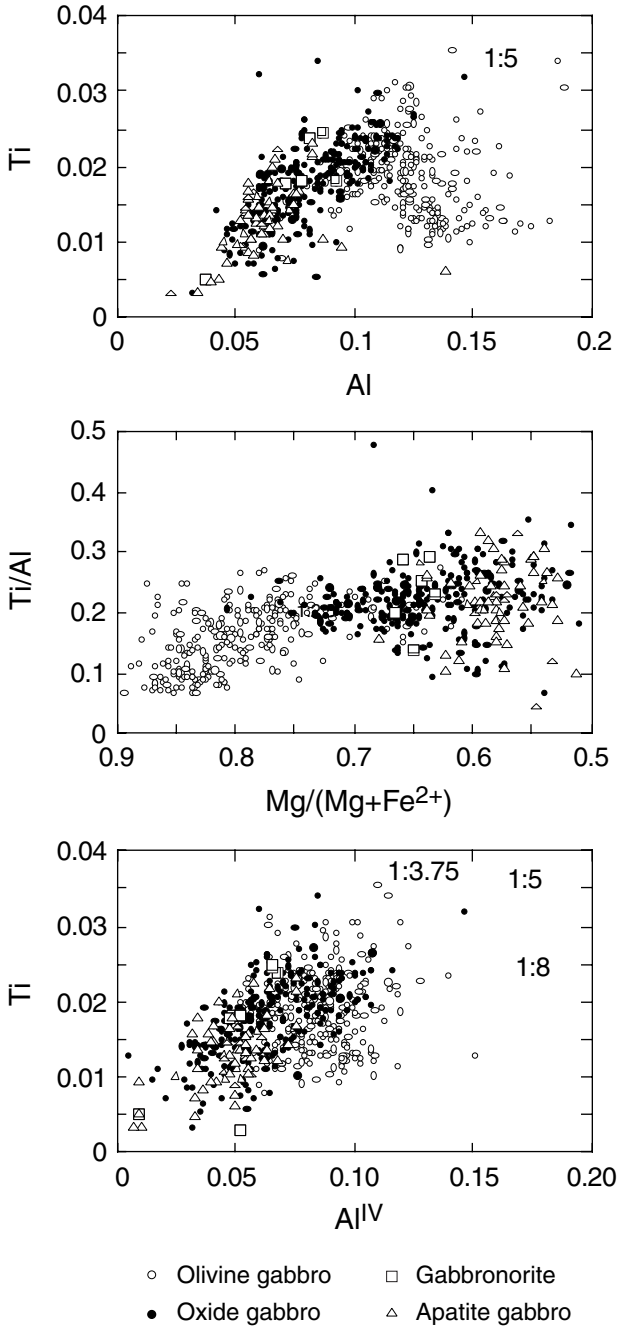

Figure F16. The elements Mg and Ca (cations per formula unit) in clinopyroxenes as a function of Fe^{2+} content. The Fe^{2+} is estimated from charge balancing cations. Pyroxenes with <10 wt% CaO are not included. The groups of gabbros are as for previous figures.

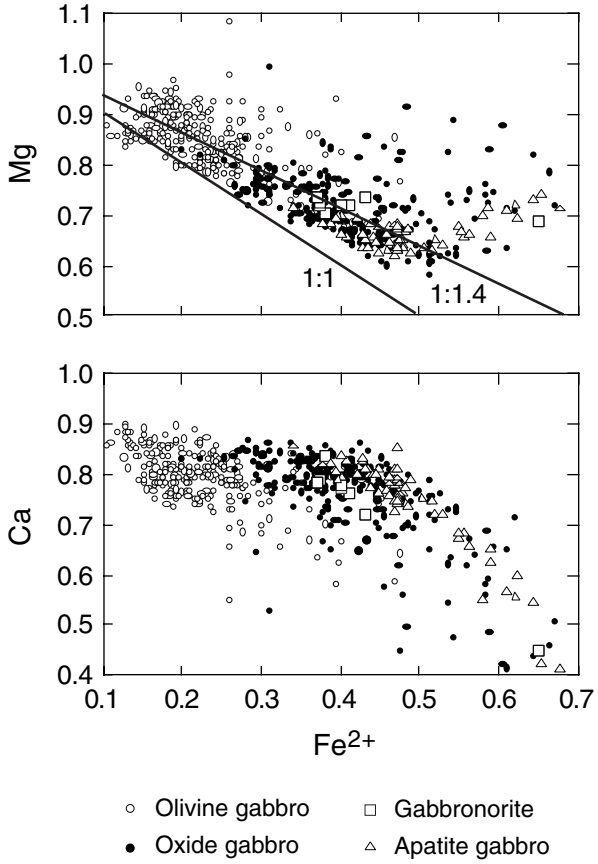

Figure F17. Fe^{2+}-Ti-Fe^{3+} variation of coexisting ilmenite and titanomagnetite. The ilmenite (il)–hematite (he) and ulvöspinel (ulv)–magnetite (mt) solid solution series are shown with the range of coexisting ilmenite and titanomagnetite pairs of the oxide gabbros. The Fe^{3+} and Fe^{2+} were calculated by assuming stoichiometry.

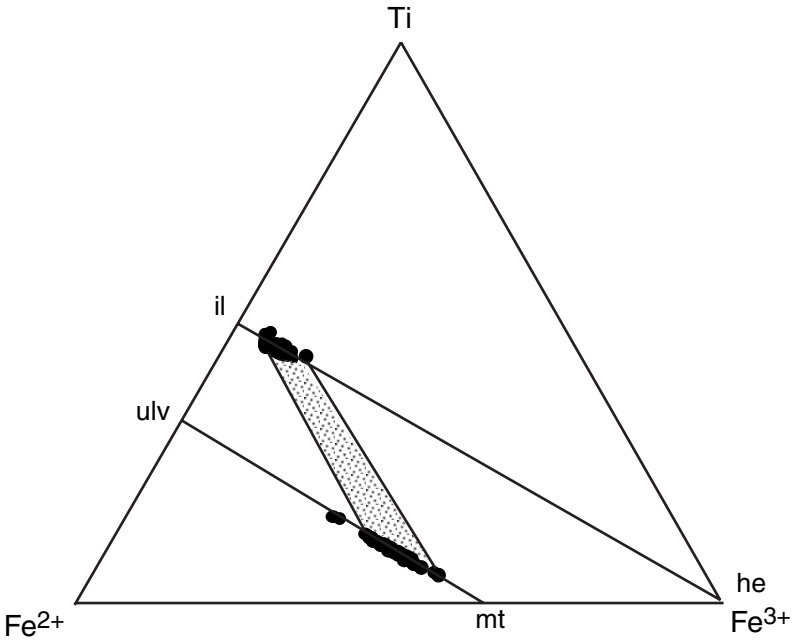

Figure F18. Mn content as a function of the Mg content of ilmenite (cations per formula units).

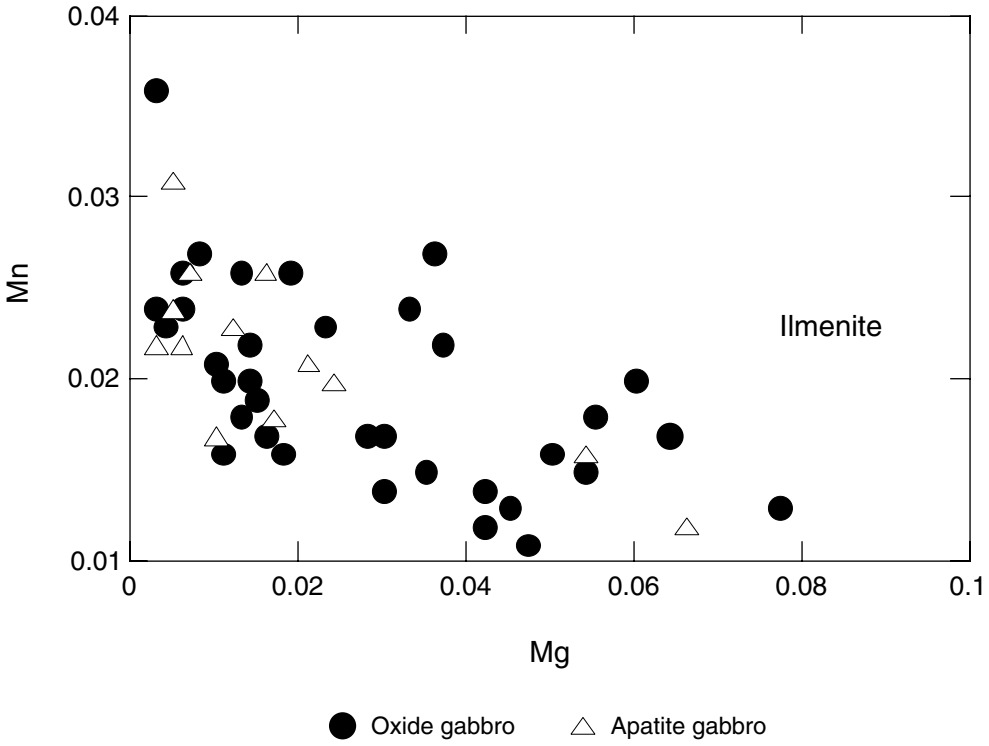

Figure F19. Oxygen fugacity (–log f_{O2}) vs. temperature for coexisting ilmenite and titanomagnetite pairs. NNO = Ni-NiO, FMQ = fayalite-magnetite-quartz, MW = magnetite-wüstite. See text for calculation methods.

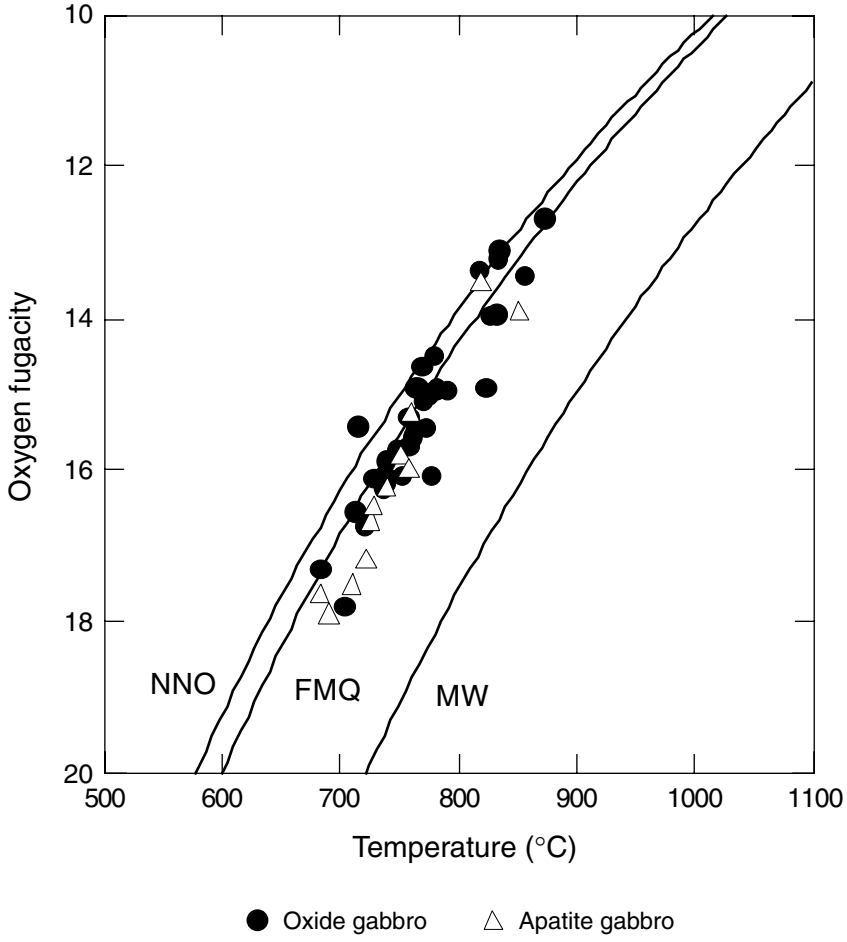

Figure F20. Anionic F, Cl, and OH components of apatite. The OH content is calculated assuming F+Cl+OH = 2.

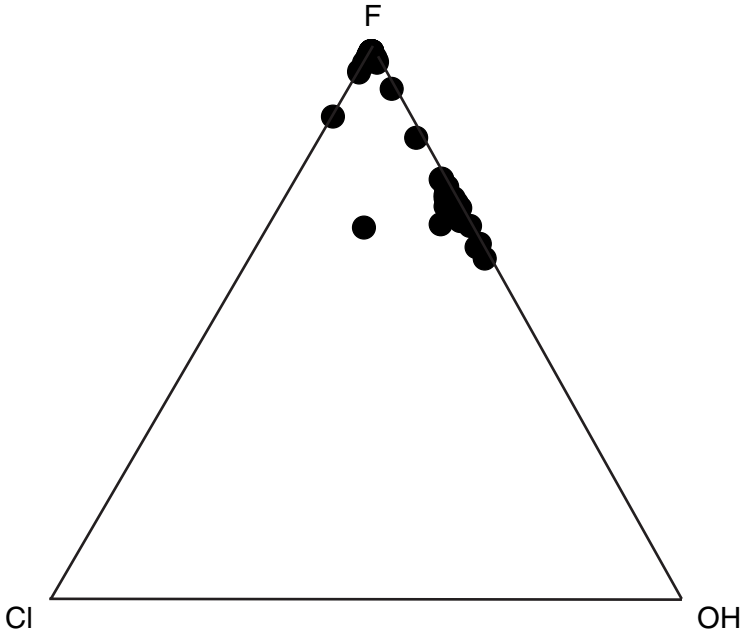

Figure F21. Compositional variation in bulk rocks identified as either Fe-Ti oxide bearing (open symbols) or Fe-Ti oxide free (closed symbols). Selected oxides are shown: TiO_2, Fe_2O_3, and P_2O_5 as well as the element ratio $Mg/(Mg+Fe^{total})$. Note that the scale for the P_2O_5 variation goes from 0 to 5 wt%. The normative anorthite is the CIPW normative plagioclase composition. Data are from Shipboard Scientific Party (1999).

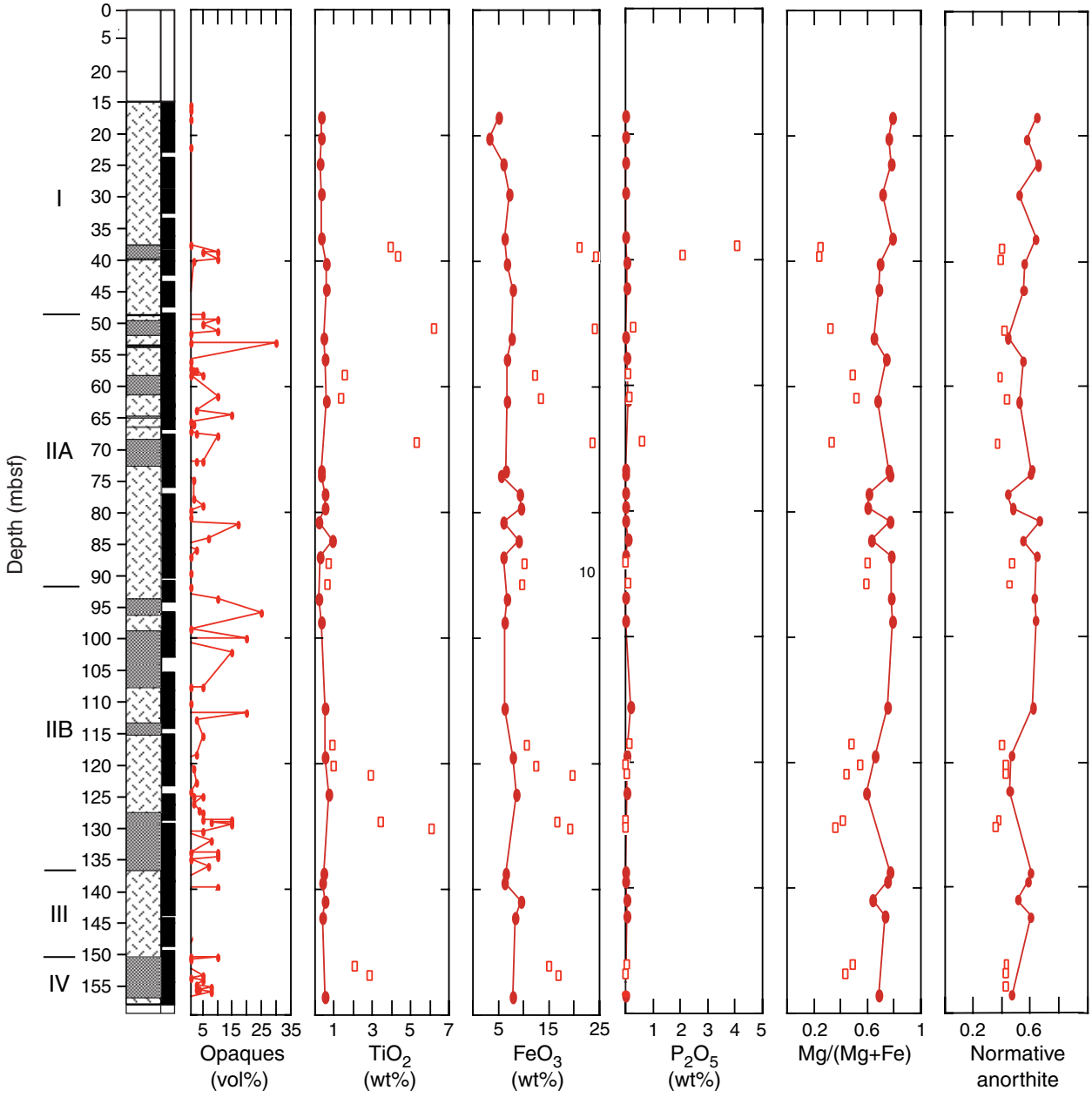

Figure F22. Bulk rock Mg/(Mg+Fe^{total}) ratio as a function of the CIPW normative composition of plagioclase (normative anorthite). Open symbols = Fe-Ti oxide bearing, closed symbols = Fe-Ti oxide free. Data are from Shipboard Scientific Party (1999).

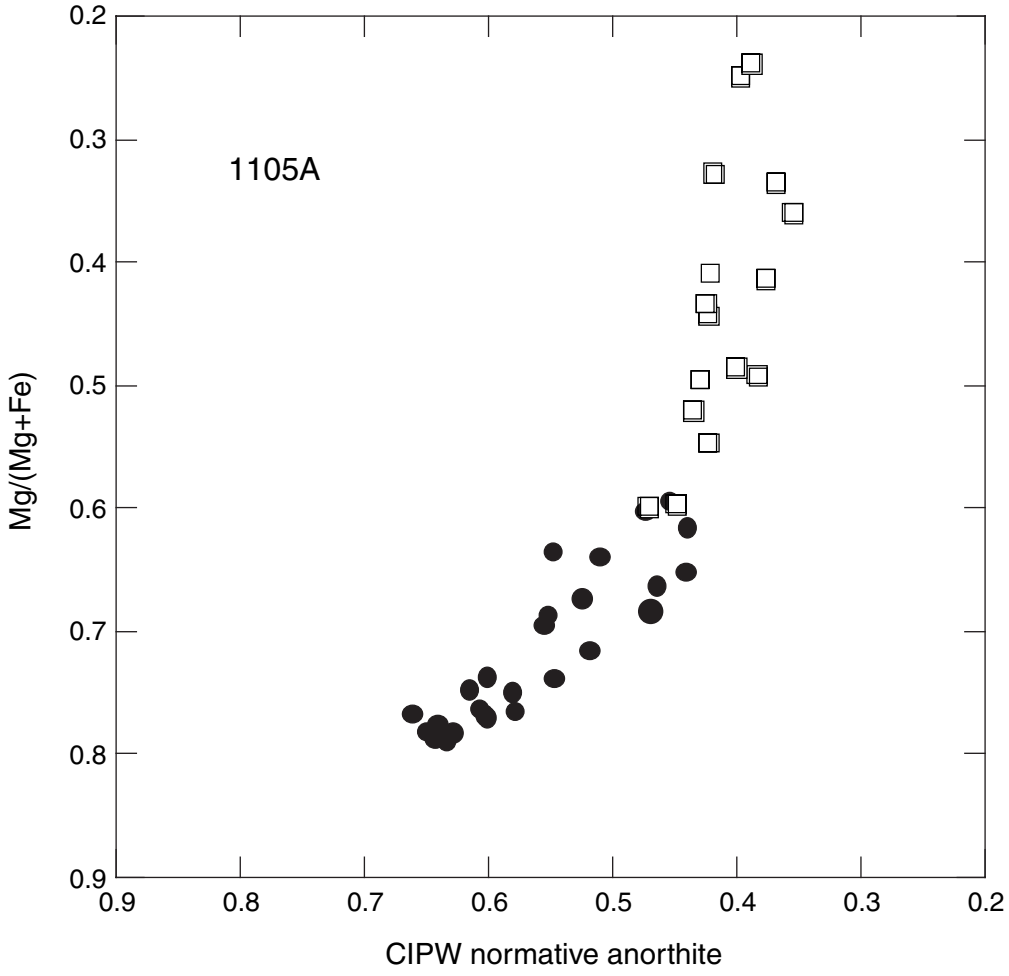

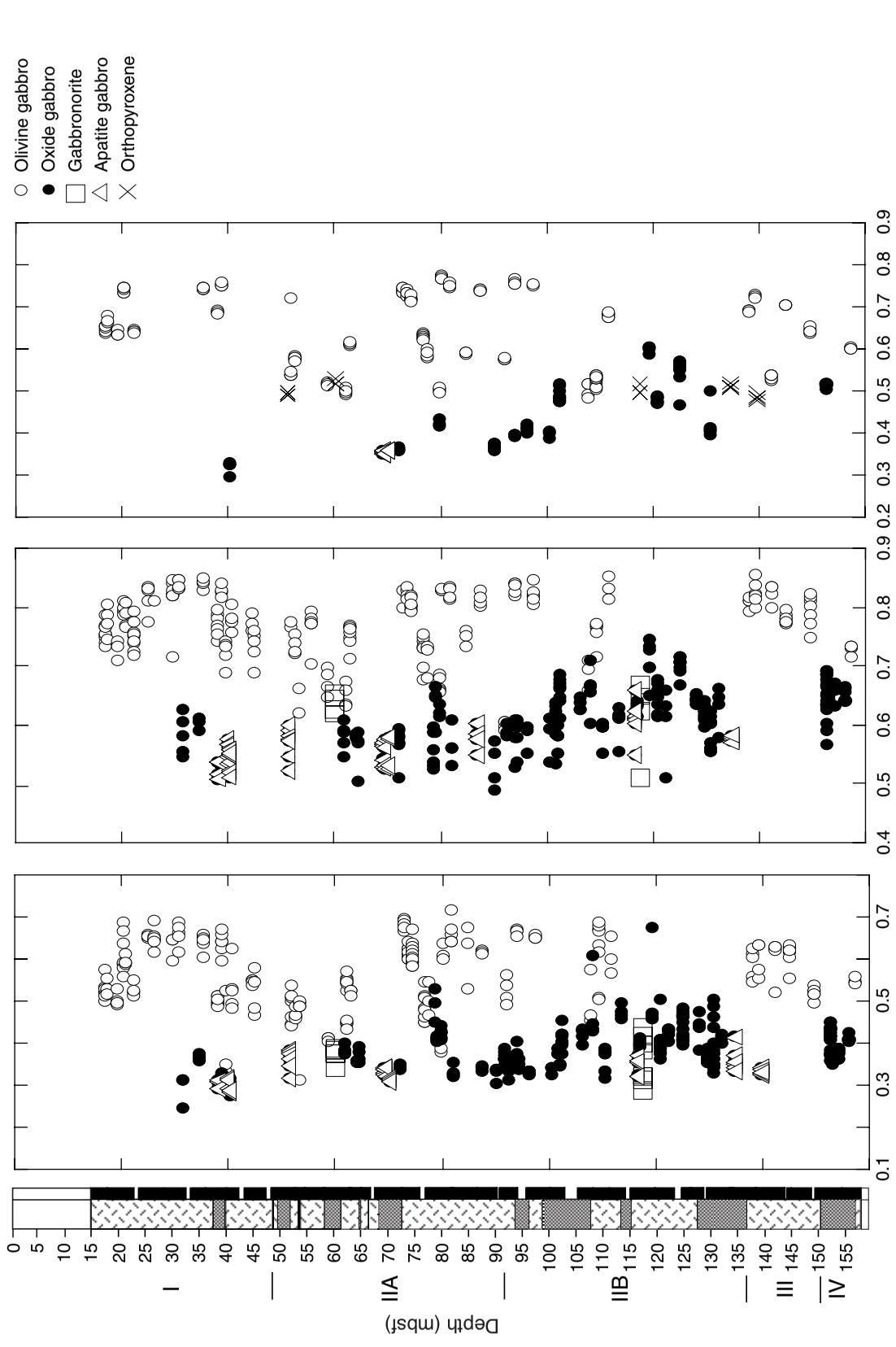

Figure F23. Cryptic mineral variation showing all analytical data in Hole 1105A revealed by cumulus olivine, plagioclase, augite, and orthopyroxene. Iron in olivine and pyroxenes has been calculated as total Fe^{2+}. All analyses are shown. An = anorthite. Mg# = $Mg/(Mg+Fe^{total})$.

Figure F24. Cryptic mineral variation showing average compositions in Hole 1105A revealed by cumulus olivine, plagioclase, augite, and orthopyroxene. Iron in olivine and augite has been calculated as total Fe^{2+}. An = anorthite. Mg# = Mg/(Mg+Fe^{total}).

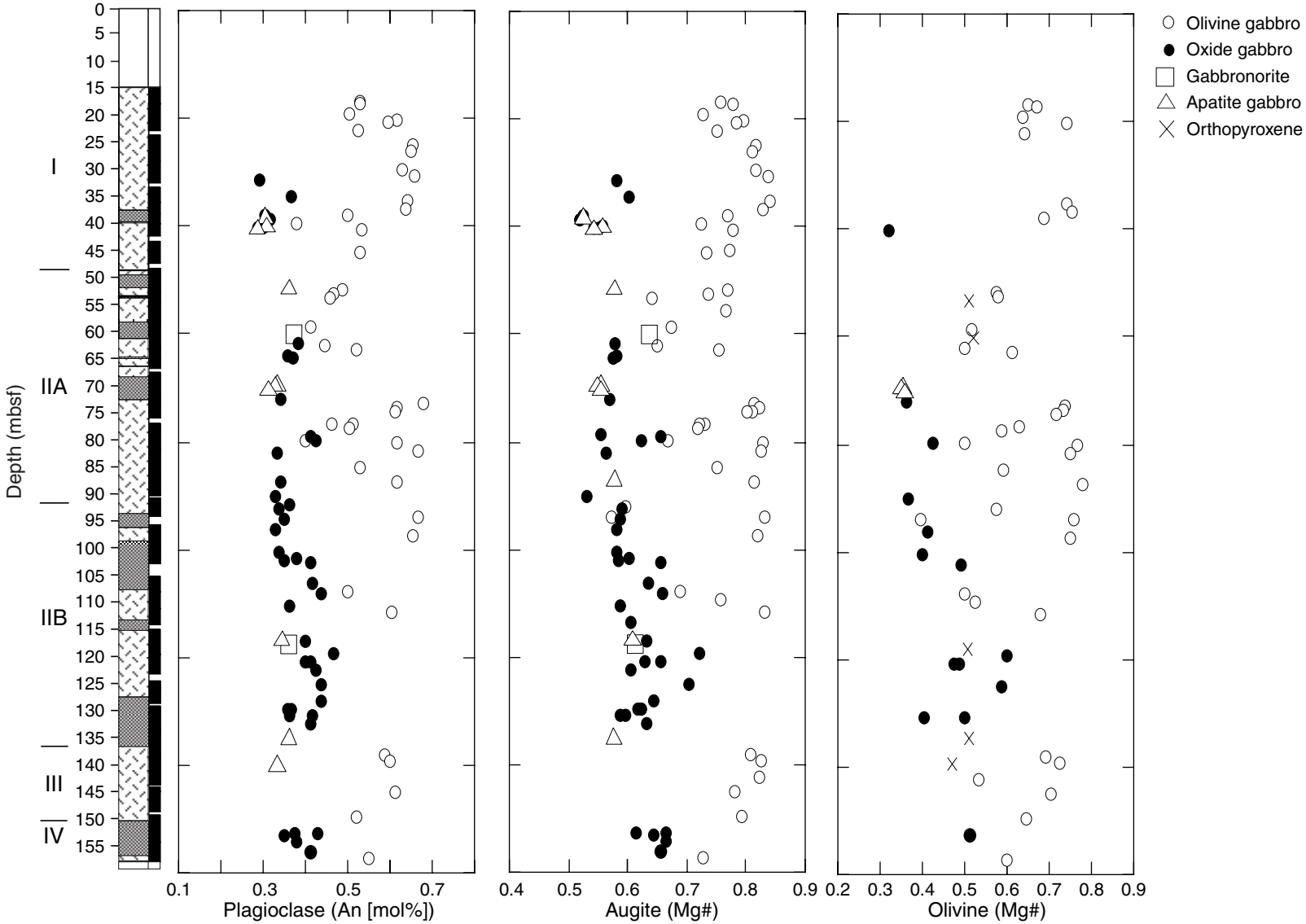

Figure F25. A. Fo (Mg/[Mg+Fe]) of olivine as a function of anthorite (An) of plagioclase. **B.** Mg# (Mg/[Mg+Fe^{total}]) ratio of augite as a function of An of plagioclase. Curves are modeled liquid lines of descent for Atlantis II Fracture Zone basaltic glass compositions (5-3, AII93-5). Near-horizontal lines mark the income of augite (aug) and Fe-Ti oxide minerals (ox), respectively. See text for calculation methods and discussion.

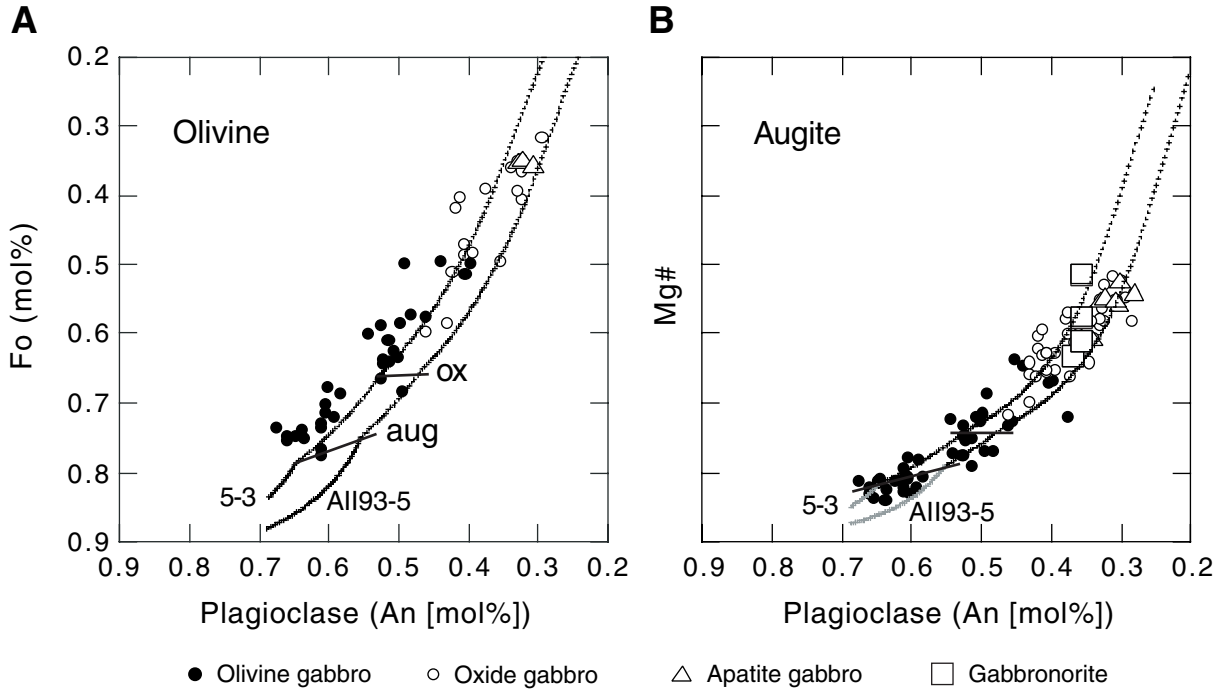

Figure F26. Compositions of bulk gabbros compared to modeled liquid line of descent (liquids) and solid fractionates (troctolite, olivine gabbro, and oxide gabbro). **A.** FeO vs. SiO_2 with all iron calculated as total FeO. Two modeled liquid trends are shown for slightly different analyses of the same sample 5-3 as given by Natland et al. (1991) and Johnson and Dick (1992), respectively. The highest iron enrichment results from the analysis of Johnson and Dick (1992). The calculated liquid line of descent for the analyses given by Natland et al. (1991) is summarized in Table T8, p. 76. **B.** P_2O_5 vs. Mg/(Mg+Fe) with iron calculated as total Fe. The solid fractionates are given with 30%, 20%, 10%, and 0% trapped liquid. The higher the trapped liquid, the closer to the liquid line of descent will the solid fractionate plot. The segmentations in the solid fractionate are caused, respectively, by the income of augite and Fe-Ti oxide minerals and by the fall-out of ilmenite as a result of liquid depletion in TiO_2. Note that the scale for P_2O_5 has been truncated at 0.4 wt% and that the diagram does not include samples with high amounts of cumulus apatite. See text for calculation methods and discussion.

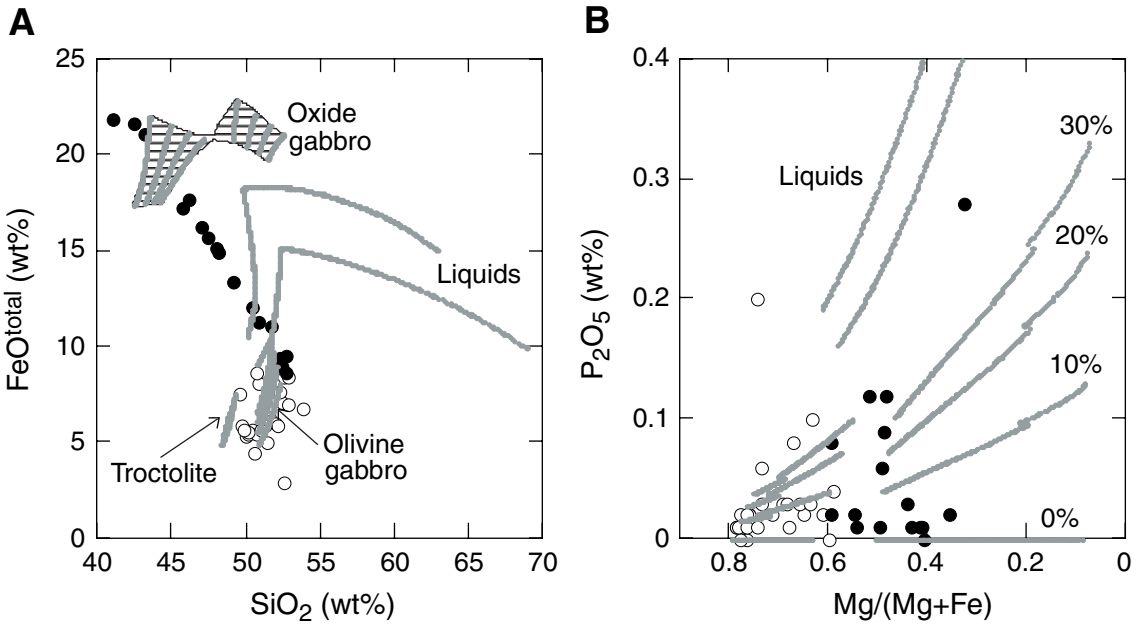

Figure F27. Anorthite (An) mole percent histograms for two selected samples. **A.** Sample 179-1105A-12R-2, 123–127 cm, is a Fe-Ti oxide gabbro. **B.** Sample 179-1105A-29R-1, 102–106 cm, is an olivine gabbro. *N* = number of analyses.

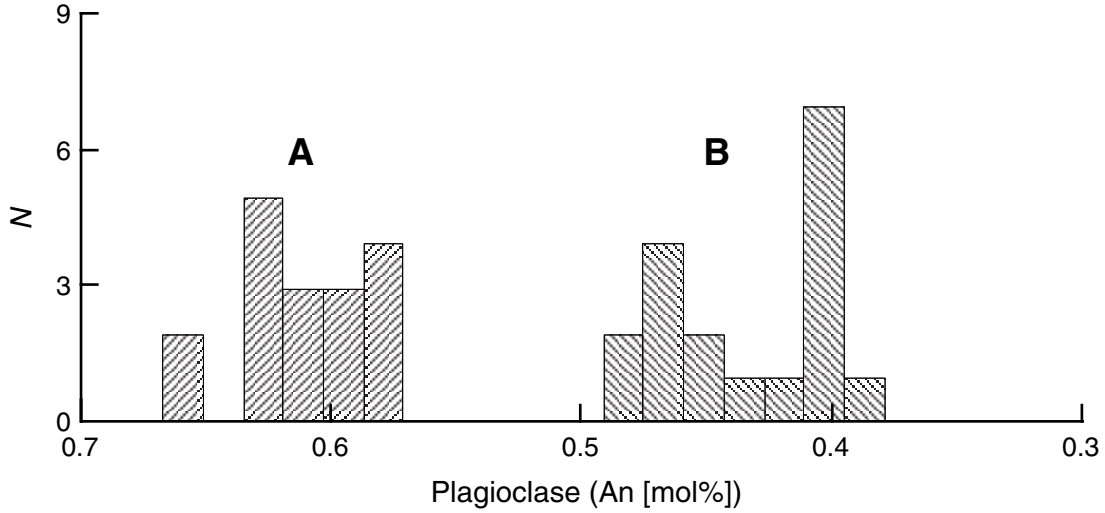

Figure F28. Compositional variation of coexisting plagioclase, olivine, and augite of Skaergaard (SK) and Hole 735B cumulus phases. **A.** Anthorite (An) content of plagioclase and forsterite (Fo) content of olivine. **B.** An content of plagioclase and Mg/(Mg+Fe) ratio of augite. Data for Hole 735B are from Ozawa et al. (1991) and Natland et al. (1991); data from Skaergaard is from Wager and Brown (1967), McBirney (1989), Maaløe (1976), and Nwe (1976). The large open symbols marked (SWIR) designate gabbros dredged along the Southwest Indian Ridge by Meyer et al. (1989) and Bloomer et al. (1989). The observed variation is compared to forward crystal fractionation modeling for potential Skaergaard parental liquids (Wager and Brown, 1987; Brooks and Nielsen, 1990) and representative Atlantis II Fracture Zone basalt glasses as shown in Figure F25, p. 49. Iron in pyroxenes has been calculated assuming all iron as Fe^{2+}.

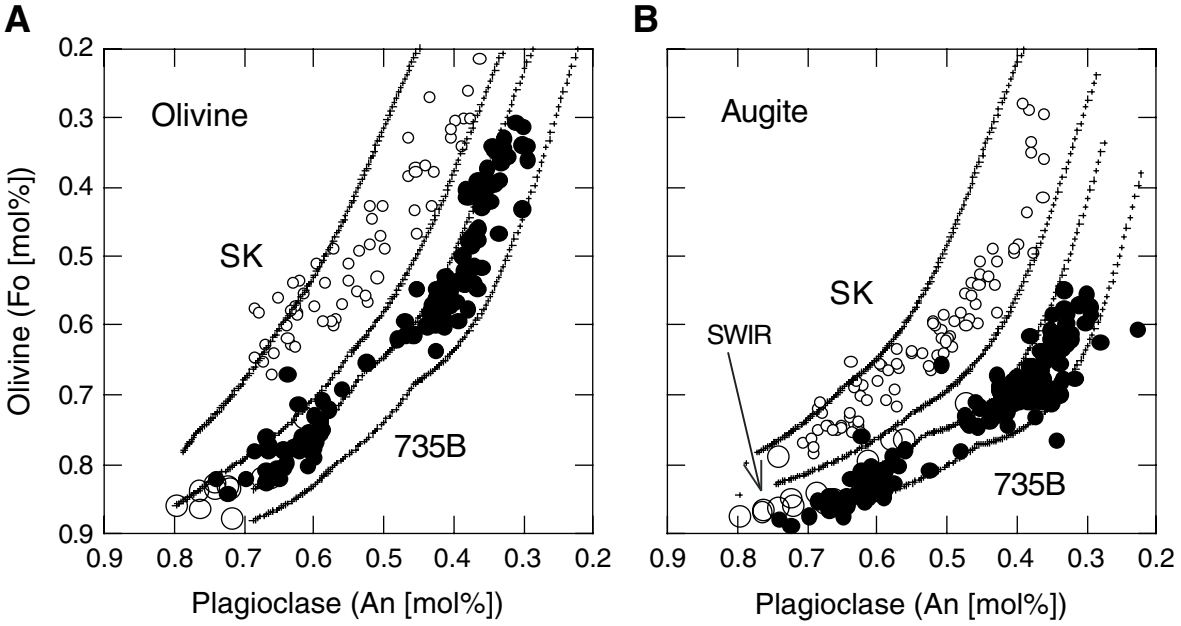

Table T1. Summary of silicate mineral compositions. (**See table notes.** Continued on next two pages.)

ID	Core, section, interval (cm)	Piece	Depth (cm)	Petrography	Plagioclase			Olivine			Augite			Orthopyroxene		
					An (mol%)	*N*	Standard deviation	Fo (mol%)	*N*	Standard deviation	Mg#	*N*	Standard deviation	Mg#	*N*	Standard deviation
	179-1105A-															
THY	1R-2, 23–26	1a	1,631	Olivine gabbro	0.524	6	0.025	0.644	7	0.007	0.753	10	0.016			
TSB	1R-2, 88–91	2b	1,696	Olivine gabbro	0.527	4	0.015	0.665	3	0.009	0.774	4	0.026			
THY	1R-3, 114–117	8b	1,859	Olivine gabbro	0.501	4	0.018	0.633	4	0.006	0.725	3	0.017			
TSB	1R-4, 95–98	5	1,985	Olivine gabbro	0.611	7	0.048	0.736	6	0.006	0.794	4	0.011			
TSB	1R-4, 141–144	8	2,031	Gabbro	0.591	4	0.012				0.780	4	0.019			
TSB	1R-5, 137–141	10	2,173	Olivine gabbro	0.523	4	0.016	0.637	5	0.003	0.747	9	0.023			
TSB	2R-1, 79–82	6	2,449	Gabbro	0.650	5	0.003				0.813	5	0.026			
THY	2R-2, 47–50	4	2,560	Olivine gabbro	0.645	7	0.001				0.808	1				
TSB	3R-1, 51–54	3	2,921	Olivine gabbro	0.625	3	0.029				0.813	12	0.033			
TSB	3R-2, 16–20	1b	3,036	Olivine gabbro	0.655	5	0.027				0.835	5	0.008			
TSB	3R-2, 87–91	9	3,107	Oxide gabbro	0.286	3	0.040				0.580	5	0.034			
THY	4R-1, 92–95	9	3,422	Oxide gabbro	0.362	4	0.008				0.600	4	0.009			
TSB	4R-2, 43–46	1b	3,491	Olivine gabbro	0.638	6	0.020	0.739	6	0.002	0.838	4	0.009			
TSB	4R-3, 46–60	3	3,628	Olivine gabbro	0.635	6	0.027	0.749	4	0.003	0.825	4	0.010			
THY	4R-4, 47–50	6	3,769	Olivine gabbro	0.497	7	0.010	0.683	4	0.003	0.767	7	0.018			
TSB	4R-4, 57–62	7	3,779	Apatite oxide gabbro	0.302	4	0.009				0.522	4	0.015			
THY	5R-1, 12–16	1	3,842	Oxide gabbro (gneissic)	0.314	6	0.007				0.517	5	0.011			
THY	5R-1, 89–93	5	3,919	Gabbro (fine grained)	0.376	4	0.098				0.721	5	0.022			
THY	5R-1, 89–93	5	3,919	Oxide gabbro (medium grained)												
TSB	5R-1, 115–118	7	3,945	Apatite oxide olivine gabbro	0.304	4	0.011				0.555	5	0.017			
TSB	5R-1, 144–147	9	3,974	Apatite oxide olivine gabbro	0.282	4	0.002				0.540	12	0.017			
THY	5R-2, 4–7	2	3,982	Oxide olivine gabbro (gneissic)	0.296	4	0.018	0.316	4	0.015	0.548	5	0.011			
TSB	5R-2, 55–58	6	4,033	Gabbro	0.528	5	0.054				0.776	4	0.020			
THY	6R-1, 124–128	16	4,404	Olivine gabbro, few oxides	0.542	4	0.005				0.771	3	0.015			
TSB	6R-2, 32–36	2	4,458	Olivine gabbro	0.527	5	0.052				0.730	5	0.029			
TSB	7R-3, 33–36	2	5,096	Orthopyroxene apatite oxide gabbro	0.356	6	0.025				0.575	6	0.018	0.489	4	0.004
THY	7R-3, 72–76	4	5,135	Olivine gabbro	0.483	7	0.037	0.573	5	0.081	0.767	2				
TSB	7R-4, 30–33	7	5,212	Olivine gabbro	0.464	5	0.010	0.574	6	0.004	0.732	4	0.014			
TSB	8R-1, 68–70	7	5,308	Microgabbro (orthopyroxene, oxides)	0.308	5	0.014				0.623	3	0.016	0.507	7	0.005
TSB	8R-1, 68–70	7	5,308	Gabbro	0.453	5	0.082				0.637	2				
TSB	8R-3, 53–56	4	5,508	Gabbro							0.762	6	0.031			
TSB	9R-1, 82–86	7	5,822	Olivine gabbro	0.406	4	0.005	0.513	4	0.003	0.671	4	0.023			
THY	9R-2, 85–89	11	5,975	Orthopyroxene oxide gabbronorite	0.369	5	0.019				0.633	4	0.017	0.518	3	0.008
THY	9R-3, 118–121	10a	6,145	Oxide gabbro	0.379	4	0.011				0.577	5	0.024			
TSB	9R-4, 12–16	1	6,181	Olivine gabbro	0.441	4	0.008	0.496	6	0.006	0.647	4	0.019			
TSB	10R-1, 38–42	3a	6,238	Olivine gabbro	0.516	3	0.008	0.608	4	0.004	0.750	8	0.019			
THY	10R-2, 38–41	4	6,373	Oxide gabbro	0.353	3	0.004				0.578	3	0.002			
TSB	10R-2, 85–88	7	6,420	Oxide gabbro	0.368	4	0.018				0.573	3	0.009			
THY	11R-2, 18–21	2	6,858	Apatite oxide olivine gabbro	0.330	5	0.007	0.351	4	0.004	0.551	5	0.019			
TSB	11R-2, 51–54	7	6,891	Apatite oxide olivine gabbro	0.324	3	0.012	0.346	4	0.001	0.546	4	0.024			
TSB	11R-2, 129–133	12	6,969	Apatite oxide olivine gabbro	0.308	3	0.005	0.355	3	0.001	0.551	4	0.029			
THY	12R-1, 28–34	3	7,158	Oxide olivine gabbro	0.339	6	0.004	0.358	6	0.005	0.567	8	0.026			
TSB	12R-1, 106–108	13	7,236	Olivine gabbro	0.677	7	0.011	0.735	6	0.006	0.811	2				
TSB	12R-2, 50–53	5	7,327	Olivine gabbro	0.611	10	0.013	0.729	4	0.006	0.820	4	0.009			
TSB	12R-2, 123–127	15	7,400	Olivine gabbro (fine grained)	0.606	13	0.025	0.714	2		0.807	2				
TSB	12R-2, 123–127	15	7,400	Olivine gabbro (coarse grained)				0.714	4	0.006	0.799	5	0.009			
TSB	13R-1, 24–26	3a	7,654	Microgabbro	0.458	5	0.014				0.726	4	0.023			

Table T1 (continued).

ID	Core, section, interval (cm)	Piece	Depth (cm)	Petrography	Plagioclase			Olivine			Augite			Orthopyroxene		
					An (mol%)	*N*	Standard deviation	Fo (mol%)	*N*	Standard deviation	Mg#	*N*	Standard deviation	Mg#	*N*	Standard deviation
TSB	13R-1, 24–26	3a	7,654	Olivine gabbro (coarse grained)	0.507	5	0.023	0.624	7	0.006	0.720	4	0.033			
TSB	13R-1, 87–89	3d	7,717	Olivine gabbro	0.500	3	0.038	0.584	4	0.008	0.715	4	0.025			
THY	13R-2, 39–43	2	7,809	Oxide gabbro	0.487	3	0.041				0.553	6	0.031			
THY	13R-2, 83–86	3a	7,853	Oxide gabbro	0.406	5	0.004				0.654	4	0.009			
TSB	13R-3, 38–42	3	7,942	Olivine gabbro (fine grained)	0.398	4	0.021	0.497	4	0.005	0.666	5	0.014			
TSB	13R-3, 38–42	3	7,942	Oxide olivine gabbro (coarse grained)	0.419	6	0.013	0.419	3	0.008	0.620	3	0.010			
TSB	13R-3, 79–82	6	7,983	Olivine gabbro	0.611	3	0.019	0.764	6	0.003	0.826	3	0.001			
TSB	14R-1, 42–45	3a	8,142	Olivine gabbro	0.662	5	0.031	0.747	5	0.004	0.821	4	0.010			
THY	14R-1, 80–84	3c	8,180	Oxide gabbro	0.328	4	0.015				0.562	4	0.032			
TSB	14R-3, 91–94	7	8,455	Olivine gabbro (foliated)	0.525	3	0.075	0.586	3	0.003	0.747	4	0.013			
THY	15R-1, 32–36	3c	8,632	Apatite oxide olivine gabbro (ultramafic)							0.575	4	0.022			
TSB	15R-1, 113–116	13	8,713	Olivine gabbro (fine grained)	0.612	3	0.004	0.775	4	0.003	0.810	4	0.012			
TSB	15R-1, 113–116	13	8,713	Oxide gabbro (coarse grained)	0.336	3	0.006									
TSB	15R-2, 71–74	9a	8,821	Microgabbro	0.352	3	0.006	0.414	3	0.003	0.617	4	0.005			
TSB	15R-3, 83–86	8	8,980	Oxide olivine gabbro (gneiss)	0.324	4	0.015	0.364	6	0.006	0.528	4	0.037			
TSB	16R-1, 56–58	4d	9,116	Oxide olivine gabbro	0.360	8	0.015									
TSB	16R-1, 91–94	10	9,151	Olivine gabbro (foliated)	0.520	4	0.030	0.572	4	0.003	0.595	5	0.007			
TSB	16R-2, 14–17	2	9,207	Oxide olivine gabbro	0.332	5	0.014				0.588	3	0.011			
TSB	16R-3, 22–25	3	9,356	Olivine gabbro/first component	0.662	4	0.007	0.755	4	0.006	0.829	5	0.009			
TSB	16R-3, 22–25	3	9,356	Olivine gabbro/second component	0.378	7	0.021	0.390	4	0.001	0.569	3	0.002			
THY	16R-3, 53–56	7	9,387	Oxide gabbro	0.347	5	0.010				0.583	5	0.029			
THY	17R-1, 47–51	4	9,607	Oxide olivine gabbro	0.326	6	0.002	0.406	4	0.008	0.580	4	0.021			
TSB	17R-2, 23–26	2	9,725	Olivine gabbro	0.649	4	0.004	0.748	3	0.001	0.816	7	0.013			
TSB	17R-4, 35–39	4	10,030	Oxide olivine gabbro	0.331	3	0.011	0.394	4	0.007	0.578	3	0.038			
THY	18R-1, 96–100	10	10,116	Oxide gabbro	0.376	3	0.007				0.599	8	0.034			
THY	18R-2, 8–11	2	10,170	Oxide gabbro	0.344	3	0.003				0.581	5	0.022			
TSB	18R-2, 53–57	7	10,215	Oxide olivine gabbro	0.407	9	0.022	0.486	9	0.016	0.654	8	0.024			
THY	19R-1, 85–89	6b	10,605	Oxide gabbro	0.414	4	0.018				0.631	4	0.010			
TSB	19R-2, 65–68	6	10,735	Olivine gabbro (troctolitic)	0.451	2		0.497	4	0.016	0.685	3	0.026			
TSB	19R-2, 95–98	8a	10,765	Oxide gabbro	0.431	3	0.008				0.657	5	0.039			
TSB	19R-3, 94–97	8a	10,899	Olivine gabbro	0.616	8	0.074	0.522	15	0.011	0.753	5	0.023			
THY	20R-1, 46–49	6	11,026	Oxide gabbro	0.359	9	0.026				0.583	4	0.024			
TSB	21R-1, 49–52	6	11,129	Olivine gabbro	0.602	3	0.045	0.676	6	0.005	0.829	3	0.020			
THY	21R-2, 121–125	14	11,335	Oxide gabbro	0.471	4	0.016				0.602	5	0.030			
TSB	22R-1, 103–106	15	11,613	Apatite oxide gabbro (mylonite)	0.341	5	0.022				0.606	8	0.031			
THY	22R-2, 27–30	2a	11,677	Oxide gabbro	0.396	5	0.008				0.628	4	0.012			
TSB	22R-2, 74–78	5	11,724	Orthopyroxene oxide gabbronorite	0.356	5	0.008				0.610	4	0.071	0.498	3	0.012
TSB	22R-3, 130–133	8	11,898	Oxide olivine gabbro (fine grained); few oxides	0.462	6	0.006	0.595	4	0.008	0.717	5	0.021			
TSB	23R-1, 94–98	8	12,034	Oxide olivine gabbro (fine grained)	0.394	9	0.010	0.481	4	0.002	0.652	5	0.023			
TSB	23R-1, 94–98	8	12,034	Oxide olivine gabbro (medium grained)	0.409	4	0.066	0.469	4	0.004	0.626	4	0.015			
TSB	23R-2, 98–101	11	12,188	Oxide gabbro	0.421	6	0.012				0.601	4	0.065			
TSB	24R-1, 32–36	3b	12,472	Oxide olivine gabbro, very few oxides	0.433	18	0.031	0.584	13	0.028	0.699	9	0.015			
THY	24R-3, 74–77	6	12,790	Oxide gabbro	0.432	5	0.003				0.641	9	0.006			
TSB	25R-1, 26–30	2	12,926	Oxide gabbro (fine grained)	0.363	6	0.011				0.619	5	0.007			
TSB	25R-1, 26–30	2	12,926	Oxide gabbro (coarse grained)	0.355	3	0.001				0.614	5	0.001			
TSB	25R-1, 133–137	5c	13,033	Oxide olivine gabbro	0.357	8	0.022	0.495	1		0.583	4	0.028			
THY	25R-2, 18–21	1	13,062	Oxide olivine gabbro	0.414	8	0.063	0.402	4	0.006	0.592	3	0.001			
TSB	25R-3, 10–13	1	13,193	Oxide gabbro (mylonitic)	0.409	5	0.008				0.628	4	0.001			

Table T1 (continued).

ID	Core, section, interval (cm)	Piece	Depth (cm)	Petrography	Plagioclase			Olivine			Augite			Orthopyroxene		
					An (mol%)	*N*	Standard deviation	Fo (mol%)	*N*	Standard deviation	Mg#	*N*	Standard deviation	Mg#	*N*	Standard deviation
THY	26R-1, 50–54	2	13,450	Orthopyroxene apatite oxide gabbro	0.357	6	0.029				0.514	4	0.005	0.507	4	0.005
TSB	26R-3, 80–81	5	13,756	Olivine gabbro	0.585	5	0.034	0.687	4	0.002	0.805	4	0.009			
TSB	27R-1, 27–28	1a	13,897	Olivine gabbro	0.595	4	0.041	0.720	4	0.003	0.822	6	0.020			
THY	27R-1, 71–75	3	13,941	Orthopyroxene apatite oxide biotite gabbro	0.328	5	0.007							0.481	4	0.007
TSB	27R-3, 93–94	2	14,195	Olivine gabbro (anorthositic); olivine interstitial	0.621	4	0.004	0.529	6	0.005	0.820	4	0.016			
TSB	28R-1, 98–99	3b	14,468	Olivine gabbro	0.607	7	0.027	0.700	5	0.001	0.777	8	0.008			
TSB	29R-1, 102–106	4	14,942	Olivine gabbro (mylonitic)	0.515	6	0.015	0.640	4	0.008	0.791	7	0.027			
TSB	29R-3, 112–114	3	15,221	Oxide olivine gabbro	0.424	18	0.013	0.509	10	0.004	0.662	24	0.023			
THY	29R-4, 13–17	1	15,253	Oxide gabbro	0.369	5	0.009				0.612	6	0.033			
TSB	29R-4, 31–33	2	15,271	Oxide gabbro	0.348	3	0.001				0.641	4	0.005			
TSB	30R-1, 27–31	3a	15,367	Oxide gabbro	0.374	10	0.010				0.662	3	0.007			
TSB	30R-2, 109–113	8	15,585	Oxide gabbro (fine grained)	0.407	3	0.012				0.653	4	0.011			
TSB	30R-3, 102–106	9	15,712	Olivine gabbro	0.544	3	0.008	0.598	4	0.001	0.724	4	0.009			

Notes: ID = shipboard sample codes. An = anorthite. Fo = forsterite. Mg# = Mg/(Mg+Fe) with iron as total FeO. *N* = number of analyses used for each average.

Table T2. Compositions of cumulus plagioclase. (**See table notes.** Continued on next four pages.)

ID	Core, section, interval (cm)	Piece	Depth (cm)	Petrography	*N*	Major element oxide (wt%)									An (mol%)
						SiO_2	TiO_2	Al_2O_3	FeO	MgO	CaO	Na_2O	K_2O	Total	
	179-1105A-														
THY	1R-2, 23–26	1a	1,631	Olivine gabbro	6	55.67	0.08	28.09	0.22	0.03	10.74	5.39	0.06	100.29	0.524
						0.78	0.04	0.31	0.04	0.00	0.54	0.29	0.02		0.025
TSB	1R-2, 88–91	2b	1,696	Olivine gabbro	4	54.33	0.08	27.97	0.12	0.01	11.05	5.48	0.07	99.11	0.527
						0.50	0.05	0.35	0.05	0.01	0.35	0.16	0.02		0.015
THY	1R-3, 114–117	8b	1,859	Olivine gabbro	4	55.35	0.06	27.79	0.25	0.03	10.27	5.65	0.07	99.47	0.501
						0.57	0.05	0.44	0.05	0.01	0.38	0.20	0.03		0.018
TSB	1R-4, 95–98	5	1,985	Olivine gabbro	7	52.49	0.04	29.31	0.22	0.04	12.69	4.46	0.06	99.32	0.611
						1.18	0.04	0.62	0.06	0.03	0.89	0.60	0.03		0.048
TSB	1R-4, 141–144	8	2,031	Gabbro	4	52.60	0.04	28.48	0.28	0.05	12.43	4.75	0.07	98.69	0.591
						0.56	0.02	0.29	0.08	0.01	0.35	0.10	0.01		0.012
TSB	1R-5, 137–141	10	2,173	Olivine gabbro	4	54.35	0.05	28.00	0.26	0.01	11.03	5.56	0.06	99.32	0.523
						0.35	0.02	0.45	0.05	0.02	0.27	0.24	0.03		0.016
TSB	2R-1, 79–82	6	2,449	Gabbro	5	51.07	0.06	29.81	0.23	0.03	13.30	3.95	0.05	98.49	0.650
						0.18	0.06	0.23	0.06	0.01	0.12	0.05	0.02		0.003
THY	2R-2, 47–50	4	2,560	Gabbro	7	52.78	0.11	27.86	0.41	0.03	13.63	4.15	0.05	99.02	0.645
						0.64	0.15	0.57	0.38	0.02	0.53	0.26	0.02		0.022
TSB	3R-1, 51–54	3	2,921	Olivine gabbro	3	51.87	0.05	29.09	0.14	0.04	12.88	4.27	0.05	98.39	0.625
						0.64	0.02	0.38	0.08	0.03	0.63	0.31	0.01		0.029
TSB	3R-2, 16–20	1b	3,036	Olivine gabbro	5	50.80	0.06	31.00	0.16	0.03	13.66	3.97	0.10	99.78	0.655
						0.70	0.06	0.33	0.05	0.01	0.68	0.31	0.09		0.027
TSB	3R-2, 87–91	9	3,107	Oxide gabbro	3	60.50	0.02	23.68	0.19	0.02	5.99	8.26	0.15	98.82	0.286
						1.10	0.02	0.89	0.02	0.01	0.85	0.42	0.01		0.039
THY	4R-1, 92–95	9	3,422	Oxide gabbro	4	59.47	0.05	24.25	0.18	0.01	7.05	6.88	0.15	98.04	0.362
						0.38	0.05	0.18	0.05	0.01	0.09	0.17	0.03		0.008
TSB	4R-2, 43–46	1b	3,491	Olivine gabbro	6	51.30	0.08	29.58	0.26	0.13	13.15	4.12	0.06	98.68	0.638
						0.23	0.02	0.55	0.37	0.26	0.42	0.25	0.03		0.020
TSB	4R-3, 46–60	3	3,628	Olivine gabbro	6	52.05	0.07	29.00	0.16	0.03	13.24	4.21	0.06	98.82	0.635
						0.72	0.06	0.59	0.03	0.01	0.56	0.31	0.02		0.027
THY	4R-4, 47–50	6	3,769	Olivine gabbro	7	57.03	0.07	26.12	0.19	0.02	10.64	5.96	0.08	100.11	0.497
						0.19	0.01	0.21	0.07	0.01	0.18	0.16	0.02		0.009
TSB	4R-4, 57–62	7	3,779	Apatite oxide gabbro	4	59.81	0.05	24.40	0.21	0.03	6.16	7.88	0.25	98.77	0.302
						0.77	0.04	0.42	0.04	0.04	0.22	0.13	0.02		0.009
THY	5R-1, 12–16	1	3,842	Oxide gabbro	6	61.05	0.03	24.85	0.30	0.02	6.47	7.81	0.20	100.75	0.314
						0.26	0.02	0.10	0.06	0.02	0.15	0.11	0.02		0.007
THY	5R-1, 89–93	5	3,919	Gabbro	4	58.64	0.07	25.69	0.23	0.02	7.54	6.89	0.18	99.26	0.377
						2.47	0.03	1.69	0.10	0.01	2.03	1.06	0.05		0.098
TSB	5R-1, 115–118	7	3,945	Apatite oxide olivine gabbro	4	60.84	0.04	24.78	0.22	0.01	6.38	8.06	0.20	100.53	0.304
						0.52	0.04	0.21	0.03	0.01	0.28	0.15	0.01		0.011
TSB	5R-1, 144–147	9	3,974	Apatite oxide olivine gabbro	4	60.93	0.03	24.70	0.20	0.01	5.94	8.36	0.16	100.34	0.282
						0.31	0.03	0.12	0.07	0.01	0.09	0.06	0.03		0.002
THY	5R-2, 4–7	2	3,982	Oxide olivine gabbro	4	61.63	0.06	24.52	0.32	0.03	6.08	7.99	0.19	100.82	0.296
						0.58	0.05	0.23	0.06	0.02	0.38	0.23	0.03		0.018
TSB	5R-2, 55–58	6	4,033	Gabbro	5	54.23	0.07	28.51	0.11	0.02	10.92	5.39	0.10	99.36	0.528
						1.05	0.04	1.05	0.07	0.01	1.24	0.58	0.01		0.054
THY	6R-1, 124–128	16	4,404	Gabbro	4	55.37	0.05	28.72	0.16	0.05	11.16	5.21	0.09	100.81	0.542
						0.23	0.02	0.11	0.07	0.02	0.07	0.07	0.02		0.005
TSB	6R-2, 32–36	2	4,458	Olivine gabbro	5	54.61	0.07	28.76	0.18	0.04	10.79	5.35	0.12	99.94	0.527
						1.41	0.03	0.88	0.07	0.01	1.13	0.55	0.03		0.052

Table T2 (continued).

ID	Core, section, interval (cm)	Piece	Depth (cm)	Petrography	*N*	Major element oxide (wt%)									An (mol%)
						SiO_2	TiO_2	Al_2O_3	FeO	MgO	CaO	Na_2O	K_2O	Total	
TSB	7R-3, 33–36	2	5,096	Orthopyroxene apatite oxide gabbro	6	58.50	0.07	25.63	0.24	0.01	7.32	7.31	0.16	99.25	0.356
						0.99	0.05	0.35	0.15	0.01	0.55	0.27	0.01		0.025
THY	7R-3, 72–76	4	5,135	Olivine gabbro	4	57.63	0.07	25.98	0.14	0.02	10.00	6.04	0.11	99.99	0.478
						1.33	0.03	0.56	0.09	0.02	0.78	0.39	0.04		0.035
TSB	7R-4, 30–33	7	5,212	Olivine gabbro	5	56.19	0.03	27.40	0.16	0.05	9.61	6.14	0.14	99.73	0.464
						0.50	0.01	0.18	0.14	0.10	0.12	0.23	0.01		0.010
TSB	8R-1, 68–70	7	5,308	Microgabbro (orthopyroxene, oxides)	5	60.17	0.04	24.92	0.22	0.04	6.42	7.96	0.16	99.93	0.308
						0.35	0.05	0.23	0.30	0.07	0.37	0.16	0.05		0.014
TSB	8R-1, 68–70	7	5,308	Gabbro	5	56.29	0.06	27.53	0.14	0.03	9.45	6.32	0.09	99.91	0.452
						2.17	0.03	1.50	0.05	0.02	1.68	0.98	0.04		0.082
TSB	8R-3, 53–56	4	5,508	Gabbro	4	66.49	0.01	20.53	0.03	0.02	1.25	11.19	0.03	99.55	0.058
						0.76	0.01	0.47	0.03	0.01	0.68	0.41	0.02		0.032
TSB	9R-1, 82–86	7	5,822	Olivine gabbro	4	59.51	0.05	26.38	0.11	0.02	8.32	6.74	0.13	101.27	0.406
						0.23	0.04	0.08	0.03	0.01	0.08	0.10	0.03		0.005
THY	9R-2, 85–89	11	5,975	Orthopyroxene oxide gabbronorite	5	60.19	0.10	25.50	0.31	0.04	7.61	7.20	0.13	101.07	0.369
						0.50	0.04	0.15	0.16	0.02	0.38	0.25	0.01		0.019
THY	9R-3, 118–121	10a	6,145	Oxide gabbro	4	59.45	0.07	24.33	0.24	0.01	7.33	6.64	0.13	98.20	0.379
						0.46	0.04	0.20	0.03	0.01	0.21	0.12	0.02		0.011
TSB	9R-4, 12–16	1	6,181	Olivine gabbro	11	56.22	0.07	27.93	0.18	0.02	10.34	5.57	0.10	100.45	0.506
						1.29	0.02	0.96	0.06	0.02	1.08	0.60	0.03		0.053
TSB	10R-1, 38–42	3a	6,238	Olivine gabbro	3	54.72	0.05	28.18	0.11	0.03	10.56	5.48	0.10	99.22	0.516
						0.44	0.03	0.14	0.01	0.02	0.17	0.13	0.01		0.008
THY	10R-2, 38–41	4	6,373	Oxide gabbro	3	60.12	0.06	25.72	0.24	0.04	7.33	7.42	0.15	101.08	0.353
						0.07	0.03	0.06	0.17	0.01	0.08	0.05	0.01		0.004
TSB	10R-2, 85–88	7	6,420	Oxide gabbro	4	60.02	0.06	25.87	0.27	0.02	7.60	7.20	0.14	101.18	0.368
						0.46	0.05	0.37	0.10	0.02	0.39	0.21	0.04		0.018
THY	11R-2, 18–21	2	6,858	Apatite oxide olivine gabbro	4	60.78	0.05	23.23	0.26	0.01	6.47	7.24	0.19	98.23	0.331
						0.47	0.03	0.13	0.10	0.01	0.09	0.17	0.05		0.008
TSB	11R-2, 51–54	7	6,891	Apatite oxide olivine gabbro	3	59.54	0.05	24.95	0.18	0.02	6.78	7.83	0.11	99.44	0.324
						0.21	0.04	0.40	0.03	0.02	0.24	0.15	0.03		0.012
TSB	11R-2, 129–133	12	6,969	Apatite oxide olivine gabbro	3	61.77	0.09	24.47	0.26	0.02	6.41	7.95	0.13	101.10	0.308
						0.08	0.03	0.27	0.13	0.01	0.17	0.06	0.03		0.005
THY	12R-1, 28–34	3	7,158	Oxide olivine gabbro	6	60.62	0.06	24.27	0.21	0.02	7.01	7.56	0.18	99.93	0.339
						0.32	0.03	0.17	0.07	0.02	0.06	0.12	0.03		0.004
TSB	12R-1, 106–108	13	7,236	Olivine gabbro	7	49.20	0.06	30.88	0.14	0.06	13.48	3.55	0.05	97.43	0.677
						1.41	0.02	0.39	0.06	0.03	0.14	0.14	0.02		0.011
TSB	12R-2, 50–53	5	7,327	Olivine gabbro	10	53.03	0.05	30.03	0.12	0.02	12.15	4.27	0.05	99.72	0.611
						0.47	0.04	0.22	0.07	0.01	0.13	0.20	0.02		0.013
TSB	12R-2, 123–127	15	7,400	Olivine gabbro (fine grained)	18	51.47	0.04	28.62	0.11	0.09	12.07	4.33	0.07	96.81	0.606
						1.63	0.02	2.44	0.06	0.17	0.83	0.44	0.03		0.040
TSB	13R-1, 24–26	3a	7,654	Microgabbro	5	56.34	0.07	26.20	0.07	0.02	9.24	6.06	0.09	98.09	0.458
						0.35	0.03	0.65	0.04	0.02	0.25	0.18	0.03		0.014
TSB	13R-1, 24–26	3a	7,654	Olivine gabbro (coarse grained)	5	54.77	0.10	28.09	0.18	0.02	10.40	5.58	0.08	99.22	0.507
						0.41	0.03	0.47	0.06	0.02	0.57	0.23	0.01		0.023
TSB	13R-1, 87–89	3d	7,717	Olivine gabbro	3	55.49	0.09	27.91	0.18	0.04	9.93	5.49	0.10	99.23	0.500
						0.63	0.08	0.59	0.03	0.03	0.88	0.39	0.05		0.038
THY	13R-2, 39–43	2	7,809	Oxide gabbro	3	57.05	0.10	27.89	0.26	0.03	10.18	5.92	0.13	101.57	0.487
						1.20	0.03	0.76	0.05	0.00	0.86	0.48	0.02		0.041
THY	13R-2, 83–86	3a	7,853	Oxide gabbro	5	58.69	0.14	26.03	0.19	0.03	8.38	6.79	0.15	100.38	0.406

Table T2 (continued).

ID	Core, section, interval (cm)	Piece	Depth (cm)	Petrography	*N*	Major element oxide (wt%)									An (mol%)
						SiO_2	TiO_2	Al_2O_3	FeO	MgO	CaO	Na_2O	K_2O	Total	
						0.56	0.05	0.27	0.07	0.02	0.09	0.07	0.04		0.004
TSB	13R-3, 38–42	3	7,942	Olivine gabbro (fine grained)	4	57.00	0.05	26.07	0.25	0.08	8.25	6.90	0.13	98.72	0.398
						0.40	0.03	0.63	0.26	0.14	0.46	0.27	0.03		0.021
TSB	13R-3, 38–42	3	7,942	Oxide olivine gabbro (coarse grained)	6	57.13	0.05	26.13	0.13	0.00	8.49	6.50	0.09	98.52	0.419
						0.35	0.03	0.33	0.10	0.01	0.27	0.16	0.02		0.013
TSB	13R-3, 79–82	6	7,983	Olivine gabbro	3	53.31	0.08	30.15	0.10	0.03	12.17	4.29	0.05	100.19	0.611
						0.49	0.02	0.33	0.06	0.01	0.38	0.22	0.01		0.019
TSB	14R-1, 42–45	3a	8,142	Olivine gabbro	5	51.69	0.05	31.10	0.11	0.02	12.98	3.67	0.04	99.67	0.662
						0.86	0.03	0.59	0.03	0.01	0.44	0.38	0.01		0.031
THY	16R-1, 80–84	3c	8,182	Oxide gabbro	4	59.78	0.05	24.81	0.33	0.03	6.76	7.66	0.19	99.61	0.328
						0.29	0.06	0.12	0.10	0.03	0.19	0.34	0.06		0.015
TSB	14R-3, 91–94	7	8,455	Olivine gabbro (foliated)	3	52.95	0.03	30.19	0.09	0.01	11.90	4.21	0.05	99.44	0.609
						2.00	0.03	1.27	0.02	0.01	1.46	0.81	0.03		0.075
TSB	15R-1, 113–116	13	8,713	Olivine gabbro (fine grained)	3	52.84	0.04	30.09	0.09	0.01	12.27	4.30	0.04	99.68	0.612
						0.31	0.04	0.24	0.03	0.01	0.23	0.08	0.02		0.004
TSB	15R-1, 113–116	13	8,713	Oxide gabbro (coarse grained)	3	59.75	0.06	25.40	0.18	0.01	6.84	7.47	0.15	99.86	0.336
						0.40	0.00	0.14	0.03	0.01	0.26	0.10	0.04		0.006
TSB	15R-2, 71–74	9a	8,821	Microgabbro	3	60.22	0.04	25.69	0.17	0.04	7.02	7.14	0.15	100.48	0.352
						0.21	0.01	0.13	0.00	0.02	0.07	0.10	0.04		0.006
TSB	15R-3, 83–86	8	8,980	Oxide olivine gabbro (gneiss)	4	59.63	0.04	25.02	0.18	0.01	6.52	7.51	0.17	99.08	0.324
						1.54	0.03	0.16	0.07	0.01	0.36	0.10	0.02		0.015
TSB	16R-1, 56–58	4d	9,116	Oxide olivine gabbro	8	58.78	0.04	25.65	0.64	0.06	7.26	7.14	0.14	99.70	0.360
						1.04	0.02	0.43	1.15	0.11	0.41	0.24	0.03		0.015
TSB	16R-1, 91–94	10	9,151	Olivine gabbro (foliated)	4	54.62	0.06	28.57	0.17	0.03	10.45	5.33	0.09	99.33	0.520
						1.42	0.03	0.28	0.06	0.02	0.53	0.38	0.02		0.030
TSB	16R-2, 14–17	2	9,207	Oxide olivine gabbro	5	60.00	0.01	24.93	0.23	0.02	6.57	7.29	0.16	99.22	0.332
						0.16	0.02	0.25	0.10	0.01	0.31	0.21	0.01		0.014
TSB	16R-3, 22–25	3	9,356	Olivine gabbro	4	51.83	0.04	31.07	0.09	0.01	13.23	3.74	0.05	100.06	0.661
						0.20	0.02	0.13	0.06	0.01	0.34	0.18	0.02		0.007
TSB	16R-3, 22–25	3	9,356	Olivine gabbro	3	58.54	0.04	26.20	0.18	0.01	7.63	6.93	0.14	99.67	0.378
						0.78	0.01	0.61	0.05	0.02	0.43	0.23	0.06		0.021
THY	16R-3, 53–56	7	9,387	Oxide olivine gabbro	5	60.43	0.05	25.51	0.27	0.03	7.18	7.48	0.15	101.10	0.347
						0.24	0.02	0.14	0.06	0.01	0.28	0.13	0.03		0.010
THY	17R-1, 47–51	4	9,607	Oxide olivine gabbro	6	61.00	0.06	24.94	0.22	0.01	6.72	7.68	0.16	100.80	0.326
						0.23	0.05	0.16	0.14	0.01	0.11	0.12	0.02		0.002
TSB	17R-2, 23–26	2	9,725	Olivine gabbro	4	52.34	0.07	30.54	0.12	0.02	12.84	3.84	0.04	99.81	0.649
						0.49	0.03	0.18	0.04	0.01	0.23	0.02	0.01		0.004
TSB	17R-4, 35–39	4	10,030	Oxide olivine gabbro	3	59.91	0.12	25.20	0.45	0.01	6.62	7.39	0.12	99.83	0.331
						1.02	0.15	0.44	0.35	0.01	0.24	0.14	0.02		0.011
THY	18R-1, 96–100	10	10,116	Oxide gabbro	3	57.13	0.02	24.55	0.13	0.01	7.39	6.78	0.11	96.11	0.376
						0.40	0.02	0.20	0.04	0.01	0.18	0.06	0.04		0.007
THY	18R-2, 8–11	2	10,170	Oxide gabbro	3	60.15	0.04	25.25	0.16	0.02	7.25	7.64	0.12	100.62	0.344
						0.18	0.02	0.11	0.01	0.01	0.07	0.11	0.03		0.003
TSB	18R-2, 53–57	7	10,215	Oxide olivine gabbro	9	58.12	0.05	26.45	0.23	0.12	8.44	6.79	0.11	100.31	0.407
						0.73	0.03	0.65	0.27	0.33	0.56	0.23	0.02		0.022
THY	19R-1, 85–89	6b	10,605	Oxide gabbro	4	56.70	0.09	25.74	0.18	0.03	8.41	6.57	0.14	97.86	0.414
						0.30	0.06	0.27	0.05	0.02	0.20	0.34	0.02		0.018
TSB	19R-2, 65–68	6	10,735	Olivine gabbro (troctolitic)	3	54.58	0.04	27.08	0.21	0.05	9.53	5.38	0.09	96.96	0.495
						3.03	0.04	1.55	0.06	0.02	1.39	0.67	0.01		0.067

Table T2 (continued).

ID	Core, section, interval (cm)	Piece	Depth (cm)	Petrography	*N*	Major element oxide (wt%)									An (mol%)
						SiO_2	TiO_2	Al_2O_3	FeO	MgO	CaO	Na_2O	K_2O	Total	
TSB	19R-2, 95–98	8a	10,765	Oxide gabbro	4	55.82	0.06	26.15	0.18	0.02	8.97	5.47	0.14	96.81	0.475
						1.52	0.04	1.27	0.10	0.01	1.82	0.82	0.04		0.086
TSB	19R-3, 94–97	8a	10,899	Olivine gabbro	8	51.92	0.06	28.82	0.19	0.02	11.99	4.12	0.08	97.20	0.617
						2.58	0.03	1.81	0.06	0.02	1.64	0.73	0.03		0.074
THY	20R-1, 46–49	6	11,026	Oxide gabbro	9	59.73	0.09	24.69	0.32	0.02	7.41	7.33	0.14	99.73	0.359
						0.81	0.08	0.39	0.23	0.01	0.51	0.36	0.03		0.026
TSB	21R-1, 49–52	6	11,129	Olivine gabbro	3	52.99	0.05	28.76	0.07	0.01	12.46	4.56	0.08	98.97	0.602
						0.86	0.02	0.88	0.08	0.01	0.69	0.60	0.00		0.045
THY	21R-2, 121–125	14	11,335	Oxide gabbro	4	56.43	0.04	27.10	0.18	0.03	9.49	5.89	0.11	99.29	0.471
						0.53	0.03	0.48	0.03	0.01	0.47	0.12	0.05		0.016
TSB	22R-1, 103–106	15	11,613	Apatite oxide gabbro (mylonite)	5	59.51	0.02	25.60	0.14	0.01	6.80	7.28	0.13	99.51	0.341
						0.80	0.02	0.44	0.05	0.01	0.40	0.36	0.05		0.022
THY	22R-2, 27–30	2a	11,677	Oxide gabbro	5	58.87	0.07	24.46	0.21	0.02	7.69	6.48	0.16	97.95	0.396
						0.53	0.05	0.21	0.07	0.02	0.15	0.16	0.01		0.008
TSB	22R-2, 74–78	5	11,724	Orthopyroxene oxide gabbronorite	8	59.32	0.05	26.07	0.18	0.03	7.25	7.26	0.17	100.33	0.356
						1.44	0.02	1.07	0.07	0.03	1.08	0.68	0.03		0.055
TSB	22R-3, 130–133	8	11,898	Oxide olivine gabbro (fine grained); few oxides	8	54.71	0.05	27.36	0.26	0.12	9.45	6.10	0.14	98.18	0.461
						0.64	0.02	0.41	0.29	0.24	0.22	0.17	0.05		0.006
TSB	23R-1, 94–98	8	12,034	Oxide olivine gabbro (fine grained)	9	57.61	0.04	26.46	0.16	0.02	8.19	6.95	0.11	99.52	0.394
						0.26	0.02	0.56	0.06	0.02	0.18	0.18	0.03		0.010
TSB	23R-1, 94–98	8	12,034	Oxide olivine gabbro (medium grained)	4	57.12	0.06	26.84	0.24	0.01	8.40	6.73	0.10	99.51	0.408
						1.61	0.01	1.08	0.12	0.01	1.34	0.76	0.03		0.066
TSB	23R-2, 98–101	11	12,188	Oxide gabbro	6	56.36	0.06	26.98	0.27	0.05	8.65	6.58	0.12	99.07	0.421
						0.60	0.04	0.19	0.16	0.06	0.19	0.21	0.02		0.012
TSB	24R-1, 32–36	3b	12,472	Oxide olivine gabbro	18	56.43	0.07	27.18	0.18	0.05	8.82	6.38	0.12	99.23	0.433
						0.97	0.03	0.79	0.16	0.10	0.64	0.34	0.03		0.031
THY	24R-3, 74–77	6	12,790	Oxide gabbro	5	57.73	0.13	25.89	0.41	0.05	8.74	6.36	0.12	99.42	0.432
						0.97	0.18	0.74	0.44	0.07	0.64	0.47	0.03		0.034
TSB	25R-1, 26–30	2	12,926	Oxide gabbro (fine grained)	6	58.09	0.03	25.77	0.16	0.02	7.31	7.10	0.13	98.61	0.363
						0.78	0.02	0.20	0.02	0.01	0.29	0.11	0.03		0.011
TSB	25R-1, 26–30	2	12,926	Oxide gabbro (medium grained)	3	58.45	0.03	25.58	0.18	0.02	7.07	7.09	0.12	98.54	0.355
						0.54	0.04	0.23	0.07	0.01	0.07	0.06	0.00		0.001
TSB	25R-1, 133–137	5c	13,033	Oxide olivine gabbro	8	57.75	0.05	24.87	0.24	0.03	7.20	7.17	0.15	97.46	0.357
						0.68	0.04	0.41	0.21	0.03	0.49	0.24	0.04		0.022
THY	25R-2, 18–21	1	13,062	Oxide olivine gabbro	8	58.51	0.08	26.71	0.25	0.03	8.59	6.73	0.13	101.03	0.414
						1.78	0.03	1.10	0.05	0.02	1.34	0.70	0.04		0.063
TSB	25R-3, 10–13	1	13,193	Oxide gabbro (mylonitic)	5	56.74	0.05	26.45	0.18	0.02	8.37	6.69	0.14	98.63	0.409
						0.90	0.03	0.71	0.03	0.02	0.15	0.18	0.03		0.008
THY	26R-1, 50–54	2	13,450	Orthopyroxene apatite oxide gabbro	6	60.08	0.10	25.59	0.18	0.02	7.40	7.37	0.16	100.89	0.357
						0.55	0.05	0.51	0.06	0.02	0.56	0.42	0.05		0.029
TSB	26R-3, 80–81	5	13,756	Olivine gabbro	5	52.50	0.07	29.74	0.14	0.03	11.75	4.61	0.06	98.90	0.585
						0.96	0.02	0.62	0.06	0.02	0.61	0.41	0.03		0.034
TSB	27R-1, 27–28	1a	13,897	Olivine gabbro	4	51.97	0.07	29.87	0.18	0.04	11.77	4.42	0.07	98.37	0.595
						1.33	0.02	0.68	0.02	0.02	0.79	0.45	0.01		0.041
THY	27R-1, 71–75	3	13,941	Orthopyroxene apatite oxide biotite gabbronorite	5	61.05	0.03	24.90	0.23	0.02	6.74	7.62	0.21	100.80	0.328
						0.35	0.03	0.23	0.12	0.02	0.08	0.19	0.05		0.007
TSB	27R-3, 93–94	2	14,195	Olivine gabbro (anorthositic)	5	51.40	0.08	29.72	0.20	0.02	12.08	4.44	0.07	98.01	0.600
						1.45	0.02	0.88	0.09	0.01	0.98	0.51	0.02		0.047
TSB	28R-1, 98–99	3b	14,468	Olivine gabbro	7	52.12	0.07	29.82	0.23	0.04	12.42	4.45	0.05	99.20	0.607

Table T2 (continued).

ID	Core, section, interval (cm)	Piece	Depth (cm)	Petrography	*N*	Major element oxide (wt%)									An (mol%)
						SiO_2	TiO_2	Al_2O_3	FeO	MgO	CaO	Na_2O	K_2O	Total	
						0.57	0.04	0.44	0.05	0.04	0.46	0.36	0.02		0.027
TSB	29R-1, 102–106	4	14,942	Olivine gabbro (mylonitic)	6	54.25	0.06	28.60	0.13	0.01	10.54	5.49	0.10	99.17	0.515
						1.05	0.03	0.27	0.06	0.01	0.31	0.20	0.04		0.015
TSB	29R-3, 112–114	3	15,221	Oxide olivine gabbro	18	56.34	0.15	26.78	0.86	0.11	8.62	6.48	0.12	99.47	0.424
						1.17	0.30	0.41	1.45	0.26	0.33	0.22	0.03		0.013
THY	29R-4, 13–17	1	15,253	Oxide gabbro	5	59.66	0.05	25.61	0.21	0.03	7.61	7.20	0.11	100.48	0.369
						0.42	0.03	0.10	0.07	0.02	0.19	0.17	0.03		0.009
TSB	29R-4, 31–33	2	15,271	Oxide gabbro	3	59.05	0.09	25.48	0.20	0.04	7.13	7.38	0.13	99.50	0.348
						0.44	0.01	0.16	0.11	0.02	0.03	0.06	0.01		0.001
TSB	30R-1, 27–31	3a	15,367	Oxide gabbro	10	57.36	0.04	25.99	0.35	0.27	7.57	7.00	0.19	98.78	0.374
						0.81	0.02	0.81	0.44	0.52	0.44	0.14	0.04		0.010
TSB	30R-2, 109–113	8	15,585	Oxide gabbro (fine grained)	3	55.97	0.04	25.93	0.18	0.01	8.17	6.57	0.11	96.98	0.407
						0.31	0.03	0.19	0.05	0.00	0.14	0.20	0.01		0.012
TSB	30R-3, 102–106	9	15,712	Olivine gabbro	3	53.19	0.04	28.97	0.20	0.03	11.11	5.15	0.08	98.76	0.544
						0.38	0.01	0.26	0.07	0.03	0.17	0.09	0.01		0.008

Notes: ID = shipboard sample codes. The first line for each sample is the average, and the second line is the standard deviation of analyses. *N* = the number of analyses included in the average. An = anorthite.

Table T3. Compositions of cumulus pyroxene. (**See table notes.** Continued on next four pages.)

ID	Core, section, interval (cm)	Piece	Depth (cm)	Petrography	*N*	Major element oxide (wt%)										
						SiO_2	TiO_2	Al_2O_3	FeO	MnO	MgO	CaO	Na_2O	Cr_2O_3	Total	Mg#
	179-1105A-															
THY	1R-2, 23–26	1a	1,631	Olivine gabbro	10	51.85	0.82	2.41	8.92	0.24	15.22	19.85	0.43	0.03	99.78	0.753
						0.60	0.10	0.16	0.88	0.07	0.45	1.13	0.10	0.03		0.016
TSB	1R-2, 88–91	2b	1,696	Olivine gabbro	4	51.36	0.74	2.43	7.98	0.20	15.26	20.92	0.53	0.06	99.54	0.773
						0.16	0.12	0.13	1.46	0.03	0.69	1.65	0.08	0.03		0.026
THY	1R-3, 114–117	8b	1,859	Olivine gabbro	3	51.48	0.78	2.60	10.12	0.27	14.94	18.67	0.37	0.04	99.66	0.725
						0.09	0.02	0.23	1.28	0.05	0.80	2.03	0.08	0.03		0.017
TSB	1R-4, 95–98	5	1,985	Gabbro	4	51.83	0.76	2.95	7.37	0.16	15.99	19.99	0.49	0.21	99.76	0.795
						0.59	0.19	0.38	0.19	0.06	0.90	1.40	0.09	0.14		0.011
TSB	1R-4, 141–144	8	2,031	Gabbro	3	51.57	0.70	2.71	7.72	0.20	15.89	20.47	0.41	0.19	99.84	0.786
						0.08	0.14	0.13	0.82	0.04	0.40	0.77	0.06	0.08		0.018
TSB	1R-5, 137–141	10	2,173	Olivine gabbro	9	51.31	0.93	2.83	9.01	0.25	14.87	20.14	0.56	0.06	99.95	0.746
						0.47	0.13	0.56	1.33	0.06	0.90	1.49	0.22	0.03		0.023
TSB	2R-1, 79–82	6	2,449	Gabbro	5	51.21	0.52	3.06	6.87	0.17	16.43	19.96	0.50	0.36	99.09	0.810
						0.79	0.12	0.41	2.11	0.06	1.95	3.36	0.11	0.12		0.026
THY	2R-2, 47–50	4	2,560	Gabbro	1	53.38	0.44	3.19	6.37	0.21	15.03	22.43	0.47	0.39	101.91	0.808
TSB	3R-1, 51–54	3	2,921	Olivine gabbro	12	51.04	0.84	2.63	6.44	0.20	15.58	21.51	0.49	0.20	98.94	0.812
						0.63	0.21	0.19	1.61	0.08	0.32	0.99	0.11	0.06		0.033
TSB	3R-2, 16–20	1b	3,036	Olivine gabbro	5	51.41	0.48	3.11	5.72	0.18	16.22	21.08	0.40	0.33	98.93	0.835
						0.48	0.07	0.22	0.12	0.05	0.93	1.05	0.03	0.12		0.008
TSB	3R-2, 87–91	9	3,107	Oxide gabbro	5	50.63	0.29	1.34	14.63	0.49	11.34	20.71	0.35	0.02	99.79	0.580
						0.86	0.11	0.47	1.18	0.09	0.69	0.37	0.04	0.03		0.034
THY	4R-1, 92–95	9	3,422	Oxide gabbro	4	51.00	0.64	1.65	14.47	0.47	12.16	19.25	0.50	0.06	100.20	0.600
						0.13	0.17	0.15	1.03	0.09	0.39	1.05	0.04	0.07		0.009
TSB	4R-2, 43–46	1b	3,491	Olivine gabbro	4	51.29	0.46	3.41	5.50	0.12	15.88	21.61	0.43	0.56	99.27	0.837
						0.48	0.09	0.36	0.38	0.06	0.16	0.82	0.07	0.06		0.009
TSB	4R-4, 57–62	7	3,779	Apatite oxide gabbro	4	51.53	0.16	1.39	20.84	0.54	12.76	9.67	0.43	0.02	97.349	0.522
						0.47	0.13	0.48	1.05	0.12	0.32	0.63	0.16	0.03		0.015
TSB	4R-3, 46–60	3	3,628	Olivine gabbro	4	51.89	0.68	2.95	6.33	0.20	16.66	20.89	0.39	0.35	100.34	0.824
						0.29	0.34	0.31	0.70	0.02	0.80	1.38	0.07	0.20		0.010
THY	4R-4, 47–50	6	3,769	Olivine gabbro	7	53.18	0.95	2.49	8.39	0.25	15.46	20.32	0.48	0.04	101.55	0.767
						0.42	0.15	0.16	1.02	0.05	0.36	1.01	0.17	0.04		0.018
THY	5R-1, 12–16	1	3,842	Oxide gabbro	3	51.62	0.53	1.23	18.31	0.64	11.06	17.93	0.49	0.05	101.86	0.518
						0.25	0.13	0.14	1.26	0.19	0.21	0.78	0.08	0.01		0.013
THY	5R-1, 89–93	5	3,919	Gabbro	5	50.94	0.56	2.99	9.90	0.28	14.37	19.65	0.56	0.22	99.48	0.721
						0.22	0.09	0.40	0.55	0.07	1.27	1.26	0.07	0.08		0.022
TSB	5R-1, 115–118	7	3,945	Apatite oxide olivine gabbro	5	50.59	0.44	1.35	16.22	0.62	11.31	19.02	0.45	0.01	100.02	0.554
						0.10	0.07	0.11	1.25	0.05	0.16	0.89	0.09	0.03		0.016
TSB	5R-1, 144–147	9	3,974	Apatite oxide olivine gabbro (mylonitic)	10	50.19	0.47	1.28	16.51	0.58	11.09	18.79	0.45	0.03	99.39	0.545
						0.30	0.12	0.07	0.95	0.07	0.18	0.90	0.04	0.03		0.011
THY	5R-2, 4–7	2	3,982	Oxide olivine gabbro	5	51.71	0.50	1.41	16.27	0.56	11.06	18.97	0.49	0.02	101.00	0.548
						0.26	0.09	0.03	0.83	0.03	0.30	1.03	0.07	0.02		0.011
TSB	5R-2, 55–58	6	4,033	Gabbro	4	51.84	0.57	2.60	8.65	0.28	16.79	18.33	0.37	0.07	99.50	0.776
						0.27	0.06	0.09	1.19	0.07	0.63	1.68	0.03	0.03		0.020
THY	6R-1, 124–128	16	4,404	Gabbro	3	52.66	0.71	2.81	8.27	0.23	15.65	20.10	0.38	0.03	100.84	0.771
						0.05	0.09	0.09	0.49	0.04	0.89	1.00	0.02	0.04		0.015
TSB	6R-2, 32–36	2	4,458	Olivine gabbro	5	50.63	0.82	2.53	8.81	0.26	14.18	21.51	0.46	0.07	99.27	0.742
						0.78	0.08	0.12	0.71	0.05	0.13	0.69	0.06	0.04		0.016
TSB	7R-3, 33–36	2	5,096	Orthopyroxene apatite oxide gabbro	6	50.54	0.40	1.17	15.10	0.51	11.45	19.73	0.47	0.04	99.39	0.575

Table T3 (continued).

ID	Core, section, interval (cm)	Piece	Depth (cm)	Petrography	*N*	Major element oxide (wt%)										Mg#
						SiO_2	TiO_2	Al_2O_3	FeO	MnO	MgO	CaO	Na_2O	Cr_2O_3	Total	
						0.87	0.13	0.17	0.80	0.06	0.33	0.71	0.05	0.03		0.018
TSB	7R-3, 33–36	2	5,096	Orthopyroxene apatite oxide gabbro	4	51.07	0.28	0.50	30.35	0.84	16.29	1.75	0.06	0.00	101.14	0.489
						0.52	0.02	0.04	0.75	0.04	0.30	0.17	0.06	0.00		0.004
THY	7R-3, 72–76	4	5,135	Olivine gabbro	2	52.35	0.72	2.28	7.84	0.31	14.49	20.97	0.47	0.01	99.43	0.767
TSB	7R-4, 30–33	7	5,212	Olivine gabbro	4	50.84	0.73	2.50	9.45	0.31	14.47	20.19	0.48	0.05	99.02	0.732
						0.26	0.04	0.10	0.78	0.07	0.15	0.71	0.07	0.06		0.014
TSB	8R-1, 68–70	7	5,308	Microgabbro (orthopyroxene, oxides)	3	51.38	0.28	1.11	13.50	0.54	12.48	20.36	0.41	0.01	100.06	0.622
						0.27	0.03	0.15	0.80	0.08	0.13	0.79	0.08	0.01		0.016
TSB	8R-1, 68–70	7	5,308	Microgabbro (orthopyroxene, oxides)	7	50.68	0.18	0.36	29.54	0.93	17.07	1.11	0.07	0.03	99.96	0.507
						0.47	0.04	0.04	0.46	0.12	0.24	0.12	0.11	0.03		0.005
TSB	8R-1, 68–70	7	5,308	Gabbro	2	51.03	0.39	1.42	12.89	0.39	12.71	20.57	0.43	0.00	99.84	0.637
TSB	8R-3, 53–56	4	5,508	Gabbro	6	51.07	0.79	2.45	8.60	0.22	15.44	20.25	0.52	0.08	99.42	0.762
						1.01	0.10	0.25	1.31	0.03	0.51	1.03	0.10	0.02		0.031
TSB	9R-1, 82–86	7	5,822	Olivine gabbro	2	52.39	0.77	2.29	11.00	0.27	13.69	20.63	0.43	0.03	101.50	0.689
THY	9R-2, 85–89	11	5,975	Orthopyroxene oxide gabbronorite	4	52.32	0.64	1.60	13.45	0.43	13.00	19.47	0.45	0.03	101.40	0.633
						0.67	0.32	0.51	1.09	0.09	0.24	1.24	0.09	0.01		0.017
THY	9R-2, 85–89	11	5,975	Orthopyroxene oxide gabbronorite	3	52.21	0.24	0.67	29.33	0.81	17.64	1.71	0.04	0.00	102.65	0.517
						0.39	0.08	0.02	1.40	0.10	0.30	1.08	0.03	0.01		0.008
THY	9R-3, 118–121	10a	6,147	Oxide gabbro	5	51.67	0.50	1.26	15.58	0.53	11.87	18.39	0.39	0.01	100.20	0.576
						0.45	0.15	0.13	1.95	0.09	0.32	1.80	0.05	0.01		0.024
THY	9R-3, 118–121	10a	6,145	Oxide gabbro	1	50.64	0.30	0.68	28.81	0.79	17.48	1.10	0.01	0.03	99.85	0.520
TSB	9R-4, 12–16	1	6,181	Olivine gabbro	3	51.64	0.69	2.43	12.09	0.44	12.72	19.91	0.44	0.04	100.40	0.652
						0.19	0.05	0.26	0.92	0.07	0.25	0.50	0.09	0.02		0.018
TSB	10R-1, 38–42	3a	6,240	Olivine gabbro	8	50.94	0.69	2.89	8.74	0.24	14.63	20.42	0.51	0.10	99.16	0.749
						0.44	0.17	0.54	1.16	0.06	0.45	1.54	0.11	0.03		0.019
THY	10R-2, 38–41	4	6,373	Oxide gabbro	3	51.64	0.40	1.70	15.44	0.43	11.87	19.69	0.37	0.02	101.54	0.578
						0.22	0.10	0.06	0.24	0.03	0.12	0.26	0.03	0.01		0.002
TSB	10R-2, 85–88	7	6,420	Oxide gabbro	3	52.04	0.50	1.52	15.94	0.46	11.97	19.14	0.46	0.01	102.04	0.572
						0.45	0.24	0.17	0.69	0.04	0.11	0.42	0.05	0.01		0.009
THY	11R-2, 18–21	2	6,858	Apatite oxide olivine gabbro	5	51.20	0.52	1.32	16.37	0.51	11.23	18.48	0.46	0.05	100.14	0.550
						0.33	0.10	0.16	1.58	0.11	0.23	1.63	0.04	0.04		0.019
TSB	11R-2, 51–54	7	6,891	Apatite oxide olivine gabbro	2	50.22	0.58	1.65	16.01	0.64	11.70	18.09	0.43	0.02	99.34	0.566
TSB	11R-2, 129–133	12	6,969	Apatite oxide olivine gabbro	2	52.01	0.76	1.50	15.77	0.46	11.99	18.95	0.47	0.01	101.94	0.575
THY	12R-1, 28–34	3	7,158	Oxide olivine gabbro	7	51.84	0.59	1.39	15.26	0.47	11.60	19.50	0.56	0.03	101.24	0.575
						0.33	0.14	0.14	1.10	0.08	0.39	0.94	0.09	0.04		0.011
TSB	12R-1, 106–108	13	7,236	Olivine gabbro	2	48.88	0.73	2.91	6.63	0.15	15.98	20.31	0.42	0.17	96.17	0.811
TSB	12R-2, 50–53	5	7,327	Olivine gabbro	4	51.61	0.77	2.99	6.11	0.14	15.64	21.15	0.43	0.31	99.15	0.820
						0.42	0.11	0.47	0.45	0.04	0.45	0.50	0.12	0.13		0.009
TSB	12R-2, 123–127	15	7,400	Olivine gabbro (fine grained)	2	51.07	0.82	2.69	6.48	0.17	15.16	21.32	0.43	0.24	98.38	0.807
TSB	12R-2, 123–127	15	7,400	Olivine gabbro (coarse grained)	5	51.78	0.70	2.51	7.12	0.15	15.88	19.97	0.37	0.16	98.64	0.799
						0.35	0.04	0.09	0.64	0.05	0.67	1.23	0.07	0.04		0.009
TSB	13R-1, 24–26	3a	7,654	Microgabbro	3	51.52	0.69	1.78	9.31	0.22	14.64	20.53	0.33		99.01	0.737
						0.50	0.38	0.61	0.27	0.02	0.41	1.26	0.10			0.010
TSB	13R-1, 24–26	3a	7,654	Olivine gabbro (coarse grained)	3	51.40	0.87	2.70	9.80	0.15	15.26	19.65	0.42		100.25	0.735
						0.19	0.22	0.13	0.67	0.09	0.23	0.56	0.02			0.013
TSB	13R-1, 87–89	3d	7,719	Olivine gabbro	3	49.74	0.75	2.74	9.93	0.23	14.99	18.89	0.61	0.06	97.74	0.729
						1.57	0.04	0.12	0.31	0.03	0.31	0.84	0.02	0.01		0.002
THY	13R-2, 39–43	2	7,809	Oxide gabbro	6	52.28	0.47	1.30	16.65	0.49	11.54	19.06	0.46	0.04	102.08	0.553
						0.48	0.11	0.35	1.32	0.10	0.70	1.14	0.07	0.03		0.031

Table T3 (continued).

ID	Core, section, interval (cm)	Piece	Depth (cm)	Petrography	*N*	Major element oxide (wt%)										
						SiO_2	TiO_2	Al_2O_3	FeO	MnO	MgO	CaO	Na_2O	Cr_2O_3	Total	Mg#
THY	13R-2, 39–43	2	7,809	Oxide gabbro	1	52.17	0.29	0.55	30.52	0.93	17.03	1.59	0.02	0.00	103.11	0.499
THY	13R-2, 83–86	3a	7,855	Oxide gabbro	4	51.64	0.92	2.47	12.48	0.37	13.23	19.28	0.54	0.03	100.88	0.654
						0.39	0.12	0.06	0.75	0.04	0.35	0.88	0.08	0.03		0.009
TSB	13R-3, 38–42	3	7,942	Olivine gabbro (fine grained)	5	49.94	0.68	1.99	12.50	0.32	13.94	18.91	0.39		98.24	0.665
						0.80	0.04	0.15	1.01	0.03	0.41	1.21	0.06			0.014
TSB	13R-3, 38–42	3	7,942	Oxide olivine gabbro (coarse grained)	1	50.23	0.82	2.31	13.20	0.44	12.68	18.50	0.45		98.64	0.631
TSB	13R-3, 79–82	6	7,983	Olivine gabbro	3	51.66	0.52	3.35	6.16	0.16	16.45	20.35	0.42	0.56	99.64	0.001
						0.44	0.15	0.30	0.29	0.03	0.85	1.12	0.10	0.21		
TSB	14R-1, 42–45	3a	8,144	Olivine gabbro	4	51.73	0.51	3.02	6.30	0.17	16.23	19.98	0.37	0.26	98.77	0.821
						0.78	0.06	0.13	0.48	0.03	0.58	0.77	0.02	0.09		0.010
THY	14R-1, 80–84	3c	8,182	Oxide gabbro	1	51.51	0.94	1.78	13.89	0.54	11.96	20.08	0.52	0.01	101.23	0.605
TSB	14R-3, 91–94	7	8,455	Olivine gabbro (foliated)	4	51.77	0.60	2.33	8.99	0.22	14.89	20.66	0.37	0.24	99.93	0.013
						0.43	0.24	0.72	0.53	0.07	0.29	1.18	0.08	0.16		
THY	15R-1, 32–36	3c	8,634	Apatite oxide olivine gabbro (ultramafic)	4	51.55	0.36	0.98	15.17	0.48	11.49	19.15	0.42	0.02	99.65	0.575
						0.63	0.27	0.45	1.48	0.05	0.23	1.66	0.02	0.02		0.022
TSB	15R-1, 113–116	13	8,713	Olivine gabbro (fine grained)	4	52.22	0.48	3.09	7.01	0.19	16.73	19.55	0.38	0.39	99.93	0.810
						0.39	0.07	0.15	0.56	0.04	0.15	0.44	0.05	0.07		0.012
TSB	15R-2, 71–74	9a	8,823	Microgabbro	4	51.37	0.60	1.80	13.69	0.32	12.37	19.66	0.40	0.00	100.10	0.617
						0.51	0.12	0.19	0.72	0.04	0.52	0.81	0.03	0.01		0.005
TSB	15R-3, 83–86	8	8,980	Oxide olivine gabbro (gneiss)	1	50.38	0.64	1.52	15.66	0.42	11.63	19.06	0.45	0.00	99.76	0.570
TSB	16R-1, 91–94	10	9,151	Olivine gabbro (foliated)	5	50.13	0.60	1.55	14.61	0.36	12.03	19.07	0.40	0.02	98.46	0.595
						0.62	0.12	0.23	0.60	0.04	0.23	1.05	0.08	0.03		0.007
TSB	16R-2, 14–17	2	9,207	Oxide olivine gabbro	3	50.79	0.60	1.58	15.06	0.41	12.04	19.12	0.43	0.02	100.06	0.588
						0.65	0.07	0.11	0.96	0.04	0.44	1.29	0.05	0.03		0.011
TSB	16R-3, 22–25	3	9,356	Olivine gabbro	6	51.43	0.51	3.52	7.46	0.23	16.03	19.49	0.44	0.52	99.74	0.793
						0.79	0.12	0.71	3.15	0.11	2.01	0.55	0.08	0.26		0.091
THY	16R-3, 53–56	7	9,387	Oxide olivine gabbro	4	51.88	0.58	1.63	15.26	0.58	12.06	18.60	0.46	0.00	101.16	0.585
						0.31	0.15	0.32	0.96	0.13	1.29	1.41	0.07	0.00		0.033
THY	17R-1, 47–51	4	9,607	Oxide olivine gabbro	3	51.77	0.74	1.69	14.60	0.46	11.79	20.07	0.53	0.01	101.22	0.590
						0.41	0.06	0.01	0.25	0.06	0.11	0.47	0.09	0.01		0.003
TSB	17R-2, 23–26	2	9,725	Olivine gabbro	7	51.95	0.65	3.14	6.44	0.14	16.03	20.72	0.35	0.39	99.81	0.816
						0.26	0.15	0.24	0.69	0.04	0.53	1.17	0.04	0.14		0.013
TSB	17R-4, 35–39	4	10,030	Oxide olivine gabbro	3	49.97	1.13	1.31	16.29	0.54	12.43	18.39	0.40	0.02	100.49	0.576
						2.38	1.17	0.10	2.37	0.08	0.18	1.16	0.07	0.03		0.038
THY	18R-1, 96–100	10	10,116	Oxide gabbro	7	49.85	0.54	1.57	13.76	0.42	12.01	19.90	0.46	0.02	98.54	0.609
						0.48	0.21	0.24	1.09	0.08	0.23	0.61	0.07	0.02		0.021
THY	18R-2, 8–11	2	10,170	Oxide gabbro	3	50.40	0.77	1.98	14.66	0.45	11.98	18.94	0.52	0.00	99.71	0.593
						1.97	0.14	0.41	0.67	0.09	0.33	0.97	0.17	0.02		0.013
TSB	18R-2, 53–57	7	10,215	Oxide olivine gabbro	6	51.91	0.64	2.21	12.93	0.34	13.90	18.44	0.42	0.04	100.84	0.657
						0.53	0.15	0.25	0.75	0.06	0.32	0.61	0.06	0.03		0.014
THY	19R-1, 85–89	6b	10,607	Oxide gabbro	4	50.81	0.81	2.16	12.92	0.36	12.40	20.04	0.56	0.03	100.09	0.631
						0.41	0.20	0.30	0.45	0.05	0.13	0.33	0.05	0.02		0.010
TSB	19R-2, 65–68	6	10,735	Olivine gabbro (troctolitic)	3	49.70	0.69	2.14	11.33	0.29	13.78	20.02	0.76	0.03	98.73	0.684
						1.01	0.18	0.10	1.38	0.09	0.24	1.12	0.09	0.04		0.026
TSB	19R-2, 95–98	8a	10,767	Oxide gabbro	3	49.98	0.83	2.52	12.08	0.34	14.07	19.03	0.40	0.02	99.27	0.675
						1.08	0.02	0.06	0.87	0.11	0.91	0.61	0.03	0.03		0.029
TSB	19R-3, 94–97	8a	10,901	Olivine gabbro	5	49.71	0.77	3.05	8.91	0.26	15.25	19.84	0.40	0.15	98.32	0.753
						0.84	0.32	0.31	0.83	0.06	0.60	0.17	0.09	0.03		0.023
THY	20R-1, 46–49	6	11,026	Oxide gabbro	3	51.89	0.69	1.49	14.98	0.50	12.35	19.05	0.44	0.01	101.40	0.595

Table T3 (continued).

ID	Core, section, interval (cm)	Piece	Depth (cm)	Petrography	*N*	Major element oxide (wt%)										Mg#
						SiO_2	TiO_2	Al_2O_3	FeO	MnO	MgO	CaO	Na_2O	Cr_2O_3	Total	
						0.33	0.08	0.06	0.56	0.06	0.38	1.37	0.05	0.01		0.003
TSB	21R-1, 49–52	6	11,129	Olivine gabbro	3	51.72	0.48	2.92	6.04	0.16	16.55	20.20	0.42	0.38	98.87	0.830
						0.74	0.19	0.26	0.45	0.05	1.09	0.87	0.11	0.13		0.020
THY	21R-2, 121–125	14	11,335	Oxide gabbro	4	50.93	0.55	1.63	14.16	0.42	11.88	19.56	0.50	0.00	99.65	0.599
						0.50	0.05	0.06	1.26	0.11	0.63	0.83	0.05	0.00		0.034
TSB	22R-1, 103–106	15	11,613	Apatite oxide gabbro (mylonite)	7	50.78	0.54	1.65	13.75	0.35	12.26	19.84	0.43	0.03	99.63	0.614
						0.85	0.24	0.30	0.86	0.10	0.31	0.82	0.07	0.04		0.020
THY	22R-2, 27–30	2a	11,679	Oxide gabbro	1	51.43	0.51	1.49	12.58	0.36	12.20	19.99	0.51	0.02	99.08	0.634
TSB	22R-2, 74–78	5	11,724	Orthopyroxene oxide gabbronorite	1	52.22	0.66	2.08	11.91	0.36	13.29	19.71	0.41	0.10	100.74	0.666
TSB	22R-2, 74–78	5	11,724	Orthopyroxene oxide gabbronorite	3	50.39	0.28	0.60	30.23	0.70	16.85	1.92	0.06	0.02	101.05	0.498
						0.27	0.00	0.03	0.54	0.02	0.50	0.30	0.04	0.01		0.012
TSB	22R-3, 130–133	8	11,898	Oxide olivine gabbro (fine grained); few oxides	2	50.01	0.84	2.32	9.21	0.35	14.48	20.45	0.51	0.01	98.16	0.737
TSB	22R-3, 130–133	8	11,898	Oxide olivine gabbro (fine grained); few oxides	1	51.00	0.32	1.11	21.94	0.59	22.61	1.63	0.04	0.07	99.31	0.648
TSB	23R-1, 94–98	8	12,034	Oxide olivine gabbro (fine grained)	5	50.17	0.74	1.94	12.85	0.36	13.48	19.46	0.42	0.03	99.44	0.651
						0.92	0.31	0.47	1.47	0.08	0.36	0.97	0.08	0.03		0.023
TSB	23R-1, 94–98	8	12,034	Oxide olivine gabbro (medium grained)	4	50.39	0.72	2.06	14.10	0.43	13.22	18.79	0.45	0.03	100.19	0.626
						0.55	0.16	0.28	1.03	0.06	0.35	1.16	0.06	0.02		0.015
TSB	23R-2, 98–101	11	12,188	Oxide gabbro	2	49.79	0.55	2.07	13.23	0.33	13.34	19.34	0.50	0.00	99.15	0.643
TSB	24R-1, 32–36	3b	12,474	Oxide olivine gabbro	9	50.64	0.92	2.40	10.89	0.31	14.15	19.26	0.44	0.03	99.04	0.698
						0.42	0.31	0.21	1.11	0.05	0.42	1.03	0.08	0.03		0.015
THY	24R-3, 74–77	6	12,790	Oxide gabbro	9	52.07	0.63	1.75	12.57	0.37	12.58	20.70	0.53	0.02	101.22	0.641
						0.46	0.18	0.39	0.33	0.05	0.12	0.49	0.06	0.03		0.006
TSB	25R-1, 26–30	2	12,926	Oxide gabbro (fine grained)	5	50.21	0.72	2.04	13.37	0.40	12.17	19.26	0.49	0.01	98.68	0.619
						0.44	0.14	0.23	0.44	0.12	0.21	0.35	0.03	0.02		0.007
TSB	25R-1, 26–30	2	12,926	Oxide gabbro (medium grained)	4	49.89	0.50	1.65	13.67	0.43	12.47	19.49	0.45	0.02	98.58	0.619
						0.67	0.19	0.30	0.79	0.06	0.27	0.78	0.12	0.03		0.016
TSB	25R-1, 133–137	5c	13,035	Oxide olivine gabbro	2	48.19	0.64	1.62	13.35	0.48	11.77	19.64	0.54	0.00	96.23	0.611
THY	25R-2, 18–21	1	13,062	Oxide olivine gabbro	2	51.71	0.65	1.82	13.82	0.52	12.08	19.92	0.47	0.00	101.01	0.609
THY	25R-2, 18–21	1	13,062	Oxide olivine gabbro	1	52.04	0.33	0.60	25.91	0.89	15.81	5.99	0.16	0.01	101.75	0.521
TSB	25R-3, 10–13	1	13,193	Oxide gabbro (mylonitic)	3	49.94	0.58	2.05	12.37	0.45	12.61	18.98	0.45	0.09	97.51	0.645
						1.25	0.19	0.41	0.80	0.05	0.33	0.63	0.04	0.01		0.014
THY	26R-1, 50–54	2	13,450	Orthopyroxene apatite oxide gabbro	4	52.01	0.45	1.37	16.05	0.56	12.15	18.69	0.43	0.02	101.73	0.574
						0.40	0.04	0.11	0.30	0.09	0.05	0.20	0.01	0.03		0.005
THY	26R-1, 50–54	2	13,450	Orthopyroxene apatite oxide gabbro	4	52.02	0.26	0.57	29.38	0.86	16.97	1.93	0.07	0.04	102.10	0.507
						0.11	0.02	0.03	0.31	0.03	0.16	0.18	0.01	0.03		0.005
TSB	26R-3, 80–81	5	13,756	Olivine gabbro	4	51.15	0.59	2.82	7.11	0.20	16.45	20.21	0.36	0.14	99.02	0.805
						0.40	0.22	0.12	0.12	0.08	0.68	1.10	0.04	0.07		0.009
TSB	27R-1, 27–28	1a	13,899	Olivine gabbro	4	51.05	0.65	3.03	6.13	0.16	16.27	19.79	0.40	0.17	97.64	0.825
						0.49	0.26	0.25	0.96	0.06	0.78	1.01	0.01	0.11		0.024
THY	27R-1, 71–75	3	13,941	Orthopyroxene apatite oxide biotite gabbro	3	51.98	0.15	0.42	31.34	0.93	16.49	1.58	0.15	0.02	103.06	0.484
						0.10	0.04	0.02	0.48	0.05	0.12	0.02	0.02	0.04		0.006
TSB	27R-3, 93–94	2	14,195	Olivine gabbro (anorthositic)	4	51.02	0.46	3.13	6.50	0.15	16.59	19.59	0.38	0.17	97.99	0.820
						1.07	0.06	0.36	0.46	0.02	0.94	0.63	0.05	0.05		0.016
TSB	28R-1, 98–99	3b	14,468	Olivine gabbro	8	51.01	0.63	2.77	8.26	0.20	16.15	19.69	0.36	0.08	99.15	0.777
						0.58	0.05	0.03	0.52	0.07	0.38	0.70	0.06	0.05		0.008
TSB	29R-1, 102–106	4	14,942	Olivine gabbro (mylonitic)	7	50.91	0.45	3.10	7.64	0.20	16.18	19.66	0.41	0.14	98.70	0.791
						1.33	0.06	0.27	1.05	0.09	0.59	0.54	0.06	0.06		0.027
TSB	29R-3, 112–114	3	15,221	Oxide olivine gabbro	22	49.76	0.73	2.21	12.11	0.37	13.43	19.95	0.53	0.03	99.11	0.664
						0.83	0.09	0.27	1.47	0.06	0.46	1.35	0.08	0.03		0.021

Table T3 (continued).

ID	Core, section, interval (cm)	Piece	Depth (cm)	Petrography	*N*	Major element oxide (wt%)										Mg#
						SiO_2	TiO_2	Al_2O_3	FeO	MnO	MgO	CaO	Na_2O	Cr_2O_3	Total	
THY	29R-4, 13–17	1	15,253	Oxide gabbro	3	52.11	0.78	2.10	13.14	0.40	13.12	19.56	0.51	0.05	101.76	0.640
						0.17	0.12	0.04	0.84	0.04	0.36	0.99	0.02	0.06		0.009
TSB	29R-4, 31–33	2	15,271	Oxide gabbro	2	50.95	0.82	2.06	13.42	0.38	13.64	18.66	0.59	0.02	100.54	0.644
TSB	30R-1, 27–31	3a	15,367	Oxide gabbro	3	49.36	0.60	1.88	11.99	0.40	13.18	20.42	0.48	0.01	98.31	0.662
						0.42	0.12	0.15	0.20	0.06	0.17	0.60	0.07	0.00		0.007
TSB	30R-2, 109–113	8	15,585	Oxide gabbro (fine grained)	4	48.59	0.65	1.89	12.05	0.41	12.72	20.28	0.50	0.01	97.10	0.653
						1.01	0.17	0.40	0.73	0.05	0.28	0.51	0.09	0.00		0.011
TSB	30R-3, 102–106	9	15,712	Olivine gabbro	3	51.04	0.59	2.28	10.29	0.31	15.51	19.51	0.35	0.03	99.91	0.729
						0.34	0.07	0.20	0.60	0.07	1.11	2.13	0.11	0.04		0.003

Notes: ID = shipboard sample codes. The first line for each sample is the average, and the second line is the standard deviation of analyses. *N* = the number of analyses used for each average. Mg# = Mg/(Mg+Fe) with all iron calculated as Fe^{2+}.

Table T4. Compositions of cumulus olivine. (**See table notes.** Continued on next two pages.)

ID	Core, section, interval (cm)	Piece	Depth (cm)	Petrography	*N*	Major element oxide (wt%)								Mg#
						SiO_2	FeO	MnO	MgO	CaO	Cr_2O_3	NiO	Total	
	179-1105A-													
TSB	1R-2, 88–91	2b	1,696	Olivine gabbro	3	37.11	30.52	0.44	34.00	0.05	0.04	0.10	102.25	0.665
						0.17	1.11	0.06	0.14	0.01	0.07	0.10		0.009
THY	1R-3, 114–117	8b	1,859	Olivine gabbro	4	37.23	33.13	0.48	31.65	0.06	0.02	0.08	102.65	0.630
						0.29	0.19	0.05	0.17	0.02	0.03	0.07		0.000
TSB	1R-4, 95–98	5	1,985	Olivine gabbro	6	38.11	24.20	0.36	37.92	0.07	0.03	0.10	100.81	0.736
						0.14	0.72	0.05	0.19	0.02	0.03	0.08		0.006
TSB	1R-5, 137–141	10	2,173	Olivine gabbro	5	36.35	32.62	0.49	32.16	0.07	0.02	0.05	101.77	0.637
						0.29	0.27	0.03	0.28	0.02	0.02	0.07		0.003
TSB	4R-2, 43–46	1b	3,491	Olivine gabbro	6	38.07	24.16	0.34	38.46	0.09	0.01	0.12	101.25	0.739
						0.30	0.30	0.06	0.14	0.02	0.01	0.09		0.002
TSB	4R-3, 46–60	3	3,628	Olivine gabbro	4	38.58	23.65	0.35	39.58	0.05	0.01	0.20	102.41	0.749
						0.19	0.45	0.02	0.21	0.04	0.01	0.04		0.003
THY	4R-4, 47–50	6	3,769	Olivine gabbro	4	38.66	29.21	0.45	35.36	0.07	0.01	0.02	103.79	0.683
						0.24	0.37	0.04	0.19	0.02	0.02	0.02		0.003
THY	5R-2, 4–7	2	3,982	Oxide olivine gabbro (gneissic)	4	32.65	54.31	1.13	14.09	0.12	0.02	0.04	102.36	0.316
						1.22	0.51	0.09	0.86	0.03	0.02	0.06		0.015
THY	7R-3, 72–76	4	5,135	Olivine gabbro	4	36.60	40.74	0.63	26.42	0.04	0.02	0.04	104.49	0.536
						0.22	0.40	0.11	0.19	0.03	0.03	0.04		0.004
TSB	7R-4, 30–33	7	5,212	Olivine gabbro	6	35.75	36.92	0.53	27.86	0.02	0.02	0.05	101.16	0.574
						0.16	0.46	0.04	0.26	0.02	0.02	0.07		0.004
TSB	9R-1, 82–86	7	5,822	Olivine gabbro	4	34.63	41.66	0.71	24.59	0.07	0.03	0.03	101.71	0.513
						0.32	0.58	0.11	0.35	0.02	0.02	0.03		0.003
TSB	9R-4, 12–16	1	6,181	Olivine gabbro	6	35.63	43.10	0.70	23.77	0.06	0.01	0.02	103.29	0.496
						0.18	0.80	0.05	0.21	0.03	0.01	0.02		0.006
TSB	10R-1, 38–42	3a	6,238	Olivine gabbro	4	36.11	34.56	0.51	30.10	0.05	0.04	0.04	101.42	0.608
						0.10	0.30	0.11	0.31	0.04	0.06	0.03		0.004
THY	11R-2, 18–21	2	6,858	Apatite Oxide olivine gabbro	4	33.39	50.52	0.99	15.33	0.12	0.02	0.03	100.40	0.351
						0.16	0.39	0.10	0.19	0.04	0.03	0.03		0.004
TSB	11R-2, 51–54	7	6,891	Apatite Oxide olivine gabbro	4	32.70	52.93	1.02	15.70	0.11	0.00	0.07	102.53	0.346
						0.06	0.66	0.09	0.19	0.04	0.00	0.05		0.001
TSB	11R-2, 129–133	12	6,969	Apatite Oxide olivine gabbro	3	33.71	52.21	0.97	16.13	0.12	0.01	0.01	103.16	0.355
						0.23	0.62	0.09	0.14	0.04	0.01	0.01		0.001
THY	12R-1, 28–34	3	7,158	Oxide olivine gabbro	6	33.88	52.52	0.99	16.46	0.10	0.02	0.03	103.99	0.358
						0.18	0.44	0.08	0.24	0.02	0.03	0.03		0.005
TSB	12R-1, 106–108	13	7,236	Olivine gabbro	6	37.01	24.07	0.31	37.49	0.09	0.01	0.06	99.03	0.735
						2.00	0.43	0.05	0.92	0.01	0.02	0.05		0.006
TSB	12R-2, 50–53	5	7,327	Olivine gabbro	4	38.60	25.13	0.34	37.95	0.03	0.02	0.05	102.10	0.729
						0.18	0.78	0.04	0.34	0.02	0.02	0.07		0.006
TSB	12R-2, 123–127	15	7,400	Olivine gabbro (fine grained)	2	38.23	26.00	0.31	36.33	0.05	0.04	0.07	101.04	0.714
TSB	12R-2, 123–127	15	7,400	Olivine gabbro (coarse grained)	4	37.51	26.20	0.32	36.75	0.04	0.01	0.06	100.89	0.714
						0.79	0.54	0.05	0.49	0.02	0.01	0.04		0.006
TSB	13R-1, 24–26	3a	7,654	Olivine gabbro (coarse grained)	7	36.55	33.88	0.42	31.60	0.08		0.04	102.56	0.624
						0.39	0.49	0.10	0.35	0.04		0.04		0.006
TSB	13R-1, 87–89	3d	7,717	Olivine gabbro	4	35.99	36.26	0.49	28.61	0.09	0.02	0.06	101.52	0.584
						0.90	0.83	0.07	0.34	0.00	0.03	0.04		0.008
TSB	13R-3, 38–42	3	7,942	Olivine gabbro (fine grained)	4	34.26	43.08	0.58	23.90	0.06		0.04	101.91	0.497
						0.37	0.38	0.06	0.30	0.02		0.03		0.005
TSB	13R-3, 38–42	3	7,942	Oxide olivine gabbro (coarse grained)	3	33.27	47.29	0.53	19.12	0.06		0.04	100.31	0.419

Table T4 (continued).

ID	Core, section, interval (cm)	Piece	Depth (cm)	Petrography	*N*	Major element oxide (wt%)								Mg#
						SiO_2	FeO	MnO	MgO	CaO	Cr_2O_3	NiO	Total	
						0.91	0.53	0.01	0.75	0.04		0.06		0.008
TSB	13R-3, 79–82	6	7,983	Olivine gabbro	6	39.13	22.25	0.23	40.40	0.04	0.00	0.06	102.12	0.764
						0.24	0.29	0.07	0.45	0.02	0.00	0.04		0.003
TSB	14R-1, 42–45	3a	8,142	Olivine gabbro	5	37.35	23.71	0.27	39.27	0.05	0.01	0.07	100.73	0.747
						0.56	0.27	0.02	0.47	0.03	0.01	0.07		0.004
TSB	14R-3, 91–94	7	8,455	Olivine gabbro (foliated)	3	35.54	36.84	0.47	29.29	0.04	0.04	0.03	102.26	0.586
						0.41	0.24	0.02	0.23	0.02	0.03	0.02		0.002
TSB	15R-1, 113–116	13	8,713	Olivine gabbro (fine grained)	4	38.18	24.68	0.27	38.46	0.04	0.02	0.08	101.74	0.735
						0.51	0.38	0.03	0.39	0.02	0.02	0.06		0.003
TSB	15R-2, 71–74	9a	8,821	microgabbro	3	33.96	49.26	0.70	19.51	0.06	0.01	0.02	103.52	0.414
						0.35	0.35	0.09	0.14	0.01	0.01	0.03		0.003
TSB	15R-3, 83–86	8	8,980	Oxide olivine gabbro (gneiss)	6	33.16	52.23	0.82	16.75	0.09	0.01	0.00	103.07	0.364
						0.55	0.60	0.08	0.27	0.03	0.02	0.01		0.006
TSB	16R-1, 91–94	10	9,151	Olivine gabbro (foliated)	4	35.69	37.64	0.54	28.21	0.04	0.01	0.04	102.16	0.572
						0.58	0.34	0.04	0.36	0.01	0.02	0.02		0.003
TSB	16R-3, 22–25	3	9,356	Olivine gabbro	4	38.55	22.66	0.31	39.20	0.03	0.00	0.03	100.78	0.755
						0.51	0.69	0.05	0.46	0.00	0.00	0.04		0.006
TSB	16R-3, 22–25	3	9,356	Olivine gabbro	4	33.04	50.03	0.68	17.97	0.08	0.01	0.03	101.84	0.390
						0.20	0.34	0.06	0.21	0.02	0.01	0.03		0.001
THY	17R-1, 47–51	4	9,607	Oxide olivine gabbro	4	34.35	49.19	1.00	18.84	0.09	0.01	0.01	103.49	0.406
						0.18	1.11	0.10	0.40	0.01	0.02	0.01		0.008
TSB	17R-2, 23–26	2	9,725	Olivine gabbro	3	38.71	23.58	0.28	39.35	0.11	0.02	0.03	102.07	0.748
						0.47	0.23	0.08	0.14	0.03	0.02	0.03		0.001
TSB	17R-4, 35–39	4	10,030	Oxide olivine gabbro	4	33.52	50.35	0.77	18.64	0.08	0.03	0.04	103.43	0.398
						0.47	0.43	0.05	0.45	0.03	0.02	0.03		0.007
TSB	18R-2, 53–57	7	10,215	Oxide olivine gabbro	9	34.31	44.21	0.66	23.48	0.08	0.02	0.01	102.77	0.486
						0.84	1.27	0.10	0.85	0.03	0.03	0.02		0.016
TSB	19R-2, 65–68	6	10,735	Olivine gabbro (troctolitic)	4	32.86	42.37	0.60	23.52	0.67	0.03	0.03	100.07	0.497
						0.71	0.77	0.09	1.23	1.15	0.04	0.03		0.020
TSB	19R-3, 94–97	8a	10,899	Olivine gabbro	15	32.81	41.04	0.58	25.18	0.08	0.02	0.03	99.74	0.522
						2.43	0.66	0.08	0.87	0.03	0.02	0.03		0.011
TSB	21R-1, 49–52	6	11,129	Olivine gabbro	6	37.66	29.41	0.39	34.50	0.05	0.01	0.07	102.09	0.676
						0.57	0.40	0.05	0.38	0.02	0.02	0.05		0.005
TSB	22R-3, 130–133	8	11,898	Oxide olivine gabbro (fine grained); few oxides	4	35.71	36.25	0.52	29.92	0.07	0.00	0.03	102.51	0.595
						0.81	0.48	0.10	0.65	0.03	0.00	0.04		0.008
TSB	23R-1, 94–98	8	12,034	Oxide olivine gabbro (fine grained)	4	34.07	44.37	0.66	23.03	0.03	0.02	0.01	102.20	0.481
						0.19	0.28	0.04	0.23	0.02	0.02	0.02		0.002
TSB	23R-1, 94–98	8	12,034	Oxide olivine gabbro (medium grained)	4	34.02	45.80	0.72	22.71	0.04	0.02	0.02	103.33	0.469
						0.15	0.51	0.07	0.25	0.03	0.02	0.02		0.004
TSB	24R-1, 32–36	3b	12,472	Oxide olivine gabbro	13	34.39	39.20	0.59	26.69	0.06	0.03	0.03	100.98	0.548
						1.71	1.87	0.05	1.72	0.03	0.03	0.03		0.028
TSB	25R-1, 133–137	5c	13,033	Oxide olivine gabbro	1	31.75	42.43	0.76	23.29	0.05	0.06	0.03	98.37	0.495
THY	25R-2, 18–21	1	13,062	Oxide olivine gabbro	4	34.36	49.23	0.94	18.57	0.09	0.01	0.03	103.22	0.402
						0.24	0.45	0.13	0.34	0.04	0.01	0.03		0.006
TSB	26R-3, 80–81	5	13,756	Olivine gabbro	4	36.93	28.72	0.42	35.35	0.05	0.01	0.08	101.58	0.687
						0.24	0.48	0.08	0.49	0.04	0.01	0.03		0.002
TSB	27R-1, 27–28	1a	13,897	Olivine gabbro	4	36.29	25.70	0.40	37.07	0.06	0.02	0.03	99.56	0.720
						0.54	0.39	0.04	0.17	0.02	0.02	0.03		0.003
TSB	27R-3, 93–94	2	14,195	Olivine gabbro (anorthositic)	6	34.91	40.70	0.72	25.64	0.04	0.04	0.05	102.12	0.529

Table T4 (continued).

ID	Core, section, interval (cm)	Piece	Depth (cm)	Petrography	*N*	Major element oxide (wt%)								Mg#
						SiO_2	FeO	MnO	MgO	CaO	Cr_2O_3	NiO	Total	
						0.06	0.68	0.07	0.33	0.02	0.05	0.05		0.005
TSB	28R-1, 98–99	3b	14,468	Olivine gabbro	5	37.45	27.75	0.39	36.38	0.09	0.02	0.06	102.14	0.700
						0.25	0.11	0.08	0.28	0.01	0.02	0.04		0.001
TSB	29R-1, 102–106	4	14,942	Olivine gabbro (mylonitic)	4	36.67	32.36	0.49	32.26	0.05	0.03	0.03	101.90	0.640
						0.18	0.99	0.10	0.09	0.04	0.03	0.03		0.008
TSB	29R-3, 112–114	3	15,221	Oxide olivine gabbro	10	34.67	42.47	0.61	24.68	0.06	0.02	0.01	102.51	0.509
						0.29	0.33	0.12	0.40	0.03	0.02	0.01		0.004
TSB	30R-3, 102–106	9	15,712	Olivine gabbro	4	35.41	36.24	0.58	30.20	0.04	0.01	0.02	102.49	0.598
						0.66	0.15	0.05	0.13	0.01	0.01	0.03		0.001

Notes: ID = shipboard sample codes. The first line for each sample is the average, and the second line is the standard deviation of analyses. *N* = the number of analyses used for each average. Mg# = forsterite content (Fo mol%).

Table T5. Compositions of coexisting ilmenite and titanomagnetite. (**See table notes.** Continued on next four pages.)

ID	Core, section, interval (cm)	Piece	Depth (cm)	Petrography	*N*	Major element oxide (wt%)										
						SiO_2	TiO_2	Al_2O_3	FeO	MnO	MgO	CaO	Cr_2O_3	NiO	Total	
	179-1105A-															
THY	4R-1, 92–95	9	3,422	Oxide gabbro	4	0.02	50.51	0.05	48.88	1.71	0.07	0.01	0.00	0.04	101.30	Il
						0.02	0.50	0.02	0.60	0.13	0.08	0.01	0.00	0.03		
THY	4R-1, 92–95	9	3,422	Oxide gabbro	4	0.09	17.42	1.82	77.71	0.69	0.09	0.01	0.01	0.02	97.86	Mt
						0.04	5.44	0.60	4.49	0.12	0.07	0.02	0.01	0.03		
TSB	4R-4, 57–62	7	3,779	Apatite oxide gabbro	4	0.01	48.85	0.08	48.58	1.24	0.43	0.03	0.02	0.01	99.24	Il
						0.01	0.50	0.08	0.67	0.29	0.37	0.02	0.02	0.02		
TSB	4R-4, 57–62	7	3,779	Apatite oxide gabbro	3	0.07	11.13	2.82	80.47	0.47	0.14	0.03	0.04	0.01	95.17	Mt
						0.02	1.67	0.07	1.24	0.07	0.08	0.02	0.03	0.01		
THY	5R-1, 12–16	1	3,842	Oxide gabbro	3	0.05	49.83	0.08	49.30	1.29	0.22	0.03	0.04	0.04	100.88	Il
						0.03	0.25	0.05	1.04	0.12	0.16	0.01	0.02	0.04		
THY	5R-1, 12–16	1	3,842	Oxide gabbro	4	0.09	10.84	2.74	83.34	0.37	0.20	0.03	0.06	0.05	97.71	Mt
						0.04	0.66	0.23	1.17	0.03	0.08	0.01	0.04	0.05		
THY	5R-1, 89–93	5	3,919	Oxide gabbro	3	0.04	49.14	0.06	49.90	1.23	0.34	0.04	0.01	0.03	100.78	Il
						0.02	0.23	0.02	0.39	0.21	0.17	0.02	0.01	0.04		
THY	5R-1, 89–93	5	3,919	Oxide gabbro	4	0.10	11.58	2.75	82.40	0.38	0.34	0.01	0.04	0.01	97.62	Mt
						0.04	0.85	0.34	0.72	0.06	0.10	0.01	0.05	0.03		
TSB	5R-1, 115–118	7	3,945	Apatite oxide olivine gabbro	3	0.04	50.08	0.06	48.81	1.22	0.18	0.02	0.02	0.00	100.43	Il
						0.03	0.12	0.02	0.29	0.16	0.10	0.03	0.03	0.00		
TSB	5R-1, 115–118	7	3,945	Apatite oxide olivine gabbro	4	0.06	10.73	2.76	82.37	0.35	0.17	0.03	0.05	0.05	96.57	Mt
						0.02	1.48	0.23	1.57	0.09	0.04	0.02	0.06	0.04		
THY	5R-2, 4–7	2	3,982	Oxide olivine gabbro (gneissic)	3	0.02	50.74	0.08	49.55	1.20	0.17	0.07	0.00	0.01	101.84	Il
						0.01	0.04	0.02	0.59	0.04	0.01	0.09	0.00	0.01		
THY	5R-2, 4–7	2	3,982	Oxide olivine gabbro (gneissic)	3	0.07	10.18	2.88	84.42	0.45	0.21	0.05	0.04	0.03	98.34	Mt
						0.03	0.77	0.44	0.73	0.12	0.03	0.03	0.03	0.02		
THY	6R-1, 124–128	16	4,404	Gabbro	5	0.02	50.99	0.10	45.71	0.62	2.55	0.01	0.09	0.02	100.11	Il
						0.02	0.51	0.12	1.46	0.05	0.64	0.02	0.05	0.02		
TSB	7R-3, 33–36	2	5,096	Orthopyroxene apatite oxide gabbro	4	0.01	49.51	0.03	48.92	0.86	0.45	0.02	0.03	0.02	99.85	Il
						0.01	0.27	0.02	1.58	0.14	0.40	0.03	0.04	0.02		
TSB	7R-3, 33–36	2	5,096	Orthopyroxene apatite oxide gabbro	4	0.09	11.16	2.65	82.14	0.25	0.11	0.02	0.04	0.06	96.51	Mt
						0.05	1.37	0.30	0.99	0.06	0.04	0.01	0.05	0.03		
TSB	8R-1, 68–70	7	5,308	Microgabbro (opx, oxides)	7	0.01	49.57	0.04	49.57	1.25	0.15	0.08	0.03	0.02	100.73	Il
						0.02	0.20	0.03	0.40	0.10	0.21	0.18	0.03	0.04		
TSB	8R-1, 68–70	7	5,308	Microgabbro (opx, oxides)	6	0.07	7.31	1.69	86.38	0.27	0.06	0.08	0.10	0.02	95.98	Mt
						0.04	1.61	0.28	2.63	0.06	0.05	0.06	0.08	0.04		
THY	9R-2, 85–89	11	5,975	Orthopyroxene oxide gabbronorite	3	0.09	49.59	0.06	48.89	0.78	1.47	0.01	0.03	0.00	100.93	Il
						0.02	0.31	0.02	0.66	0.18	0.41	0.01	0.01	0.00		
THY	9R-2, 85–89	11	5,975	Orthopyroxene oxide gabbronorite	3	0.14	10.38	3.11	82.67	0.33	0.81	0.03	0.04	0.01	97.52	Mt
						0.04	0.71	0.30	0.87	0.04	0.12	0.02	0.00	0.02		
THY	9R-3, 118–121	10a	6,147	Oxide gabbro	2	0.04	49.31	0.07	49.84	0.75	0.50	0.01	0.01	0.01	100.53	Il
THY	9R-3, 118–121	10a	6,147	Oxide gabbro	3	0.53	13.64	3.08	79.05	0.42	0.80	0.06	0.11	0.03	97.71	Mt
						0.75	6.97	0.42	5.46	0.14	0.65	0.08	0.02	0.04		

Table T5 (continued).

ID	Core, section, interval (cm)	Piece	Depth (cm)	Petrography	*N*	Major element oxide (wt%)										
						SiO_2	TiO_2	Al_2O_3	FeO	MnO	MgO	CaO	Cr_2O_3	NiO	Total	
THY	10R-2, 38–41	4	6,373	Oxide gabbro	5	0.05	49.60	0.04	48.95	0.93	0.29	0.02	0.02	0.04	99.92	Il
						0.04	0.52	0.03	0.91	0.17	0.18	0.01	0.03	0.06		
THY	10R-2, 38–41	4	6,373	Oxide gabbro	3	0.15	17.47	3.13	76.35	0.41	0.33	0.03	0.04	0.05	97.98	Mt
						0.12	3.20	0.51	2.54	0.09	0.17	0.01	0.04	0.05		
TSB	10R-2, 85–88	7	6,420	Oxide gabbro	4	0.01	50.26	0.08	49.88	0.91	0.38	0.01	0.02	0.06	101.60	Il
						0.01	0.12	0.05	0.53	0.14	0.25	0.01	0.03	0.02		
TSB	10R-2, 85–88	7	6,420	Oxide gabbro	3	0.05	12.39	3.09	81.34	0.35	0.12	0.02	0.02	0.02	97.40	Mt
						0.04	0.55	0.13	0.84	0.10	0.04	0.01	0.03	0.03		
THY	11R-2, 18–21	2	6,858	Apatite oxide olivine gabbro	3	0.04	50.06	0.07	48.29	0.98	0.56	0.02	0.01	0.02	100.05	Il
						0.03	0.44	0.07	0.82	0.30	0.19	0.01	0.01	0.02		
THY	11R-2, 18–21	2	6,858	Apatite oxide olivine gabbro	3	0.09	11.93	3.17	81.14	0.34	0.29	0.03	0.03	0.01	97.04	Mt
						0.01	0.71	0.28	0.88	0.10	0.09	0.02	0.04	0.01		
TSB	11R-2, 51–54	7	6,891	Apatite oxide olivine gabbro	3	0.04	50.64	0.09	49.70	0.84	0.27	0.01	0.06	0.03	101.68	Il
						0.03	0.12	0.06	0.69	0.16	0.12	0.02	0.02	0.05		
TSB	11R-2, 51–54	7	6,891	Apatite oxide olivine gabbro	6	0.06	12.21	3.33	80.54	0.29	0.14	0.01	0.07	0.02	96.68	Mt
						0.04	1.17	0.24	0.89	0.06	0.15	0.01	0.04	0.04		
TSB	11R-2, 129–133	12	6,969	Apatite oxide olivine gabbro	4	0.01	50.18	0.07	49.15	0.95	0.66	0.02	0.03	0.07	101.14	Il
						0.01	0.49	0.02	0.79	0.34	0.49	0.01	0.02	0.08		
TSB	11R-2, 129–133	12	6,969	Apatite oxide olivine gabbro	2	0.08	12.99	3.03	80.95	0.36	0.31	0.01	0.06	0.00	97.79	Mt
THY	12R-1, 28–34	3	7,158	Oxide olivine gabbro	3	0.05	50.13	0.18	48.85	0.63	1.22	0.03	0.02	0.02	101.12	Il
						0.04	0.23	0.21	0.64	0.17	0.04	0.01	0.03	0.02		
THY	12R-1, 28–34	3	7,158	Oxide olivine gabbro	4	0.08	10.94	3.22	82.20	0.31	0.57	0.01	0.07	0.00	97.38	Mt
						0.04	1.15	0.46	1.10	0.06	0.01	0.01	0.05	0.00		
THY	13R-2, 39–43	2	7,809	Oxide gabbro	9	0.03	49.85	0.06	50.41	1.14	0.09	0.01	0.02	0.02	101.64	Il
						0.02	0.42	0.03	0.76	0.16	0.04	0.01	0.02	0.05		
THY	13R-2, 39–43	2	7,809	Oxide gabbro	4	0.08	10.77	2.36	83.64	0.28	0.07	0.01	0.05	0.01	97.27	Mt
						0.05	0.78	0.06	0.60	0.06	0.04	0.01	0.06	0.02		
THY	13R-2, 83–86	3a	7,855	Oxide gabbro	3	0.01	47.51	0.07	48.65	0.77	0.73	0.02	0.04	0.05	97.86	Il
						0.01	0.67	0.02	0.83	0.07	0.26	0.02	0.06	0.06		
THY	13R-2, 83–86	3a	7,855	Oxide gabbro	3	0.08	13.95	3.49	77.35	0.38	0.68	0.02	0.11	0.08	96.14	Mt
						0.03	1.78	0.80	2.33	0.08	0.35	0.03	0.05	0.02		
TSB	13R-3, 38–42	3	7,942	Oxide olivine gabbro (coarse grained)	4	0.03	48.86	0.04	48.03	0.54	1.25	0.03		0.04	98.81	Il
						0.03	0.56	0.02	1.09	0.11	0.14	0.02		0.03		
TSB	13R-3, 38–42	3	7,942	Oxide olivine gabbro (coarse grained)	2	0.04	8.87	3.06	78.27	0.17	0.48	0.01		0.04	90.95	Mt
THY	14R-1, 80–84	3c	8,182	Oxide gabbro	3	0.06	49.55	0.09	49.99	0.82	0.47	0.02	0.03	0.03	101.05	Il
						0.05	0.33	0.02	0.88	0.16	0.47	0.02	0.04	0.04		
THY	14R-1, 80–84	3c	8,182	Oxide gabbro	3	0.10	13.41	2.60	80.10	0.31	0.18	0.01	0.07	0.02	96.80	Mt
						0.03	1.34	0.17	1.68	0.08	0.08	0.01	0.03	0.02		
THY	15R-1, 32–36	3c	8,634	Apatite oxide olivine gabbro (ultramafic)	3	0.03	49.85	0.06	49.54	1.11	0.33	0.01	0.02	0.04	100.98	Il
						0.03	0.15	0.02	0.26	0.20	0.29	0.00	0.02	0.06		
THY	15R-1, 32–36	3c	8,634	Apatite oxide olivine gabbro (ultramafic)	3	0.09	11.02	2.50	83.00	0.28	0.25	0.01	0.04	0.05	97.24	Mt
						0.01	0.53	0.02	0.59	0.08	0.06	0.02	0.04	0.05		

Table T5 (continued).

ID	Core, section, interval (cm)	Piece	Depth (cm)	Petrography	*N*	Major element oxide (wt%)										
						SiO_2	TiO_2	Al_2O_3	FeO	MnO	MgO	CaO	Cr_2O_3	NiO	Total	
TSB	15R-1, 113–116	13	8,713	Oxide gabbro (coarse grained)	6	0.01	50.32	0.08	50.02	0.82	0.85	0.02	0.02	0.01	102.15	Il
						0.01	0.28	0.03	0.93	0.17	0.38	0.02	0.02	0.01		
TSB	15R-1, 113–116	13	8,713	Oxide gabbro (coarse grained)	3	0.06	11.96	2.82	82.78	0.34	0.41	0.03	0.07	0.01	98.48	Mt
						0.02	1.87	0.06	1.99	0.14	0.28	0.02	0.04	0.01		
TSB	15R-2, 71–74	9a	8,823	Microgabbro	3	0.02	47.83	0.05	49.99	0.66	0.69	0.01	0.07	0.06	99.39	Il
						0.02	0.99	0.01	0.78	0.12	0.22	0.01	0.06	0.06		
TSB	15R-3, 83–86	8	8,980	Oxide olivine gabbro (gneiss)	4	0.03	50.71	0.08	49.31	0.59	1.15	0.02	0.02	0.02	101.93	Il
						0.01	0.18	0.06	0.66	0.17	0.33	0.01	0.02	0.03		
TSB	15R-3, 83–86	8	8,980	Oxide olivine gabbro (gneiss)	3	0.06	9.66	3.28	84.73	0.23	0.33	0.01	0.09	0.01	98.41	Mt
						0.03	0.96	0.34	1.50	0.06	0.12	0.02	0.04	0.01		
TSB	16R-1, 56–58	4d	9,118	Oxide olivine gabbro	1	0.03	49.84	0.06	50.10	0.82	0.43	0.03	0.00	0.00	101.32	Il
TSB	16R-1, 56–58	4d	9,118	Oxide olivine gabbro	3	0.06	11.51	3.11	81.62	0.35	0.24	0.03	0.17	0.01	97.10	Mt
						0.03	2.58	0.34	1.65	0.11	0.03	0.01	0.03	0.02		
TSB	16R-2, 14–17	2	9,207	Oxide olivine gabbro	3	0.02	49.58	0.08	49.33	1.17	0.91	0.02	0.04	0.04	101.18	Il
						0.02	0.28	0.03	1.01	0.47	0.41	0.02	0.06	0.07		
TSB	16R-2, 14–17	2	9,207	Oxide olivine gabbro	3	0.94	11.03	2.62	81.44	0.54	0.51	0.01	0.07	0.03	97.19	Mt
						1.36	0.72	0.91	3.30	0.21	0.38	0.02	0.04	0.03		
THY	16R-3, 53–56	7	9,387	Oxide olivine gabbro	4	0.03	49.27	0.10	48.86	1.06	1.00	0.01	0.05	0.06	100.45	Il
						0.01	0.35	0.02	1.24	0.14	0.50	0.02	0.03	0.06		
THY	16R-3, 53–56	7	9,387	Oxide olivine gabbro	3	0.08	11.62	3.77	79.78	0.41	1.09	0.01	0.12	0.00	96.88	Mt
						0.01	1.49	0.34	1.68	0.11	0.04	0.02	0.03	0.00		
THY	17R-1, 47–51	4	9,607	Oxide olivine gabbro	5	0.03	49.76	0.09	48.37	0.71	1.48	0.01	0.01	0.04	100.51	Il
						0.03	0.18	0.03	0.26	0.08	0.17	0.01	0.01	0.04		
THY	17R-1, 47–51	4	9,607	Oxide olivine gabbro	4	0.08	10.74	3.33	82.66	0.30	0.73	0.02	0.06	0.00	97.91	Mt
						0.05	1.17	0.34	0.99	0.05	0.18	0.02	0.04	0.00		
TSB	17R-4, 35–39	4	10,030	Oxide olivine gabbro	3	0.01	50.16	0.05	49.40	0.71	0.95	0.01	0.00	0.04	101.33	Il
						0.00	0.14	0.04	0.32	0.03	0.16	0.00	0.00	0.02		
TSB	17R-4, 35–39	4	10,030	Oxide olivine gabbro	3	0.05	12.74	3.16	80.92	0.36	0.25	0.01	0.08	0.04	97.62	Mt
						0.04	0.22	0.39	0.89	0.05	0.01	0.01	0.07	0.06		
THY	18R-1, 96–100	10	10,116	Oxide gabbro	3	0.03	50.56	0.04	49.24	0.89	0.40	0.01	0.03	0.02	101.22	Il
						0.02	0.39	0.03	1.26	0.27	0.53	0.01	0.05	0.03		
THY	18R-1, 96–100	10	10,116	Oxide gabbro	3	0.07	9.42	2.26	83.97	0.19	0.14	0.01	0.12	0.03	96.20	Mt
						0.02	2.47	1.08	2.41	0.06	0.16	0.01	0.08	0.04		
THY	18R-2, 8–11	2	10,170	Oxide gabbro	4	0.02	50.39	0.17	47.62	0.68	1.15	0.02	0.02	0.01	100.07	Il
						0.04	0.52	0.07	0.79	0.10	0.27	0.02	0.03	0.01		
THY	18R-2, 8–11	2	10,170	Oxide gabbro	3	0.08	12.25	3.25	80.86	0.26	0.64	0.01	0.08	0.02	97.45	Mt
						0.02	0.43	0.09	0.40	0.09	0.21	0.01	0.08	0.03		
TSB	18R-2, 53–57	7	10,215	Oxide olivine gabbro	6	0.02	45.89	0.08	48.77	0.60	2.05	0.00	0.07	0.02	97.49	Il
						0.02	1.12	0.04	0.56	0.13	0.31	0.00	0.05	0.02		
TSB	18R-2, 53–57	7	10,215	Oxide olivine gabbro	2	0.07	10.79	3.61	79.94	0.32	1.11	0.01	0.25	0.03	96.14	Mt
THY	19R-1, 85–89	6b	10,607	Oxide gabbro	8	0.03	48.63	0.08	50.48	0.78	0.31	0.02	0.04	0.01	100.37	Il
						0.03	0.31	0.05	0.63	0.15	0.26	0.02	0.03	0.02		
THY	19R-1, 85–89	6b	10,607	Oxide gabbro	1	0.04	13.05	3.36	80.65	0.25	0.09	0.01	0.03	0.14	97.62	Mt

Table T5 (continued).

ID	Core, section, interval (cm)	Piece	Depth (cm)	Petrography	*N*	Major element oxide (wt%)										
						SiO_2	TiO_2	Al_2O_3	FeO	MnO	MgO	CaO	Cr_2O_3	NiO	Total	
TSB	19R-2, 95–98	8a	10,767	Oxide gabbro	4	0.02	46.41	0.08	49.58	1.08	0.60	0.01	0.09	0.02	97.88	Il
						0.02	0.48	0.01	0.99	0.38	0.45	0.01	0.05	0.03		
TSB	19R-2, 95–98	8a	10,767	Oxide gabbro	2	0.07	9.43	3.83	82.29	0.36	0.19	0.03	0.33	0.02	96.54	Mt
THY	20R-1, 46–49	6	11,026	Oxide gabbro	4	0.06	48.81	0.06	48.38	0.88	1.34	0.01	0.05	0.01	99.58	Il
						0.03	1.47	0.03	0.72	0.16	0.24	0.01	0.06	0.01		
THY	20R-1, 46–49	6	11,026	Oxide gabbro	3	0.10	13.35	4.38	78.66	0.32	1.10	0.02	0.10	0.02	98.03	Mt
						0.03	8.61	0.57	8.55	0.23	0.35	0.01	0.04	0.02		
THY	21R-2, 121–125	14	11,335	Oxide gabbro	5	0.02	50.46	0.05	50.03	0.88	0.07	0.02	0.01	0.02	101.56	Il
						0.01	0.37	0.02	0.75	0.12	0.05	0.02	0.01	0.02		
TSB	22R-1, 103–106	15	11,613	Apatite oxide gabbro (mylonite)	5	0.03	48.54	0.05	49.88	1.04	0.09	0.01	0.02	0.02	99.69	Il
						0.04	1.52	0.04	0.50	0.13	0.05	0.02	0.02	0.04		
TSB	22R-1, 103–106	15	11,613	Apatite oxide gabbro (mylonite)	6	0.07	10.60	2.91	82.68	0.34	0.06	0.01	0.12	0.04	96.83	Mt
						0.03	1.34	0.28	1.83	0.08	0.03	0.01	0.03	0.06		
THY	22R-2, 27–30	2a	11,679	Oxide gabbro	3	0.04	49.67	0.06	49.65	1.09	0.11	0.01	0.03	0.05	100.72	Il
						0.02	0.66	0.02	0.49	0.14	0.06	0.01	0.03	0.07		
THY	22R-2, 27–30	2a	11,679	Oxide gabbro	3	0.06	10.59	2.90	82.47	0.25	0.33	0.01	0.12	0.07	96.81	Mt
						0.03	0.87	0.70	0.71	0.03	0.43	0.02	0.05	0.07		
TSB	22R-2, 74–78	5	11,724	Orthopyroxene oxide gabbronorite	5	0.01	46.80	0.05	50.33	1.45	0.13	0.01	0.02	0.04	98.83	Il
						0.01	0.44	0.03	0.65	0.14	0.07	0.01	0.03	0.05		
TSB	22R-2, 74–78	5	11,724	Orthopyroxene oxide gabbronorite	3	0.07	11.10	2.62	82.85	0.52	0.11	0.01	0.06	0.02	97.38	Mt
						0.01	0.51	0.26	0.40	0.05	0.07	0.01	0.09	0.03		
TSB	23R-1, 94–98	8	12,034	Oxide olivine gabbro (fine grained)	4	0.02	50.42	0.05	48.92	1.24	0.51	0.06	0.04	0.04	101.30	Il
						0.02	0.36	0.04	0.60	0.35	0.38	0.05	0.02	0.02		
TSB	23R-1, 94–98	8	12,034	Oxide olivine gabbro (medium grained)	3	0.02	49.87	0.15	48.75	0.58	1.82	0.01	0.06	0.07	101.34	Il
						0.02	0.41	0.16	0.34	0.18	0.15	0.02	0.05	0.08		
TSB	23R-1, 94–98	8	12,034	Oxide olivine gabbro (medium grained)	4	0.06	8.74	3.71	82.66	0.20	0.59	0.01	0.46	0.05	96.48	Mt
						0.04	0.95	0.15	0.32	0.11	0.23	0.02	0.04	0.05		
TSB	23R-2, 98–101	11	12,188	Oxide gabbro	3	0.06	50.20	0.02	49.17	1.30	0.98	0.02	0.04	0.03	101.83	Il
						0.07	0.56	0.01	0.80	0.60	0.94	0.04	0.04	0.04		
TSB	23R-2, 98–101	11	12,188	Oxide gabbro	4	0.09	11.36	3.78	81.32	0.46	0.70	0.01	0.26	0.02	97.99	Mt
						0.01	0.33	0.50	1.65	0.05	0.19	0.01	0.10	0.04		
TSB	24R-1, 32–36	3b	12,474	Oxide olivine gabbro	4	0.05	50.39	0.04	45.92	0.94	1.60	0.01	0.06	0.01	99.02	Il
						0.02	0.59	0.03	0.93	0.23	0.33	0.01	0.04	0.01		
THY	24R-3, 74–77	6	12,790	Oxide gabbro	4	0.03	49.30	0.06	49.99	0.85	0.36	0.00	0.04	0.02	100.67	Il
						0.01	0.28	0.07	0.63	0.07	0.23	0.00	0.02	0.05		
THY	24R-3, 74–77	6	12,790	Oxide gabbro	3	0.10	9.43	3.66	82.62	0.25	0.12	0.01	0.21	0.04	96.44	Mt
						0.03	1.67	0.21	1.27	0.11	0.02	0.01	0.04	0.04		
TSB	25R-1, 26–30	2	12,926	Oxide gabbro (fine grained)	6	0.13	49.02	0.05	49.01	1.15	0.17	0.02	0.06	0.02	99.64	Il
						0.28	1.04	0.06	0.71	0.22	0.09	0.02	0.05	0.03		
TSB	25R-1, 26–30	2	12,926	Oxide gabbro (fine grained)	2	0.03	7.94	2.92	83.65	0.36	0.02	0.03	0.51	0.07	95.54	Mt
TSB	25R-1, 26–30	2	12,926	Oxide gabbro (medium grained)	5	0.01	49.63	0.06	49.67	1.01	0.27	0.00	0.02	0.02	100.69	Il
						0.01	0.32	0.03	0.68	0.19	0.32	0.00	0.03	0.02		
TSB	25R-1, 26–30	2	12,926	Oxide gabbro (medium grained)	1	0.05	10.79	2.69	80.73	0.33	0.11	0.00	0.14	0.03	94.87	Mt

Table T5 (continued).

ID	Core, section, interval (cm)	Piece	Depth (cm)	Petrography	*N*	Major element oxide (wt%)										
						SiO_2	TiO_2	Al_2O_3	FeO	MnO	MgO	CaO	Cr_2O_3	NiO	Total	
TSB	25R-1, 133–137	5c	13,035	Oxide olivine gabbro	2	0.00	49.26	0.10	49.51	0.82	0.82	0.01	0.08	0.00	100.61	Il
TSB	25R-1, 133–137	5c	13,035	Oxide olivine gabbro	4	0.05	11.93	2.69	80.70	0.37	0.39	0.00	0.15	0.01	96.30	Mt
						0.02	0.98	0.28	0.98	0.14	0.15	0.01	0.08	0.02		
THY	25R-2, 18–21	1	13,062	Oxide olivine gabbro	4	0.14	49.81	0.14	48.60	0.77	1.38	0.02	0.01	0.00	100.88	Il
						0.14	0.90	0.12	0.39	0.29	0.35	0.02	0.02	0.00		
THY	25R-2, 18–21	1	13,062	Oxide olivine gabbro	5	0.16	11.80	2.92	81.40	0.40	0.51	0.01	0.08	0.04	97.32	Mt
						0.12	1.93	0.41	1.56	0.10	0.15	0.01	0.06	0.05		
THY	26R-1, 50–54	2	13,450	Orthopyroxene apatite oxide gabbro	4	0.12	48.12	0.07	51.01	1.12	0.14	0.03	0.03	0.03	100.68	Il
						0.22	1.49	0.01	0.39	0.16	0.08	0.02	0.03	0.03		
THY	26R-1, 50–54	2	13,450	Orthopyroxene apatite oxide gabbro	3	0.09	6.87	1.61	88.16	0.22	0.08	0.03	0.09	0.03	97.17	Mt
						0.02	0.37	0.13	0.23	0.07	0.00	0.02	0.03	0.03		
THY	27R-1, 71–75	3	13,941	Opx apatite oxide biotite gabbro	6	0.03	48.39	0.05	50.95	1.06	0.17	0.01	0.01	0.04	100.72	Il
						0.04	0.56	0.02	0.55	0.06	0.07	0.01	0.01	0.05		
THY	27R-1, 71–75	3	13,941	Opx apatite oxide biotite gabbro	3	0.14	10.19	1.63	85.48	0.32	0.26	0.01	0.03	0.01	98.07	Mt
						0.04	2.52	0.21	1.69	0.09	0.17	0.02	0.03	0.01		
TSB	29R-3, 112–114	3	15,221	Oxide olivine gabbro	6	0.09	48.17	0.24	49.58	0.85	1.50	0.00	0.05	0.02	100.51	Il
						0.13	0.31	0.29	0.78	0.06	0.13	0.00	0.06	0.01		
TSB	29R-3, 112–114	3	15,221	Oxide olivine gabbro	6	0.13	10.64	3.33	82.82	0.35	0.64	0.01	0.21	0.03	98.16	Mt
						0.16	0.95	0.25	0.44	0.04	0.19	0.01	0.07	0.03		
THY	29R-4, 13–17	1	15,253	Oxide gabbro	3	0.04	50.00	0.10	49.21	0.67	0.83	0.07	0.01	0.00	100.93	Il
						0.03	0.11	0.07	1.01	0.15	0.53	0.12	0.01	0.00		
THY	29R-4, 13–17	1	15,253	Oxide gabbro	3	0.05	10.96	3.76	81.00	0.27	0.66	0.02	0.18	0.01	96.90	Mt
						0.01	1.05	0.31	1.14	0.05	0.16	0.03	0.02	0.01		
TSB	29R-4, 31–33	2	15,271	Oxide gabbro	4	0.01	48.42	0.07	50.67	0.97	0.37	0.00	0.03	0.04	100.57	Il
						0.01	0.20	0.04	0.26	0.12	0.47	0.00	0.03	0.02		
TSB	29R-4, 31–33	2	15,271	Oxide gabbro	3	0.07	9.96	3.16	83.94	0.24	0.54	0.01	0.17	0.01	98.09	Mt
						0.03	0.49	0.38	0.74	0.04	0.25	0.00	0.05	0.01		
TSB	30R-1, 27–31	3a	15,369	Oxide gabbro	3	0.01	46.68	0.03	50.54	1.04	0.38	0.01	0.04	0.01	98.75	Il
						0.01	0.38	0.03	0.81	0.12	0.20	0.01	0.01	0.02		
TSB	30R-1, 27–31	3a	15,369	Oxide gabbro	1	0.02	10.77	3.11	82.15	0.35	0.73	0.00	0.25	0.04	97.42	Mt
TSB	30R-2, 109–113	8	15,585	Oxide gabbro (fine grained)	3	0.01	49.13	0.06	48.39	0.79	1.74	0.02	0.02	0.02	100.17	Il
						0.01	0.26	0.02	0.58	0.12	0.32	0.01	0.03	0.03		
TSB	30R-2, 109–113	8	15,585	Oxide gabbro (fine grained)	3	0.02	9.65	3.44	82.00	0.33	0.83	0.01	0.21	0.03	96.51	Mt
						0.01	1.81	0.21	1.95	0.03	0.24	0.02	0.07	0.04		

Notes: ID = shipboard sample codes. The first line for each sample is the average, and the second line is the standard deviation of analyses. *N* = the number of analyses used for each average. Il = ilmenite, Mt = magnetite. Vertical line indicates coexisting magnetite and ilmenite. All iron is given as FeO.

Table T6. Compositions of cumulus apatite.

ID	Core, section, interval (cm)	Piece	Depth (cm)	Petrography	*N*	Major element oxide (wt%)							Element (wt%)		Total
						SiO_2	FeO	MnO	MgO	CaO	Na_2O	P_2O_5	F	Cl	
TSB	4R-4, 57–62	7	3,779	Apatite oxide gabbro	6	0.16	0.23	0.09	0.06	55.49	0.07	40.22	3.87	0.03	100.23
						0.02	0.09	0.04	0.02	0.74	0.03	1.94	0.23	0.02	
TSB	5R-1, 115–118	7	3,945	Apatite oxide olivine gabbro	10	0.23	0.15	0.06	0.04	54.97	0.06	41.94	3.86	0.04	101.36
						0.14	0.08	0.05	0.02	0.57	0.03	0.51	0.13	0.02	
TSB	5R-1, 144–147	9	3,974	Apatite oxide olivine gabbro	8	0.18	0.29	0.05	0.03	55.19	0.03	40.36	3.91	0.02	100.07
						0.03	0.18	0.05	0.02	0.43	0.03	1.76	0.08	0.01	
TSB	7R-3, 33–36	2	5,096	Orthopyroxene apatite oxide gabbro	5	0.22	0.14	0.07	0.03	55.35	0.06	39.49	4.03	0.03	99.42
						0.05	0.03	0.05	0.02	0.58	0.03	0.44	0.15	0.02	
THY	11R-2, 18–21	2	6,858	Apatite oxide olivine gabbro	6	0.28	0.37	0.06	0.07	54.08	0.15	41.26	2.56	0.36	99.19
						0.30	0.55	0.04	0.11	0.84	0.13	0.58	0.12	0.59	
TSB	11R-2, 51–54	7	6,891	Apatite oxide olivine gabbro	6	0.13	0.15	0.06	0.05	55.48	0.05	41.65	3.98	0.18	101.73
						0.04	0.10	0.06	0.02	0.75	0.03	0.29	0.11	0.40	
TSB	11R-2, 129–133	12	6,969	Apatite oxide olivine gabbro	7	0.12	0.19	0.10	0.04	54.95	0.04	40.92	3.96	0.09	100.41
						0.02	0.06	0.06	0.02	0.66	0.01	1.06	0.13	0.12	
THY	15R-1, 32–36	3c	8,634	Apatite oxide olivine gabbro (ultramafic)	8	0.12	0.18	0.10	0.08	54.21	0.16	41.72	2.69	0.11	99.37
						0.05	0.05	0.04	0.02	0.22	0.12	0.59	0.21	0.06	
TSB	22R-1, 103–106	15	11,613	Apatite oxide gabbro (mylonite)	2	0.88	0.96	0.04	0.30	53.16	0.09	41.31	2.77	0.08	99.59
THY	26R-1, 50–54	2	13,450	Orthopyroxene apatite oxide gabbro	3	0.16	0.18	0.02	0.02	53.79	0.03	41.02	2.68	0.04	97.96
						0.02	0.05	0.02	0.02	0.27	0.03	0.94	0.14	0.00	
THY	27R-1, 71–75	3	13,941	Orthopyroxene apatite oxide biotite gabbro	7	0.24	0.19	0.07	0.03	53.77	0.22	41.49	2.75	0.11	98.86
						0.07	0.11	0.03	0.01	0.57	0.06	0.33	0.08	0.04	

Notes: ID = shipboard sample codes. The first line for each sample is the average; second line is the standard deviation. *N* = the number of analyses used for each average.

Table T7. Composition of cumulus biotite.

Oxide	Composition (wt%)	Element	Cations to 20 O and 4 OH		
179-1105A-17R-1, 71-75 cm					
SiO_2	36.2	Si	5.626	Z	7.957
TiO_2	3.53	Ti	0.413	Y	5.959
Al_2O_3	12.72	Al^{IV}	2.331	X	1.758
FeO	29.26	Fe	3.803	O	20
MnO	0.17	Mn	0.022	OH	4
MgO	7.43	Mg	1.721		
CaO	0.01	Ca	0.002		
Na_2O	0.37	Na	0.112		
K_2O	8.29	K	1.644		
Total	97.98	Total	15.674		

Notes: Z, Y, and X refer to the ideal chemical formulas of biotite ($X_2Y_6Z_8O_{20}OH_4$), where X = Na + K + Ca, Y = Ti + Fe + Mn + Mg, and Z = Si + Al. O = oxygen, OH = hydroxyl groups.

Table T8. Modeling of fractional crystallization.

Solid fraction	Temperature (°C)	Major element oxide (wt%)												Density (g/cm^3)	Liquid (Mg#)	Augite (Mg#)	Plagioclase An (mol%)	Olivine Fo (mol%)
		SiO_2	TiO_2	Al_2O_3	Fe_2O_3	FeO	MnO	MgO	CaO	Na_2O	K_2O	P_2O_5	FeO*					
0.00	1184	50.70	1.71	16.05	1.26	8.00	0.20	7.17	11.35	3.17	0.19	0.19	9.13	2.67	0.615	(0.849)	0.687	0.837
0.05	1180	50.86	1.80	15.67	1.31	8.20	0.21	6.96	11.40	3.20	0.20	0.20	9.37	2.67	0.602		0.680	0.830
0.10	1174	51.02	1.89	15.28	1.36	8.39	0.22	6.75	11.45	3.22	0.21	0.21	9.62	2.67	0.589		0.672	0.821
0.15	1168	51.22	2.00	14.80	1.42	8.64	0.22	6.49	11.52	3.25	0.22	0.23	9.91	2.68	0.573		0.663	0.810
0.20	1161	51.42	2.12	14.29	1.48	8.88	0.23	6.23	11.61	3.27	0.23	0.24	10.21	2.68	0.556		0.655	0.798
0.25	1154	51.61	2.25	13.79	1.55	9.13	0.24	5.99	11.66	3.30	0.24	0.26	10.52	2.68	0.539	0.816	0.647	0.785
0.35	1143	51.81	2.57	12.92	1.72	9.96	0.26	5.56	11.23	3.41	0.27	0.30	11.51	2.69	0.499	0.796	0.617	0.754
0.40	1137	51.89	2.73	12.49	1.81	10.36	0.27	5.34	11.04	3.46	0.29	0.32	11.99	2.69	0.479	0.785	0.603	0.738
0.45	1130	51.99	2.96	11.91	1.93	10.90	0.28	5.06	10.80	3.51	0.31	0.35	12.64	2.70	0.453	0.770	0.585	0.716
0.50	1122	52.07	3.21	11.30	2.06	11.45	0.30	4.76	10.57	3.56	0.34	0.38	13.30	2.71	0.426	0.753	0.567	0.691
0.55	1112	52.16	3.55	10.51	2.23	12.14	0.32	4.39	10.30	3.62	0.37	0.43	14.15	2.72	0.392	0.731	0.546	0.658
0.60	1102	52.24	3.92	9.66	2.41	12.87	0.33	4.01	10.03	3.66	0.40	0.48	15.04	2.73	0.357	0.706	0.527	0.622
0.65	1087	53.41	3.60	9.25	2.45	12.86	0.34	3.43	9.85	3.83	0.45	0.54	15.06	2.71	0.322	0.682	0.496	0.580
0.69	1069	55.16	2.98	8.92	2.43	12.57	0.35	2.74	9.64	4.06	0.51	0.63	14.76	2.69	0.280	0.649	0.459	0.526
0.75	1048	57.60	2.12	8.53	2.37	12.07	0.35	1.95	9.31	4.35	0.60	0.76	14.20	2.66	0.224	0.597	0.416	0.447
0.80	1026	61.19	0.83	8.03	2.21	11.15	0.35	1.13	8.70	4.73	0.73	0.94	13.14	2.60	0.153	0.503	0.363	0.333
0.85	1006	66.03		7.18	1.88	9.60	0.35	0.38	7.23	5.18	0.92	1.25	11.29	2.53	0.066	0.308	0.290	0.164
0.87	1000	68.78		6.61	1.63	8.52	0.35	0.16	6.06	5.41	1.04	1.45	9.98	2.49	0.033	0.182	0.245	0.086

Notes: Parental melt is glass in dredge sample 5-3, Conrad Cruise 27-09 (Natland et al., 1991, table 1; Johnson and Dick, 1992, table 5). Perfect fractional crystallization is modeled in steps of 1 wt% of the remaining liquid. The conditions were assumed to be open with respect to oxygen and iron oxidation constrained by the fayalite-magnetite-quartz oxygen buffer. For details of calculations see the text. FeO* = total iron calculated as FeO. Mg# = Mg/(Mg+Fe^{2+}) for liquid and Mg/(Mg+Fe^{total}) for augite. An = anorthite, Fo = forsterite.